Technical University of Denmark

DTU

Field rotor measurements. Data sets prepared for analysis of stall hysteresis

Aagaard Madsen , Helge; Thirstrup Petersen, J.; Bruining, A.; Brand, A.; Graham, M.

Link back to DTU Orbit

DTU Library
Technical Information Center of Denmark

RISØ   DK 9801605   Risø-R-1046(EN)

MASTER

Field Rotor Measurements

Data Sets Prepared for Analysis of Stall Hysteresis

Helge Aagaard Madsen, Jørgen Thirstrup Petersen,
Albert Bruining, Arno Brand and Mike Graham

RECEIVED
OCT 05 1998
OSTI

Risø National Laboratory, Roskilde, Denmark
May 1998

DISCLAIMER

Portions of this document may be illegible
in electronic image products. Images are
produced from the best available original
document.

FIELD ROTOR MEASUREMENTS
Data sets prepared for analysis of stall hysteresis

Helge Aagaard Madsen   Risø (DK)
Jørgen Thirstrup Petersen Risø (DK)
Albert Bruining   Delft University (NL)
Arno Brand   ECN (NL)
Mike Graham   Imperial College (UK)

Abstract

As part of the JOULE-3 project "STALLVIB" an analysis and synthesis of the data from the field rotor experiments at ECN, Delft University, Imperial College, NREL and Risø has been carried out. This has been done in order to see to what extent the data could be used for further development and validation of engineering dynamic stall models.

A detailed investigation of the influence of the post-processing of the different data sets has been performed. Further, important statistical functions such as PSD spectra, coherence and transfer functions have been derived for the data sets which can be used as basis for evaluation of the quality of the data seen relative to actual application of the data. The importance of using an appropriate low-pass filtering to remove high frequency noise has been demonstrated when the relation between instantaneous values of e.g. α and C_N is considered.

In general, the complicated measurement on a rotor of α and w and the interpretation of these parameters combined with the strongly three-dimensional, turbulent flow field around the rotating blade has the consequence that it seems difficult to derive systematic information from the different data sets about stall hysteresis. In particular, the measurement of α, which has been performed by different methods, is complicated. Derivation of α on basis of determination of the stagnation point gives reasonable data below stall but fails in stall. On the other hand, measurements of α with a five hole pitot tube can be used also in the stall region. Another main problem is the non-dimensionalization of the coefficients C_N and C_T. If the dynamic pressure used for the non-dimensionalization is not fully correlated with the aerodynamic pressure over the considered airfoil section due to e.g. influence of the gravity on the pressure pipes, the hysteresis loops will be distorted.

However, using the data with caution and applying a suitable post-processing as described by the different participants, it will probably be possible to obtain some information on stall hysteresis from the field rotor data. An example of use of the data for derivation of the empirical constants in the fgh dynamic stall model is shown at the end of the report.

Content

Preface

The present report is one of two final reports from the project "Prediction of Dynamic Loads and Induced Vibrations in Stall STALLVIB". In the present report the work within one of totally seven work packages is reported.

The title of the other main report is:

> Petersen, J.T. (Risø), Madsen, H.A. (Risø), Björck, A. (FFA), Enevoldsen, P. (Bonus), Øye, S. (DTU), Ganander, H. (Teknikgruppen), Winkelaar, D. (ECN) *"Prediction of Dynamic Loads and Induced Vibrations in Stall"*. Risø-R-1045(EN), Risø National Laboratory, Roskilde, May 1998

The participants in the STALLVIB project are the following:

Teknikgruppen AB (Sweden)	Hans Ganander
FFA (Sweden)	Anders Björck
ECN (NL)	Danny Winkelaar Arno Brand
Delft University of Technology (NL)	Albert Bruining
The Technical University of Denmark (DK)	Stig Øye
Bonus Energy A/S (DK)	Peder Enevoldsen
Imperial College (UK)	Mike Graham
Risø National Laboratory (DK)	Jørgen T. Petersen Helge A. Madsen

1 Introduction

The importance of stall hysteresis and 3D effects for the dynamic loading on turbines in stall is well-known and experimental verification and quantification of these phenomena has been the main theme in a number of projects in the past. A comprehensive project with a number of European participants was carried out under the JOULE II programme [1-1] with the aim to increase the understanding of the three-dimensional and unsteady aerodynamics of stall controlled HAWT's. Results from the different field rotor experiments at ECN, Delft, Imperial College, NREL in US and at Risø were investigated in this project in order to provide insight into the physics of three-dimensional flow and unsteady flow of wind turbines and in order to provide guidance to how engineering methods for these phenomena should be constructed. However, more of the field rotor experiments were still ongoing during the JOULE II project so that it was typically preliminary data that were available.

It was therefor decided to included a work package in the present project STALLVIB containing an analysis and synthesis of the existing field rotor ·measurements in order to establish a common, firm basis for use of the data in the further development and verification of engineering stall hysteresis models (ESHM). Most of the different ESHM used for wind turbines originate from classical models for helicopter rotors (e.g. the Beddoes model and the ONERA model) and the verification and choice of model parameters has mainly been based upon 2D wind tunnel results on dynamic stall. However, there are some major principal differences in the operational conditions of wind turbines and helicopter rotors (e.g. continues operation of HAWT´s in stall and deep stall; HAWT´s operate in the near earth boundary layer causing a high stochastic component in the inflow parameters), which might have the influence that the parameters in the ESHM should be modified when used on wind turbines. Further, the STALLVIB project focuses on the edgewise vibrations and the influence of variations in the relative velocity to the blade. These conditions are difficult to simulate in wind tunnel tests and the different stall models are therefor mainly tuned against pitch and ramp experiments in wind tunnels.

1.1 References

[1-1]
Bjørck, A. "Dynamic Stall and Three-Dimensional Effects". Final Report for the EC DGXII Joule II Project, JOU2-CT93-0345 "Dynamic Stall and Three-dimensional Effects". FFA TN 1995-31.

2 Data Analysis

The Field rotor experiments carried out during the past decade at NREL, ECN, DELFT, Imperial College (IC) and Risø contain some new elements in the experimental set-up which has not previously been used in measurements on wind turbines. This is the measurement of the inflow parameters, angle of attack α and the relative velocity w. Additionally, the aerodynamic forces at different radial stations are measured, either by surface pressure measurements (NREL, ECN, DELFT, IC) or by force measurements (Risø). The aerodynamic forces have then to be non-dimensionalized in order to derive the normal and tangential force coefficients C_N, C_T or the lift and drag coefficients C_L, C_D. In the process of measurement and data acquisition as well as in the postprocessing many different ways exist of performing the different tasks and in particular as concerns the non-dimensionalization of the force coefficients and as concerns the derivation of α and w. Many of these subjects have been discussed thoroughly within the framework of IEA Annex XIV [2-1] which had the main objective to establish a data base of the field rotor experiments.

However, in the present project the aim is to investigate the influence on the data characteristics from the postprocessing and to see if the data can be used specifically to give details about stall hysteresis on a rotor and to be used for tuning the parameters in the stall models. It is obvious that this put strong demands on the data quality (frequency content, minimum of spikes, correlation etc.) and the postprocessing as for example time averaging.

A major problem is of course that "the correct data set" are not known so a straight forward validation cannot be carried out. Instead the approach is to perform some statistical investigations in a common way for each of the data sets and then use a more "soft" validation based on these results. A few comparisons have also been made with simulations of inflow (α and w) as done in advanced aeroelastic modelling. Finally, careful study of the time traces of e.g. α could reveal major problems in the data set The same could the appearance of much bigger hysteresis loops C_N vs. α well below stall than normally seen in aeroelastic simulations.

2.1   Common analysis and procedures

It was decided to consider measurements from only one radial station at 60-70 % radius where the flow is expected to be less influenced of 3D effects. Further, it was found convenient to look only at a few data sets but so that a wide α interval from well below stall to well above is covered.

As the major stochastic loading on a rotor is on the rotational frequency 1p and multiples of this frequency; 2p, 4p etc. for a two-bladed rotor and 3p, 6p etc. for a three-bladed rotor it was decided to low pass filter the data with a cut off frequency slightly above 3p (three-bladed rotors) and 2p (two-bladed rotors), respectively. For example for the NREL turbine running 72 rpm, 3p is equal to 3.6 Hz and a filter with a cut of frequency between 4 and 4.5 was used for this data set.

The first task has now been to describe how the data are influenced by the standard postprocessing carried out by the individual participants and then the agreed, common low pass filtering of the data. Risoe distributed at the start of the task a design programme for digital filters based on the Kaiser window theory and this has been used by some of the participants.

Next the influence from the filtering is visualised on basis of Power Spectral Density (PSD) of the angle of attack α and the relative velocity w. Risoe distributed also a data analysis package for this purpose, (the DAP-1 programme) [2-2] for spectral analysis which has been used by most of the participants.

The total signal of α and w has been split into its deterministic and stochastic parts. The reason to do this is that the more site specific parameters as tower shadow and wind shear mainly influence the deterministic part whereas the stochastic part should be more directly comparable for the different data sets. For the Risoe data set a comparison of the PSD spectra of α and w with simulations using a state of the art aeroelastic code has also been performed.

As the data are intended for analysis of stall hysteresis which express the instantaneous correlation between α and C_N or C_L a high coherence between α and C_N is important. The coherence has therefor been derived for the data sets below stall. Likewise, the transfer function for the same two parameters has been worked out where the amplitude gives information about the average slope of the α, C_N relation.

Finally, an example of use of one of the data sets for derivation of the empirical functions in the fgh stall hysteresis model [2-3] is shown.

2.2 References

[2-1]
Schepers, J.G. et al. "Final report of IEA Annex XIV: Field Rotor Aerodynamics". ECN-C-97-027, ECN June 1997.

[2-2]
Madsen, P.H. "DAP –1 A Data Analysis Package for Spectral Analysis Version 1.2". Wind Energy Research Centre, Solar Energy Research Institute, Golden, Colerado.

[2-3]
Rasmussen, F., Petersen, J.T. and Madsen, H.A. "Response Predictions by Application of a New Dynamic Stall Model". Proceedings of the 1996 European Union Wind Energy Conference, Göteborg, Sweden, May 20-24, 1996, pp 838-842.

3 Data from ECN

3.1 Background

In the framework of ECN's Field Rotor-Aerodynamics research programme aerodynamic measurements were performed at the HAT25 experimental wind turbine. To this end an Aerpac 25WPX rotor blade is equipped with a high-speed pressure scanning system. This system measures blade surface pressures at three stations (30%, 60% and 80% of the blade span; 47 taps per station) and velocity probe pressures at one location (35% of the blade span; 5 taps). In addition to the pressure data, signals from the HAT25 (e.g. rotor speed) and the environment (e.g. wind speed) are acquired. The facility allows different experimental conditions to be set by changing independently the blade pitch angle, the rotor speed, and/or the yaw angle. Also active yawing and periodic pitch variation is possible. Conditions for the experiments were defined on basis of an analysis of the effects which may induce dynamic stall and/or three-dimensional flow. In the corresponding measuring programmes ten types of experiment were identified; apart from the high wind-speed cases all measurements were performed by 30th June 1996. A detailed description of the working methods and overview of the available data have been published separately [3-1], [3-2]. Analyses of the data, mainly comprising conditional averages against the angle of attack, have also been presented separately [3-3], [3-4].

In this chapter an analysis of the time series, thus unsteady rather than averaged data, is presented for the first time. This analysis consists of an investigation of the effect of the actual data pre-processing on the aerodynamic data. The material presented is mainly a condensation of the methods and results that were reported earlier in the course of the 'Stallvib' project [3-5], [3-6], but includes also a description of the datasets selected for stall hysteresis analysis. First, a description of the data handling is presented, identifying the standard and the specific procedures (section 3.2). Next, the approach is introduced which was used in order to prepare data sets for analysis (section 3.3). Next follow discussions on the effect of filtering and decomposing (section 3.4 and 3.5), as well as how these affect the normal force curve (section 3.6). Finally, the datasets selected for stall hysteresis analysis and the conclusions regarding the ECN data are presented (section 3.7 and 3.8).

3.2 Data handling

Standard methods

The experimental procedure is organised into two stages: the data acquisition stage and the data reduction stage. In the data acquisition stage blade and probe surface pressure differences, and, in addition, signals form the HAT25 and the environment are measured. In the data reduction stage aerodynamic quantities are derived form these pressure difference and additional signals. This stage consists of three sub-stages: the pre-processing of the acquired pressure differences, the processing of the acquired pressure differences into aerodynamic

quantities, and the post-processing of the aerodynamic quantities. Figure 3-1 presents an outline of this data handling.

In the framework of the 'Stallvib' project the pre-processing stage is addressed. In the standard form (i.e. prior to the start of the 'Stallvib' project) in this stage the acquired data is filtered by using:

- A three-point median filter, and
- A first-order Butterworth filter (bandwidth 10 Hz).

These filters, which are to remove binary and gaussian noise, respectively, are described in the first report on the ECN aerodynamic field measurements [3-1].

Methods specific to the 'Stallvib' project

In the 'Stallvib' project the investigation on the effect of pre-processing the (time series of) aerodynamic data was organised into a study on the effect of filtering and an investigation on the effect of decomposing. In both cases the effects were to be evaluated on basis of power spectra, phase spectra, coherence functions, and amplitude and phase of transfer functions. In order to harmonise this evaluation the spectral analysis programme DAP was provided by Risø.

In order to evaluate the effect of filtering, in addition to the standard one another four first-order Butterworth filters with bandwidths ranging from 2.5 Hz to 40 Hz were considered by ECN. In combination with the options median filter 'ON/OFF' and the non-filtering Butterworth filter with bandwidth ∞ Hz, this resulted in ten different types of filtering. Although these ten types were considered in the first progress report [3-5], the evaluation was limited to three different types in the second progress report [3-6]:

- Raw: Median filter 'OFF' plus Butterworth filter 'OFF',
- Standard: Median filter 'ON' plus Butterworth filter 'ON' with bandwidth 10 Hz, and
- Most: Median filter 'ON' plus Butterworth filter 'ON' with bandwidth 2.5 Hz.

Additionally, in order to further harmonise the analyses, a Kaiser window Finite Impulse Response low-pass filter was obtained from Risø. By using the associated filter design programme, this Kaiser filter was tailored to ECN's needs defined by a data rate of 128 Hz and a 1P frequency of about 0.625 Hz. This Kaiser filter is described in ECN's second progress report [3-6]. The transfer functions of the 'standard', 'most' and Kaiser filter are shown in *Figure 3-2*.

The idea behind decomposing a measured signal is that it contains a 'real' signal which is hidden in noise. The method to decompose a signal which was chosen by ECN is triple decomposition in combination with phase averaging. In the associated terminology (which is somewhat different from the one in the common approach), this allows one to identify the coherent and the random component of a signal, and, in addition, its deterministic component. Apart from its average value, the 'real' signal can be recovered by determining the coherent part of the measured signal. The deterministic component of the measured signal represents the 'real' signal but for the average noise. The second progress report by ECN contains a description of this decomposing procedure [3-6].

3.3 Approach

The test case addressing the effects of filtering and decomposing consists of data from the 80% station in the measurement 'h215397' [3-1], pp. 137-143. This measurement, one of the seven in the measurement series 'nov95f', was selected because here for the outboard station the angle of attack α and the normal force coefficient c_n are in the linear region ($\alpha = 3.7°$ en $c_n = 0.71$). It contains 70.3 s of data acquired at 128 Hz effectively for a blade pitch angle of 6.5°, a rotor speed of 37.3 rpm, a wind speed of 9.7 m/s, and a yaw misalignment of 3.6° (average values).

In the remainder of ECN's contribution to the 'Stallvib' project, as described in the second progress report [3-6], it is assumed that the coherent/deterministic component represents the 'real' signal if it is hidden in noise. Subsequently, by analysing the outboard data from measurement 'h215397' it was concluded that this coherent/deterministic component must be obtained from the raw (i.e. not filtered) signal, if low as well as high-frequency components are to be included in analyses of the 'real' signal. If, on the other hand, high-frequency components must be removed from the 'real' signal, application of the Kaiser-window low-pass filter must be preferred over the first-order Butterworth filters. Anyway, the Butterworth filter with the smaller bandwidth must not be used. As to c_n and α, if the relation between the time series of the two quantities is considered, 'coherent, Kaiser filtered' data must be preferred. On the other hand, normal force curves $c_n(\alpha)$ must be based on 'deterministic, raw' data.

So far, in the ECN investigations, angle of attack has been determined by using the stagnation point method. In the angle-of-attack studies which were performed in the framework of IEA Annex XIV 'Field Rotor-Aerodynamics' [3-7], it was discovered that stagnation angles have some serious flaws. (Regarding stagnation velocities serious problems were not noted.) Consequently, it was concluded stagnation angles are a good estimate to the angle of attack *in the linear region* only. Although this warrants a thorough review of the stagnation angle method, in which new calibration functions and a new interpolation scheme must be developed, in the 'Stallvib' investigations this method is used in its original form.

3.4 Effect of filtering

In order to show qualitatively the effect of filtering, part of the time series of normal force coefficient c_n (Figure 3-3), angle of attack α (Figure 3-4) and effective wind speed W (Figure 3-5) are presented. These 8 s records contain about 5 revolutions. It is clear the raw data contain narrow peaks, particularly the angle of attack and the effective wind speed. (Also note the spike in W due to the data rejection mechanism in the stagnation point method.) Application of the Butterworth filters attenuates the peaks as required, but also causes an undesired time shift in the data. Attenuation and shift are largest in the most filtered data. By applying the Kaiser filter, on the other hand, low-frequency components are neither attenuated nor shifted. This is in contrast to the high-frequency components, which are effectively removed. This effect of the Kaiser filter is also quantitatively shown in the power spectra of the three time series (Figure 3-6, Figure 3-7 and Figure 3-8).

3.5 Effect of decomposing

Since high-frequency components must not be present in the data to be analysed, in the following the examples are limited to Kaiser filtered data. The effect of decomposing the three aerodynamic quantities is shown in the Figure 3-9 to Figure 3-11 in the form of the coherent component and the random component of the measured signals. The corresponding power spectra are presented in the Figure 3-12 through Figure 3-17. On basis of the assumption that the coherent component represents the real signal apart from its average value, these figures present the low-frequency component of the three aerodynamic quantities. Inspection of the spectra reveals that mainly nP components are present in the coherent components. Note however that neither low-pass filtering nor decomposing could prevent a spike from entering the coherent component of the effective wind speed signal.

The coherence between α and c_n, as expressed in the coherence function and the phase spectrum, is presented in the Figure 3-18 and Figure 3-19. From the coherences it follows that generally the correlation between the coherent components of α and c_n is better (i.e. closer to 1) than the one of the not-decomposed components. Also it follows that application of the Kaiser filter has given a good correlation between α and c_n at the low frequencies but a poor correlation at the high frequencies. In addition, the phase spectra show that the phase shift between α and c_n is small for the low frequencies. Note however that the irregularities in the phase spectrum suggest that large random phase shifts are present in the not-decomposed data.

The transfer between α and c_n, as expressed in the amplitude and the phase of the transfer function, is presented in Figure 3-20 and Figure 3-21. From the amplitudes it follows that for frequencies up to 10 Hz the lift curve slope is of the order 0.1 1/deg. (This is in contrast to the not-decomposed and Butterworth filtered data where the lift curve slope is 0.1 1/deg at a frequency of about 1P only.) Due to its erratic behaviour, information can not be obtained from the phase of the transfer function.

3.6 Normal force coefficient versus angle of attack

Next, the decomposing procedure is applied to Kaiser filtered data so that plots of the instantaneous realisations of the deterministic components of c_n and α are obtained. The result is presented in Figure 3-22. The corresponding normal force curve, obtained by conditionally averaging c_n against α using a 'bin width' of 1°, is shown in Figure 3-23. A comparison of these figures reveals that, instantaneously as well as on average, most datapoints are on a straight line. This supports the point of view that the aerodynamic data from the 80% station in data set 'h215397' is in the linear region.

3.7 Selected data sets

In the course of the 'Stallvib' project three datasets were prepared for analysis. These datasets contain aerodynamic data from the outboard station (radial position 82%) as available in the measurement series 'nov95f' [3-1]. The duration is 70.3 s and the data rate is 128 Hz. Together these cover an incidence range from well below to well above '2D steady' stall:

1) 'pro80_e215.397': linear region ($\alpha = 3.7°$); origin: measurement 'h215397',
2) 'pro80_e215.395': near stall ($\alpha = 9.3°$); origin: measurement 'h215395', and

3) 'pro80_e215.393': above stall ($\alpha = 18.3°$); origin: measurement 'h215393'.

Note in these measurements a different average angle of attack was obtained by changing the blade pitch angle at a given wind speed. Data in these files comprise time series of angle of attack, effective wind speed, normal force coefficient and tangential force coefficient. The Figure 3-24 to Figure 3-26 show these data and the tables 1 to 3 present the statistics. The time series are 'raw' (i.e. as measured), which means that post-processing has not been applied. In other words: neither filtering nor decomposing has been applied. As a consequence, spikes originating from the data rejection mechanism of the stagnation point method are present.

The three datasets must be prepared before any further analysis is performed. On basis of the results presented in the sections 2.4 to 2.6, the following procedures are recommended:

- If high-frequency components must be removed from the measured signals, the Kaiser window FIR low-pass filter must be used; in order to include frequencies up to 4P in the filtered time series, the upper edge of the pass band must be 2.5 Hz and the transition band must have a width of 0.5 Hz,
- If noise is to be removed from the data, the coherent or deterministic component of the measured signals must be determined.

Furthermore, it is recommended

- To use 'coherent, Kaiser filtered' data if the instantaneous values of the time series of a quantity are to be considered (e.g. power spectra, coherence function, or transfer function), and
- To use 'deterministic, raw' data if the average values of a quantity are to be considered (e.g. normal force curves, or azimuthal averages).

Finally, the enhancement is shown which is obtained by preparing the three selected data files along these guidelines. Figure 3-27 presents the normal force curve as obtained by conditionally averaging the 'deterministic, raw' time series of c_n and α against the angle of attack. The slope of this curve is of the order 0.1 1/deg for angles of attack up to 10°, and gradually decreases to about zero in the interval from 10° to 23°. Figure 3-28 presents plots of the original instantaneous 'not-decomposed, raw' realisations of c_n and α, as obtained from records with a duration of 3 s. This figure shows that the shape of the 'not-decomposed, raw' loops is convex in the linear and the near stall region. Above stall, on the other hand, these loops are horizontally elongated. The decomposing procedure thus has given more realistic data.

3.8 Conclusion

On basis of an analysis of the effect of pre-processing on the ECN aerodynamic field data, three datasets have been selected for further analysis. These datasets are 'raw' in the sense that pre-processing has not been applied. Before any further analysis is applied these datasets must be pre-processed. To this end guidelines have been specified.

It must however be noted that in these investigations it has been assumed that the stagnation point method (giving angle of attack and effective wind speed) is worthwhile, and the flaws in this method have been taken for granted.

3.9 References

[3-1]
Brand A.J., Dekker J.W.M., De Groot C.M. and Späth M., 1996,
Overview of aerodynamic measurements on an Aerpac 25WPX wind turbine
blade at the HAT25 experimental wind turbine (fourth quarter 1995), ECN -
Renewable Energy, Report DE-Memo-96-014.

[3-2]
Brand A.J., Dekker J.W.M., De Groot C.M. and Späth M., 1997,
Overview of aerodynamic measurements on an Aerpac 25WPX wind turbine
blade at the HAT25 experimental wind turbine (first and second quarter 1996),
ECN - Renewable Energy, Report DE-Memo-96-044

[3-3]
Brand A.J., Dekker J.W.M., De Groot C.M. and Späth M., 1996,
Aerodynamic field data form the HAT25 experimental wind turbine - Contri-
bution to the EC/NOVEM project 'Dynamic Stall and Three-dimensional Ef-
fects', ECN - Renewable Energy, Report ECN-C--96-037

[3-4]
Montgomerie B.O.G., Brand A.J., Bosschers J. and Van Rooij R.P.J.O.M.,
1997, Three-dimensional effects in stall, ECN - Renewable Energy, Report
ECN-C--96-079

[3-5]
Brand A.J., 1996, ECN progress report Work Package #1 EC 'Stallvib' project
- Actions M-1, M-2 and M-4, ECN - Renewable Energy, Report DE-Memo-96-
045

[3-6]
Brand A.J., 1997, Second ECN progress report Work Package #1 EC 'Stallvib'
project - Actions M-1, M-4 and M-5, ECN - Renewable Energy, Report DE-
Memo-97-034

[3-7]
Schepers J.G. (ed.), 1997, Final report of IEA Annex XIV: Field Rotor-
Aerodynamics ECN - Renewable Energy, Report ECN-C--97-027

3.10 Figures

```
+-------------------------------------------------------------------------+
|                          PHYSICAL QUANTITIES                            |
|                                                                         |
| pressures              ref press   rotor speed   rotor azimuth   etc    |
+-------------------------------------------------------------------------+
    | | |               |           |             |               |
+---+-+-+---------------+-----------+-------------+---------------+-------+
| |   | | |             |           |             |               |      |
| | +-----------------------------------------------------------------+  | |
| | |                    DATA ACQUISITION                             |  | |
| | |                                                                 |  | |
| | | +-------------------------+  +----------------------------+     |  | |
| | | | Time series of pressure difference | | Time series of additional signals | |  | |
| | | | (1) at three rotor blade sections  sync e.g. rotor speed          | |  | |
| | | | (2) at one velocity probe          | |     rotor azimuth          | |  | |
| | | +-------------------------+  +----------------------------+     |  | |
| | |             |                            |                      |  | |
| | +-------------+----------------------------+----------------------+  | |
| |               +----------------------------+                         | |
| |                            ||                                        | |
| |                           \||/                                       | |
| |                            \/                                        | |
| | +-----------------------------------------------------------------+  | |
| | |                    DATA REDUCTION                               |  | |
| | |                                                                 |  | |
| | |    +--------------------------------------------+               |  | |
| | |    | Pre-processing (optional):                 |               |  | |
| | |    | Filtering of measured data                 |               |  | |
| | |    | (a) three-point median filter              |               |  | |
| | |    | (b) first-order Butterworth filter         |               |  | |
| | |    +--------------------------------------------+               |  | |
| | |                            ||                                   |  | |
| | |                           \||/                                  |  | |
| | |                            \/                                   |  | |
| | |    +--------------------------------------------+               |  | |
| | |    | Processing:                                |               |  | |
| | |    | Derivation of aerodynamic quantities       |               |  | |
| | |    | e.g. compensated pressure differences      |               |  | |
| | |    |         stagnation angles                  |               |  | |
| | |    |         stagnation pressures               |               |  | |
| | |    |         probe inflow angles                |               |  | |
| | |    |         probe 'dynamic pressures'          |               |  | |
| | |    |         normal and tangential force coefficients |         |  | |
| | |    |         non-dimensional pressure distributions  |          |  | |
| | |    +--------------------------------------------+               |  | |
| | |                            ||                                   |  | |
| | |                           \||/                                  |  | |
| | |                            \/                                   |  | |
| | |    +--------------------------------------------+               |  | |
| | |    | Post-processing:                           |               |  | |
| | |    | Manipulation of aerodynamic quantities     |               |  | |
| | |    | (a) Additional filtering (optional)        |               |  | |
| | |    |     (1) three-point median filter          |               |  | |
| | |    |     (2) first-order Butterworth filter     |               |  | |
| | |    | (b) Outlier removal (optional)             |               |  | |
| | |    | (c) Presentation of aerodynamic quantities |               |  | |
| | |    |     e.g. (1) single realisations           |               |  | |
| | |    |          (2) average and st. dev. of quantity |            |  | |
| | |    |               - over time                  |               |  | |
| | |    |               - binned against angle of attack |           |  | |
| | |    |               - binned against rotor azimuth  |            |  | |
| | |    +--------------------------------------------+               |  | |
| | |                            ||                                   |  | |
| | +-----------------------------------------------------------------+  | |
| |                            ||                                        | |
| |                           \||/                                       | |
| |                            \/                                        | |
| | +-----------------------------------------------------------------+  | |
| | |                       ASSESSMENT                                |  | |
| | |                                                                 |  | |
| | |     Step #1: Quality                                            |  | |
| | |     Step #2: Statistical overview                               |  | |
| | |     Step #3: Error analysis                                     |  | |
| | +-----------------------------------------------------------------+  | |
| |                            ||                                        | |
| |                            ||                                        | |
+-+------------------------------------------------------------------------+
                             ||
                            \||/
                             \/
+-------------------------------------------------------------------------+
|                          APPLICATION                                    |
+-------------------------------------------------------------------------+
```

Figure 3-1 An outline of the data handling in the ECN aerodynamic field meas-urements
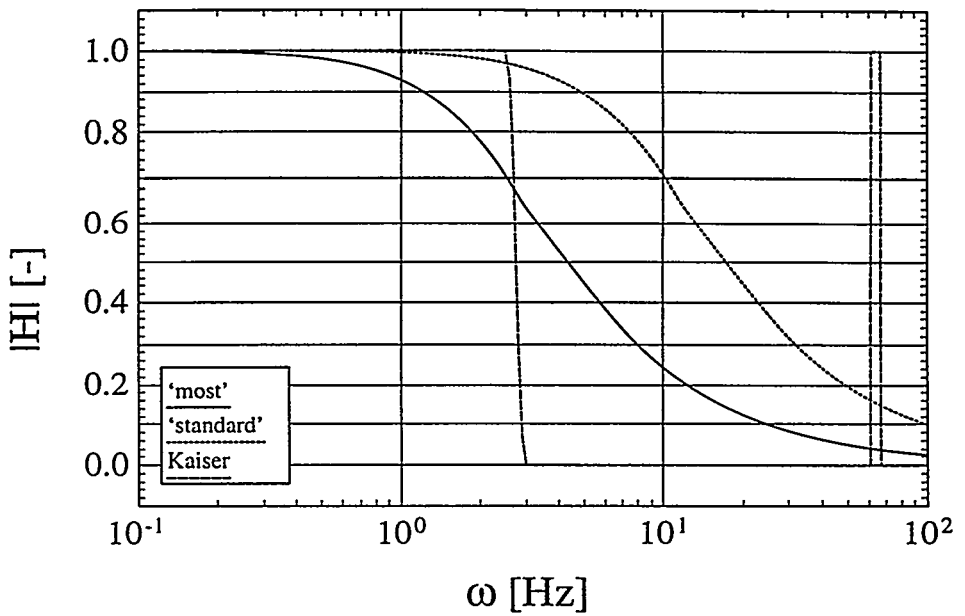
Figure 3-2 Amplitude of the transfer function of the two first-order Butterworth and the Kaiser window low-pass filters

h215397, 80% station
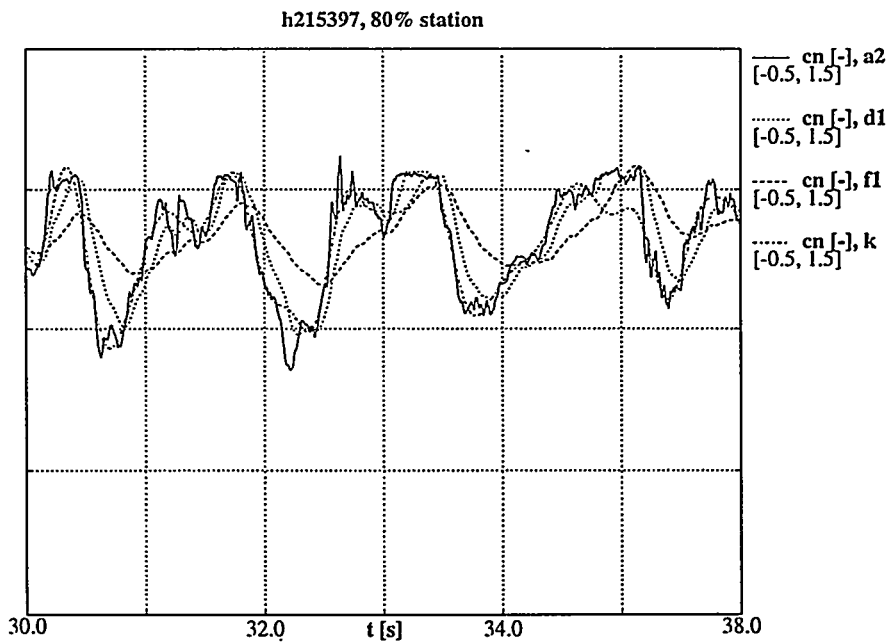
Figure 3-3 Part of the c_n time series: raw data (a2) plus standard (d1), 'most' (f1) and Kaiser (k) filtered data.

h215397, 80% station
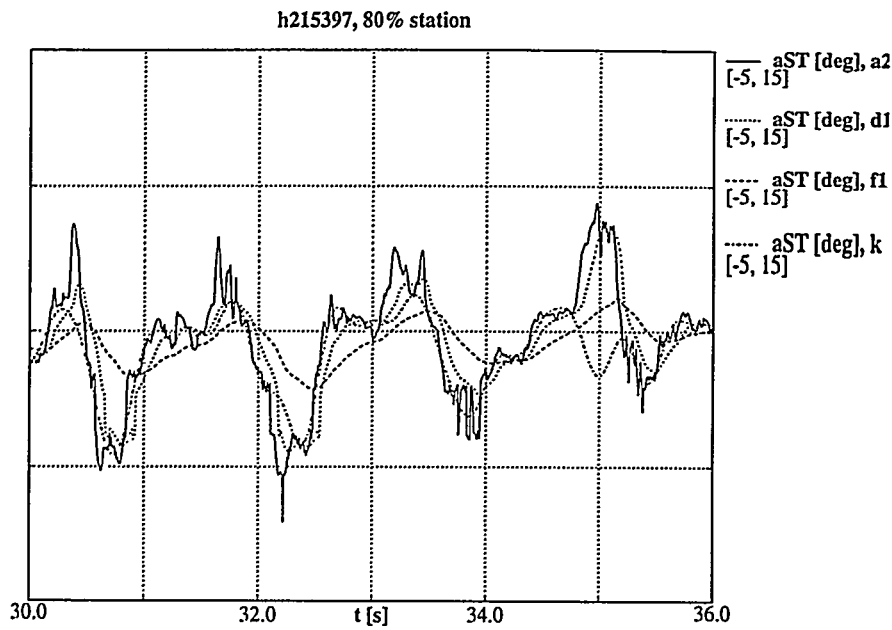
Figure 3-4 Part of the α time series: raw data (a2) plus standard (d1), 'most' (f1) and Kaiser (k) filtered data.

h215397, 80% station
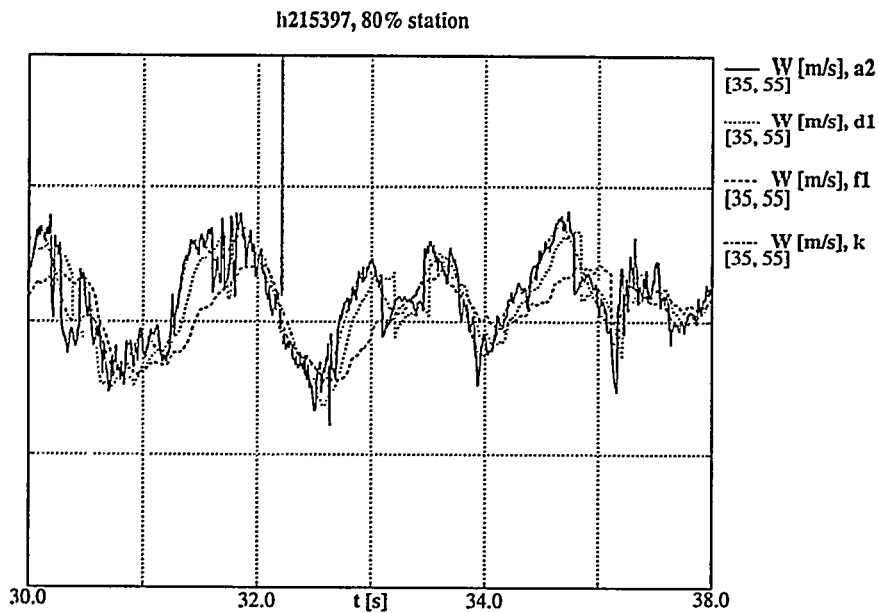
Figure 3-5 Part of the W time series: raw data (a2) plus standard (d1), 'most' (f1) and Kaiser (k) filtered data
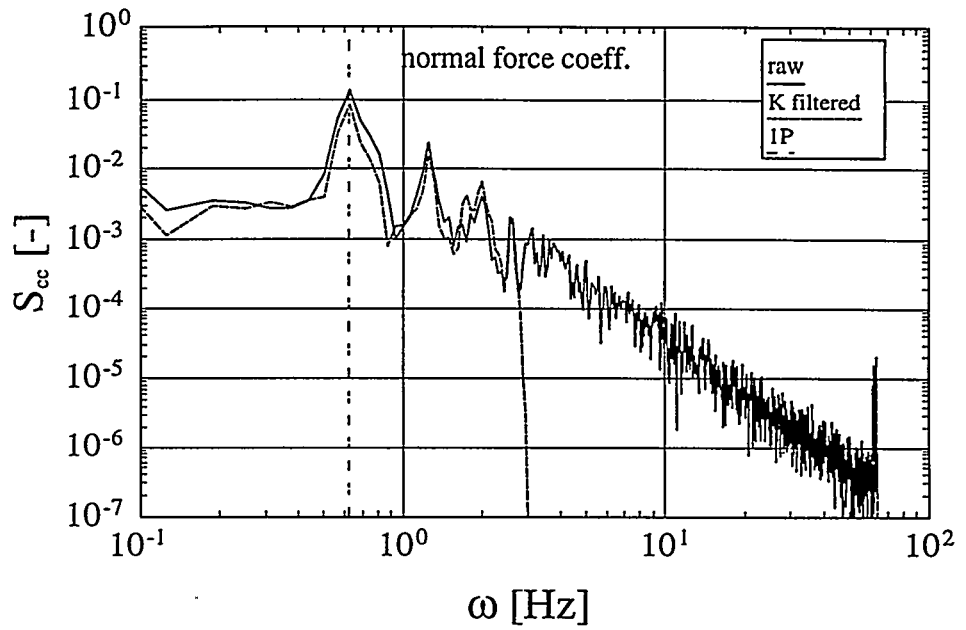
Figure 3-6 Power spectrum of the not-decomposed c_n time series, without and with application of the Kaiser filter
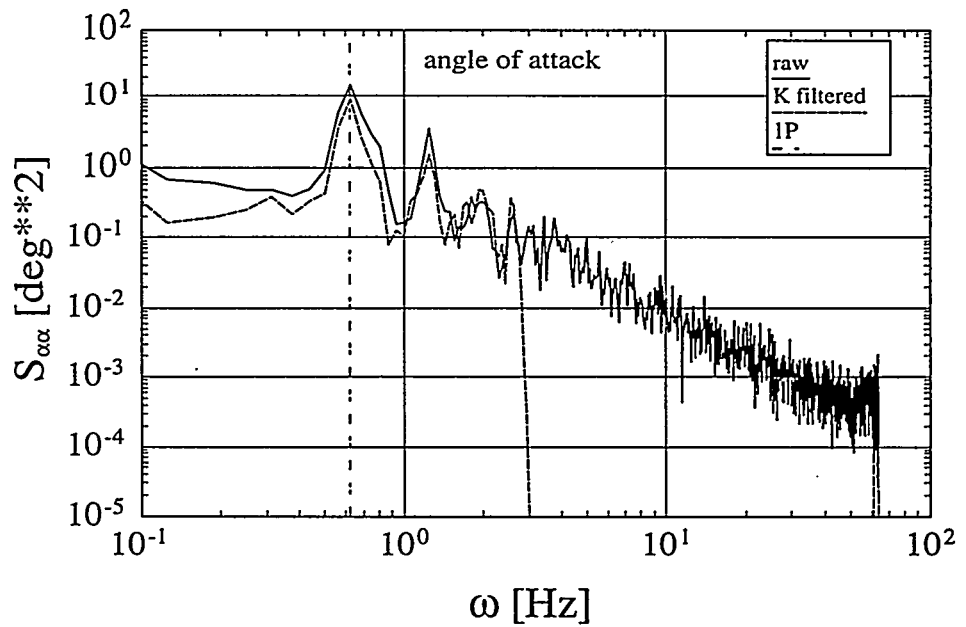
Figure 3-7 Power spectrum of the not-decomposed α time series, without and with application of the Kaiser filter
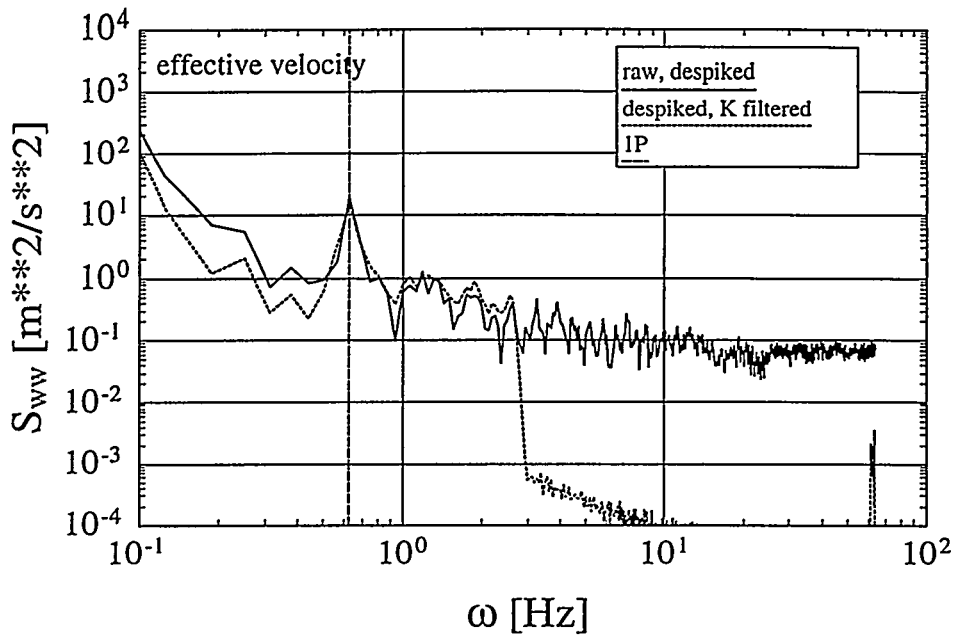
Figure 3-8 Power spectrum of the not-decomposed W time series, without and with application of the Kaiser filter.
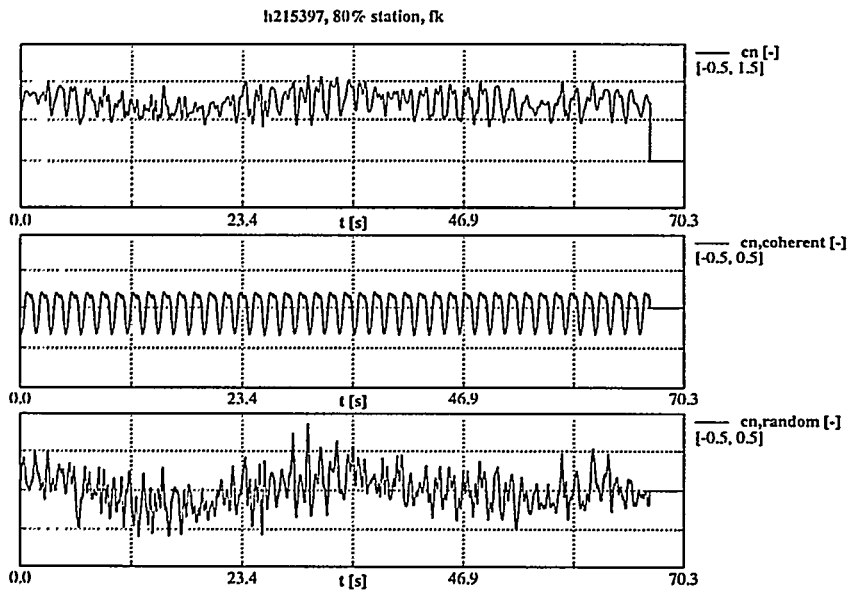
Figure 3-9 Kaiser filtered time series of C_n: not-decomposed data, coherent component and random component.
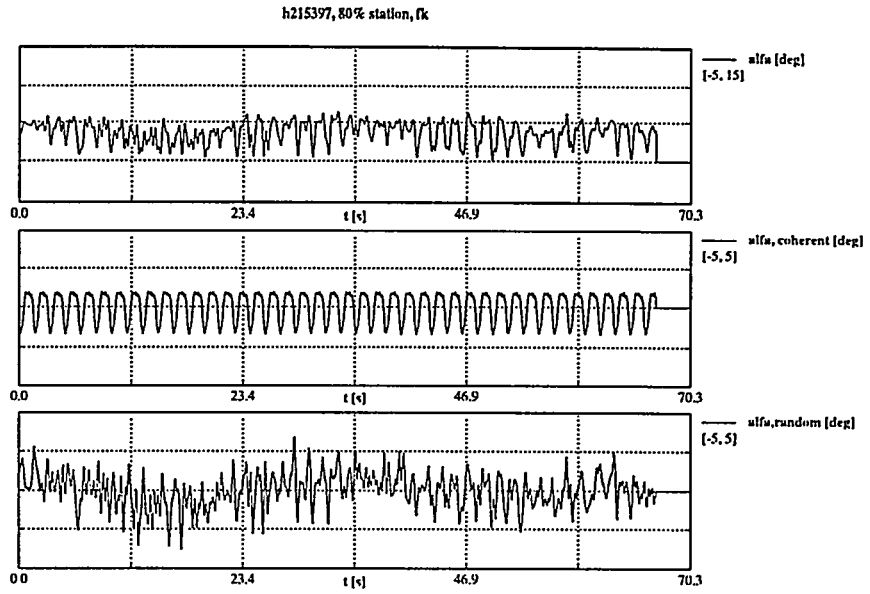
Figure 3-10 Kaiser filtered time series of α: not-decomposed data, coherent component and random component.
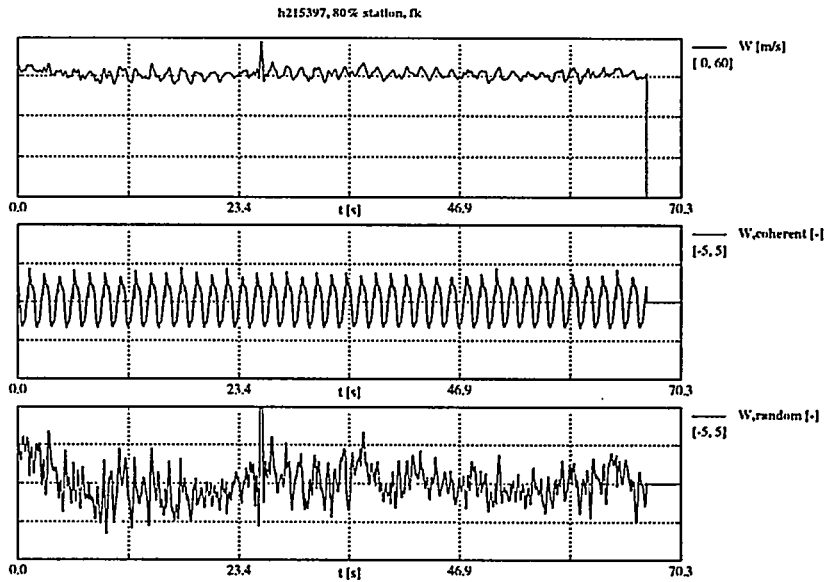
Figure 3-11 Kaiser filtered time series of despiked W: not-decomposed data, coherent component and random component.
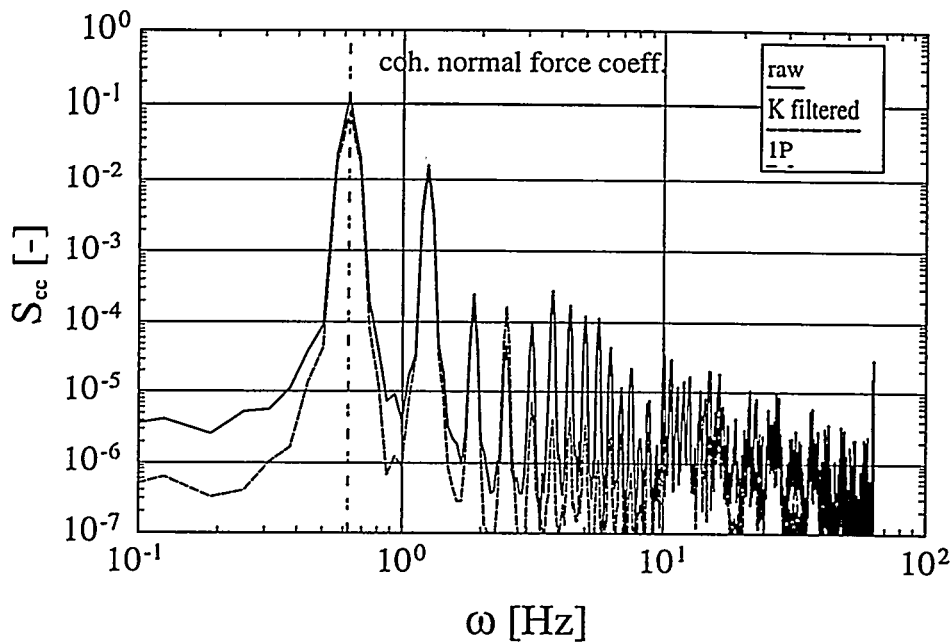
Figure 3-12 Power spectrum of the coherent component of the c_n time series, without and with application of the Kaiser filter.
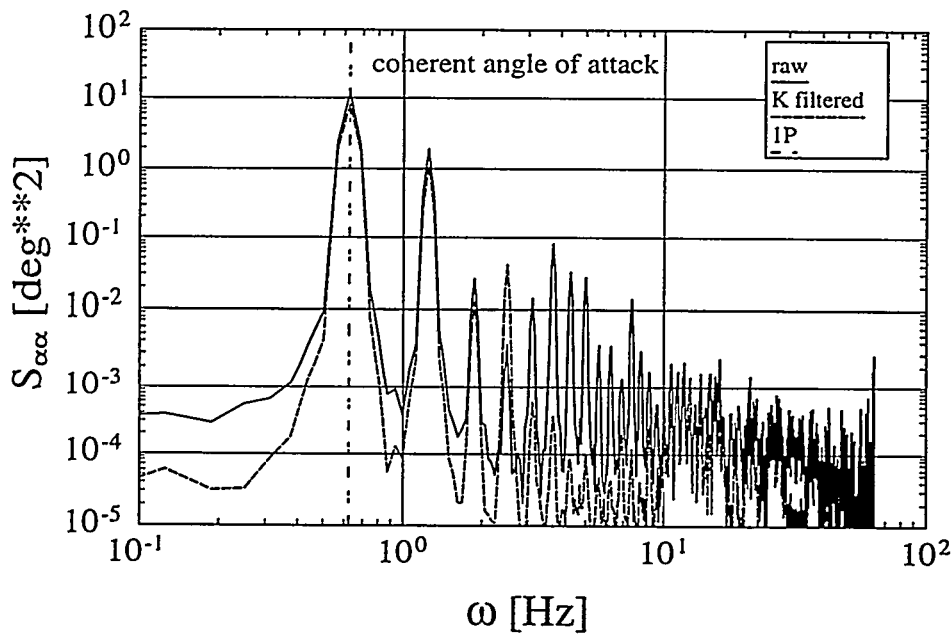
Figure 3-13 Power spectrum of the coherent component of the α time series, without and with application of the Kaiser filter.
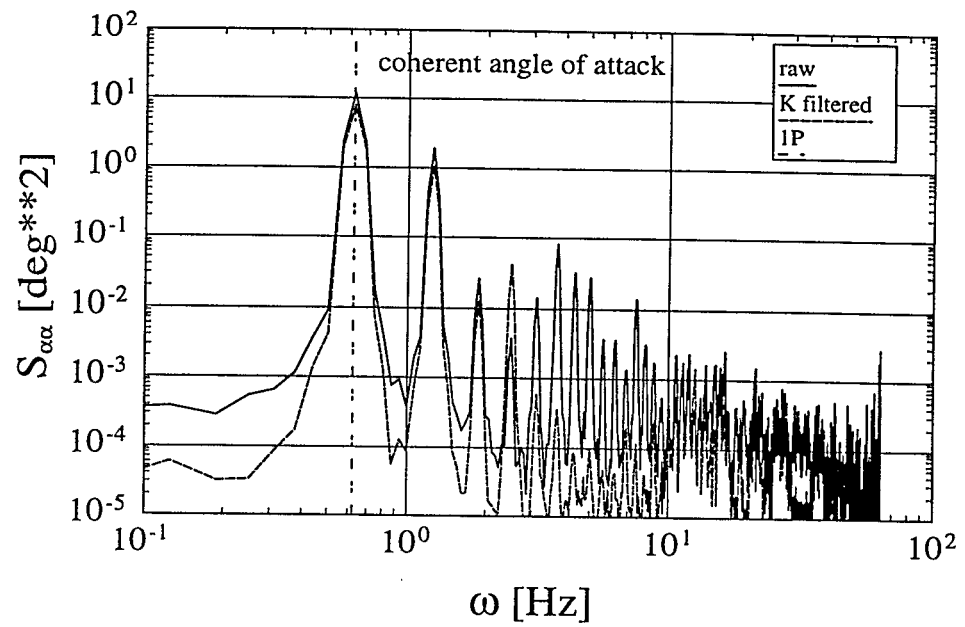
Figure 3-14 Power spectrum of the coherent component of the W time series, without and with application of the Kaiser filter.
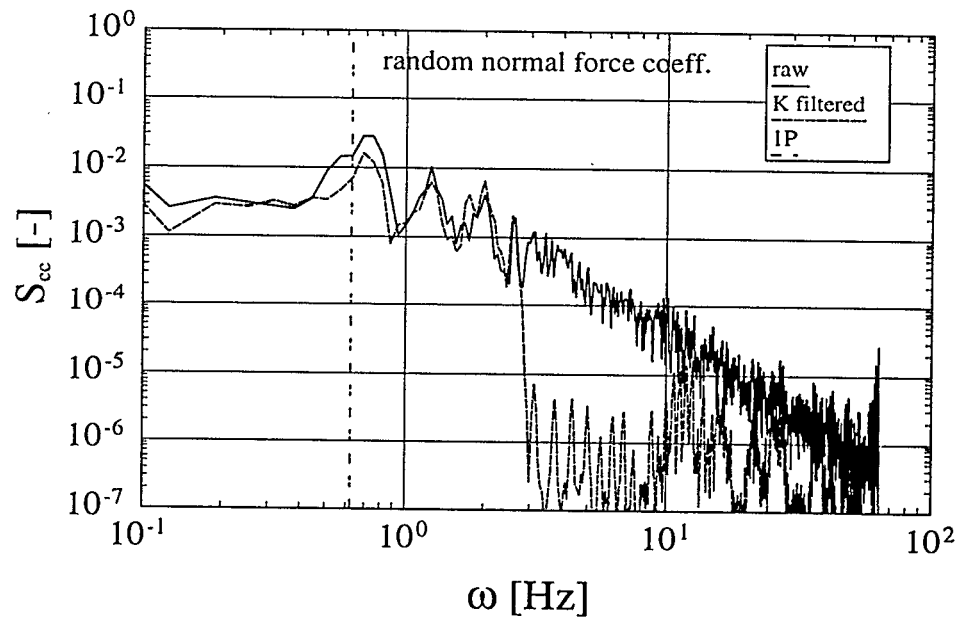
Figure 3-15 Power spectrum of the random component of the c_n time series, without and with application of the Kaiser filter.
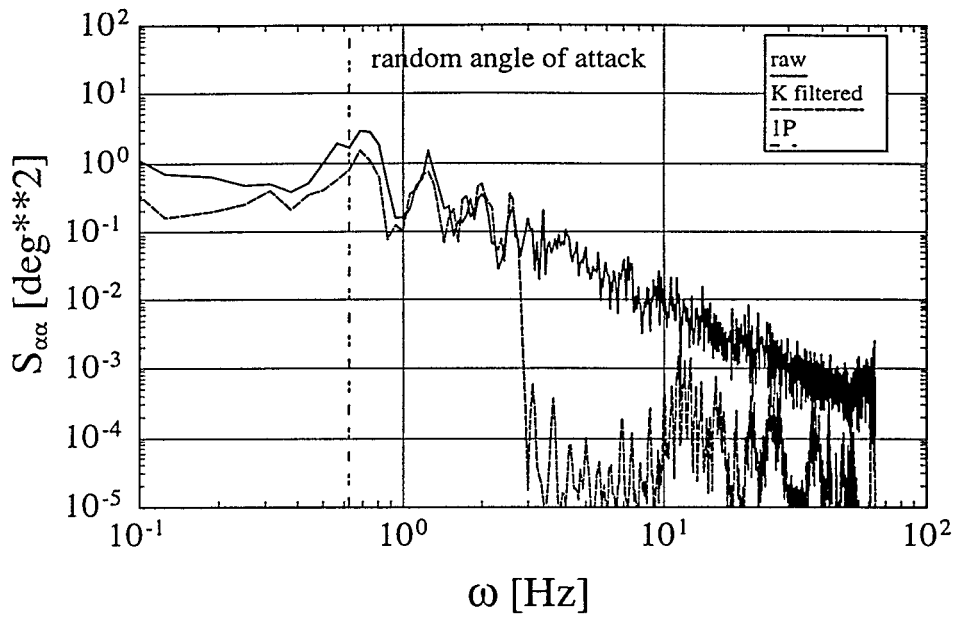
Figure 3-16 Power spectrum of the random component of the α time series, without and with application of the Kaiser filter.
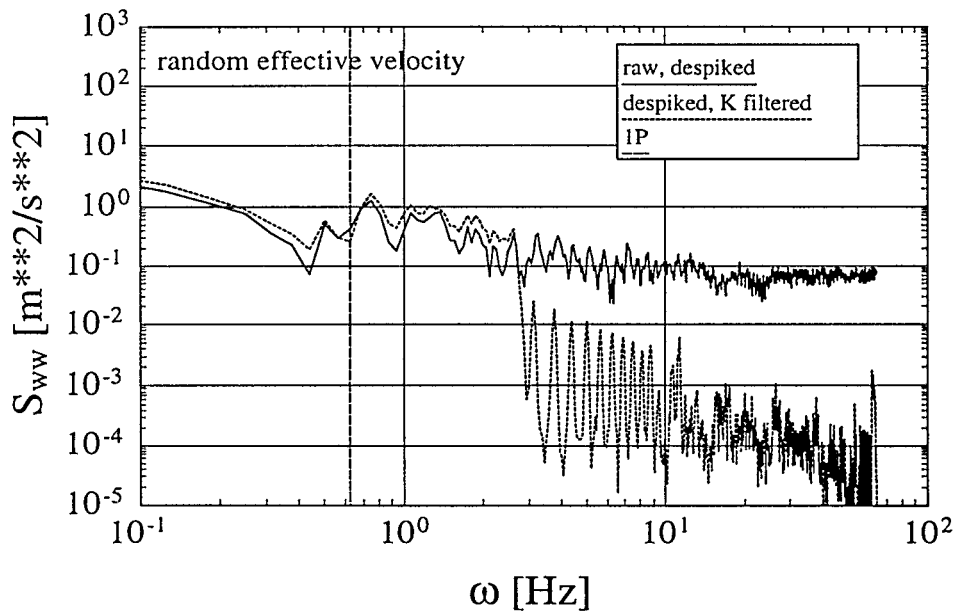
Figure 3-17 Power spectrum of the random component of the despiked W time series, without and with application of the Kaiser filter.
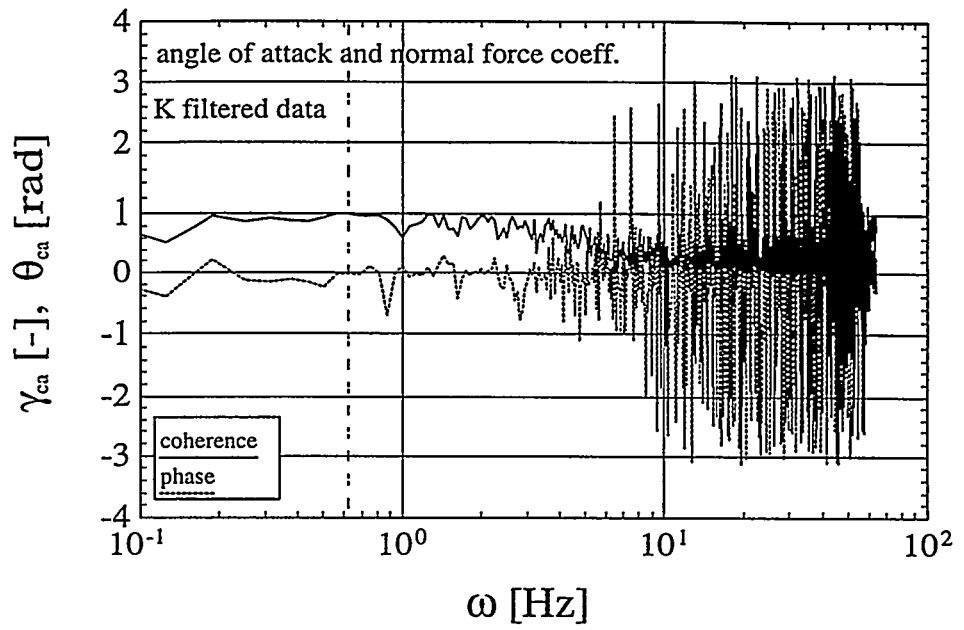
Figure 3-18 Coherence function and phase spectrum of the not-decomposed
Kaiser filtered c_n and α time series.
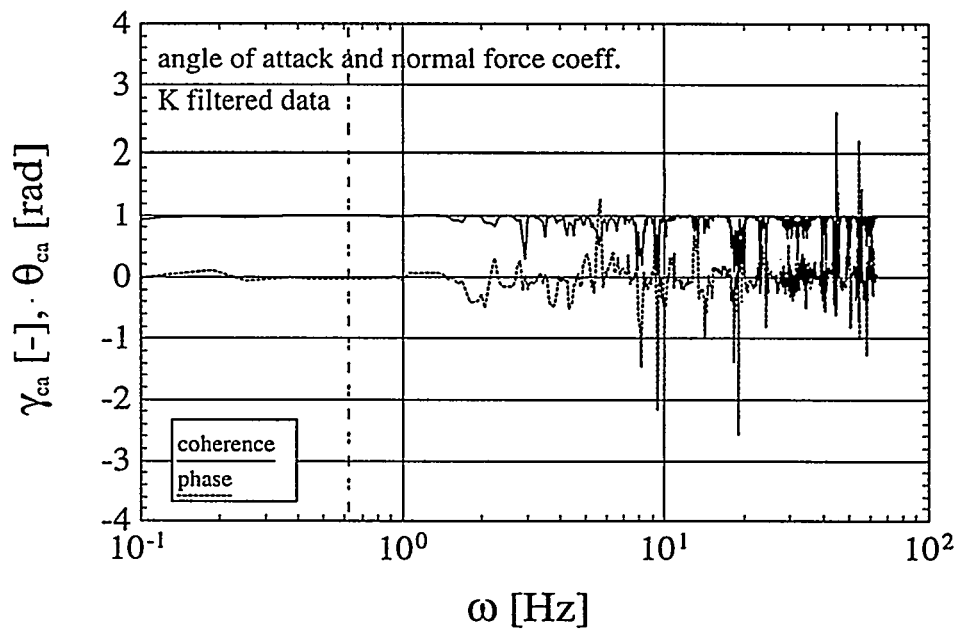
Figure 3-19 Coherence function and phase spectrum of the coherent component
of the Kaiser filtered c_n and α time series.
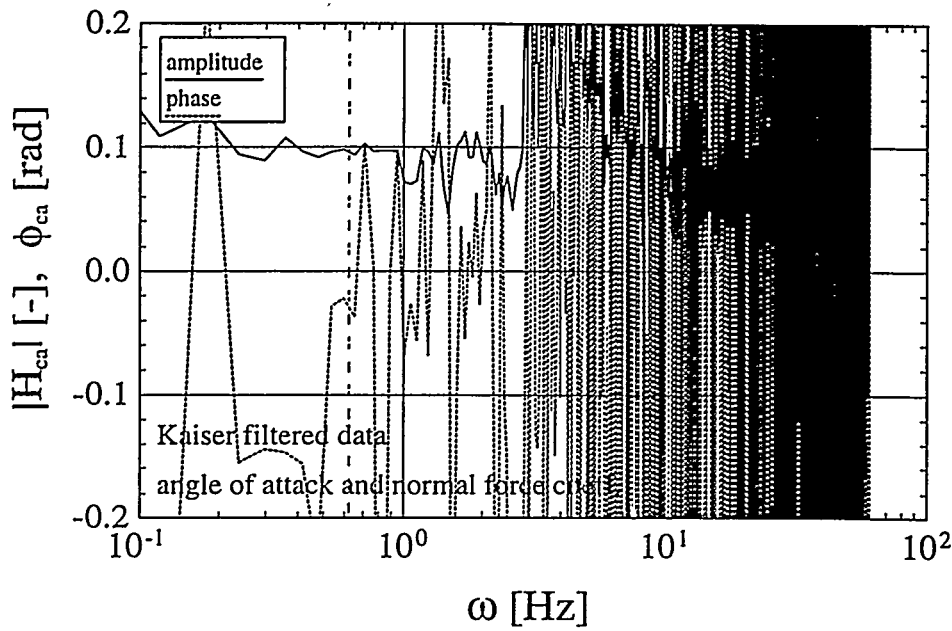
Figure 3-20 Amplitude and phase of the transfer function for the not-decomposed Kaiser filtered c_n and α time series.
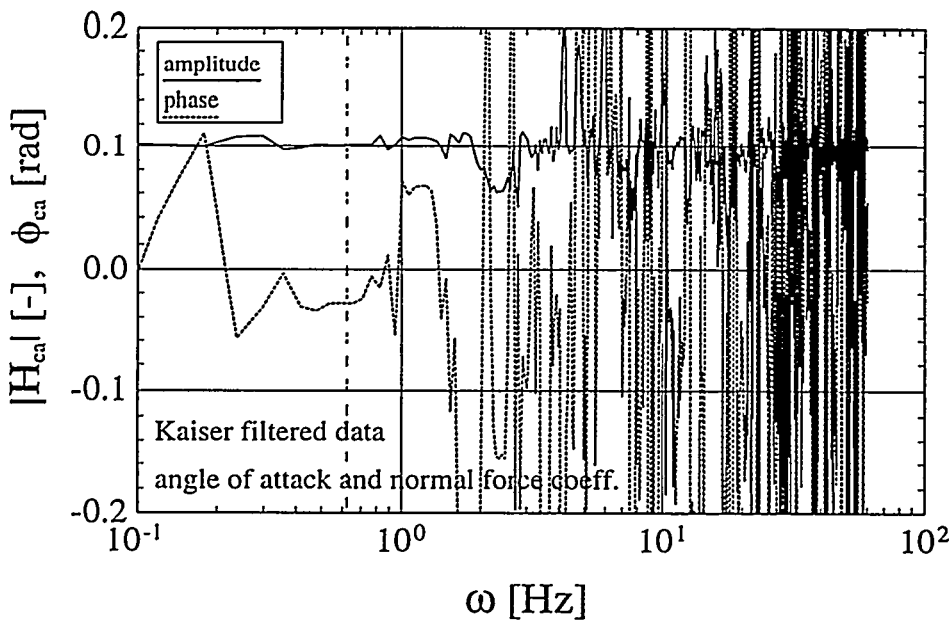
Figure 3-21 Amplitude and phase of the transfer function for the coherent components of the Kaiser filtered c_n and α time series.
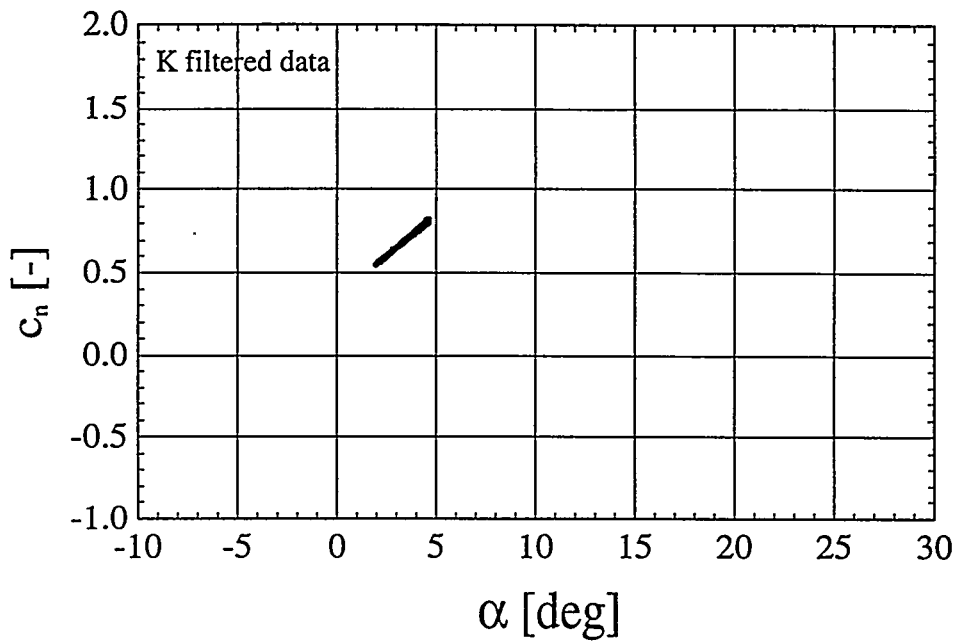
Figure 3-22 Plot of the instantaneous deterministic values of the Kaiser filtered c_n and α time series.
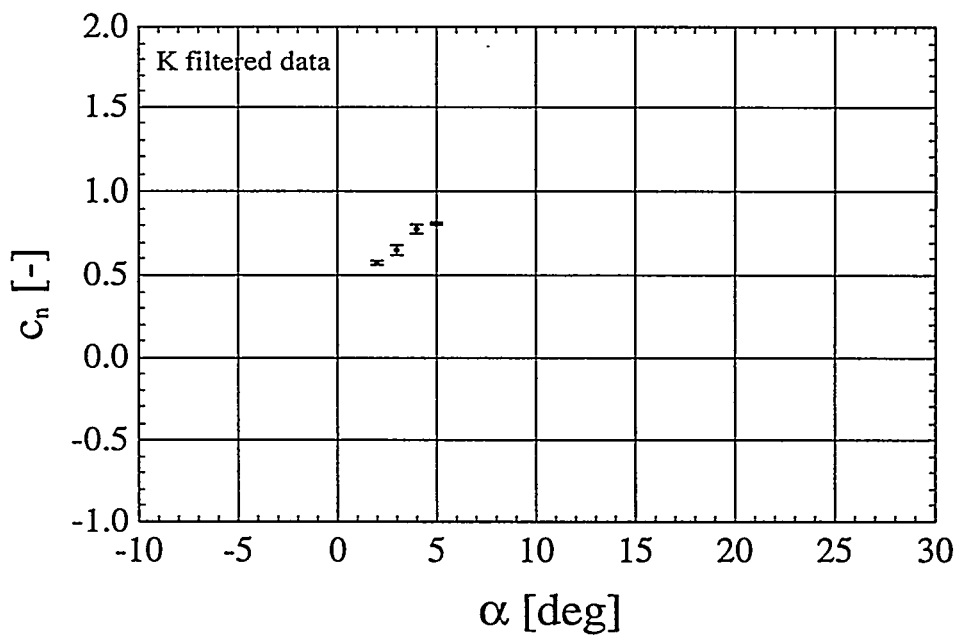
Figure 3-23 Normal force curve based on the instantaneous deterministic values of the Kaiser filtered c_n and α time series.
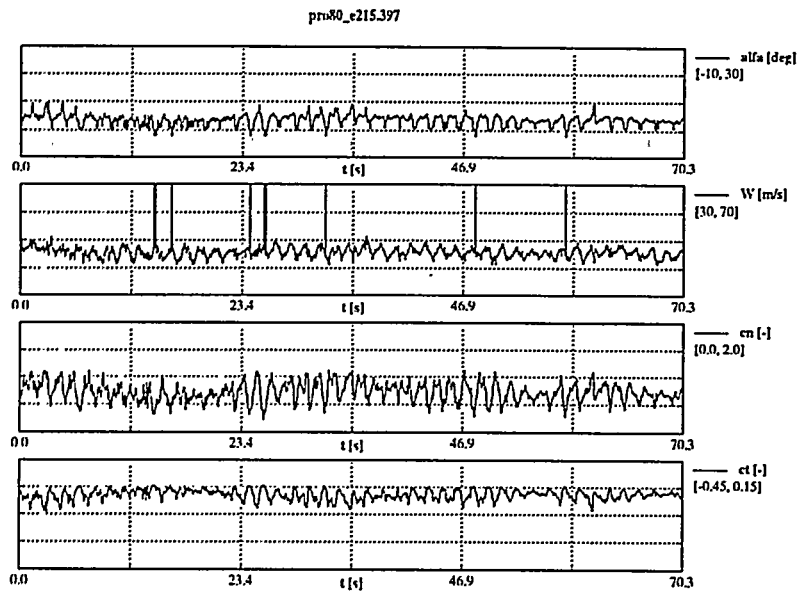
pro80_e215.397

Figure 3-24 Content of datafile 'pro80_e215.397': time series of α, W, c_n and c_t.
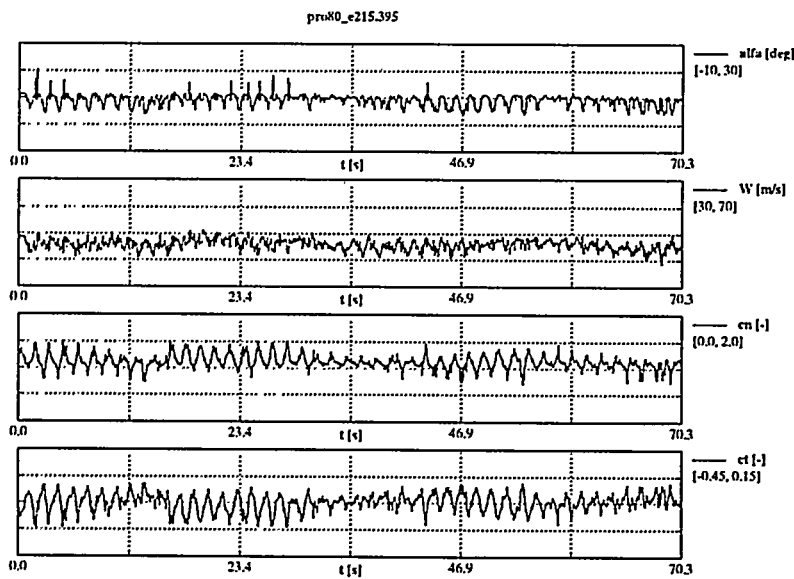
pro80_e215.395

Figure 3-25 Content of datafile 'pro80_e215.395': time series of α, W, c_n and c_t.
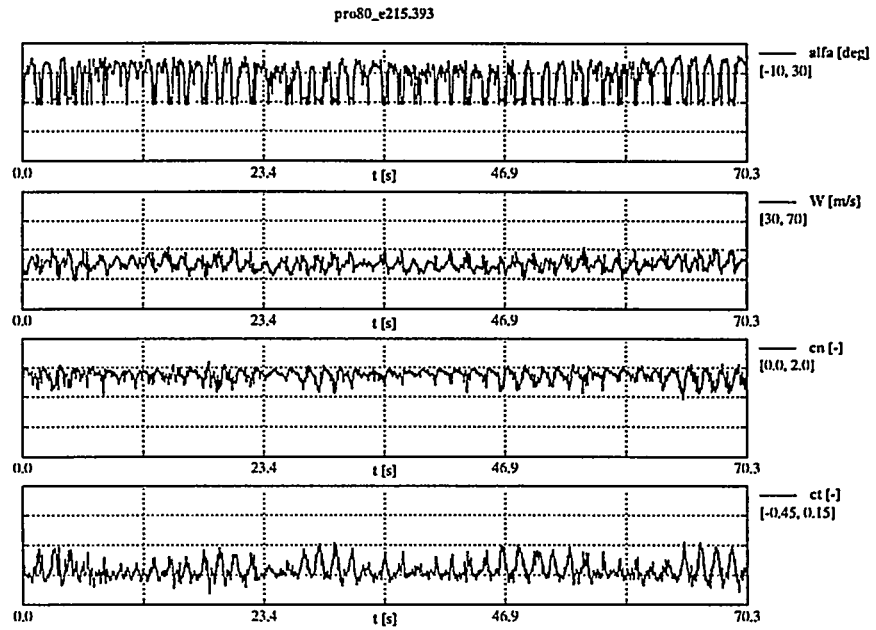
pro80_e215.393

Figure 3-26 Content of datafile 'pro80_e215.393': time series of α, W, c_n and c_t.
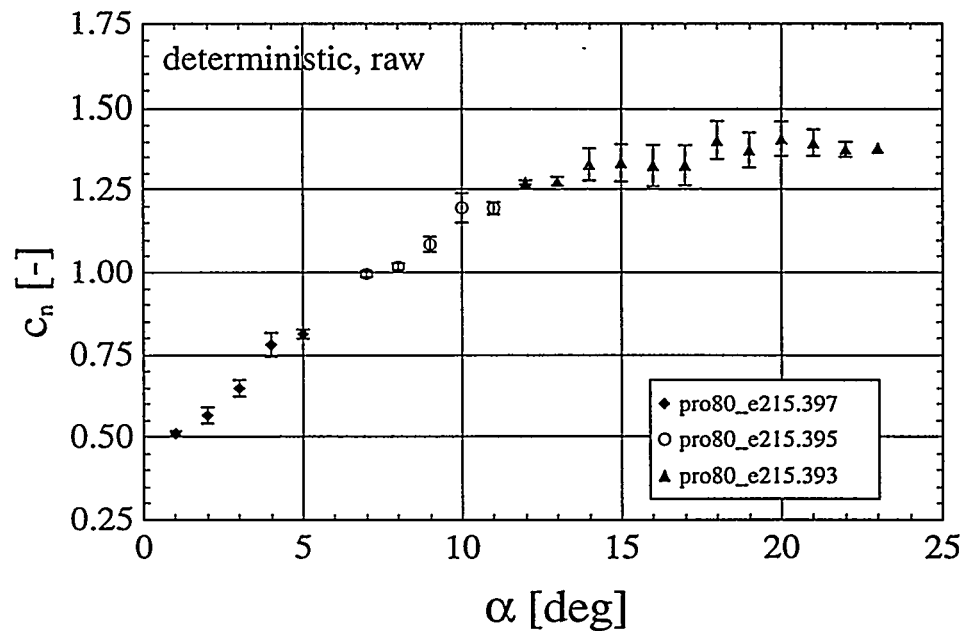
Figure 3-27 Normal force curve based on the instantaneous deterministic values of the not-filtered c_n and α in the three datafiles.
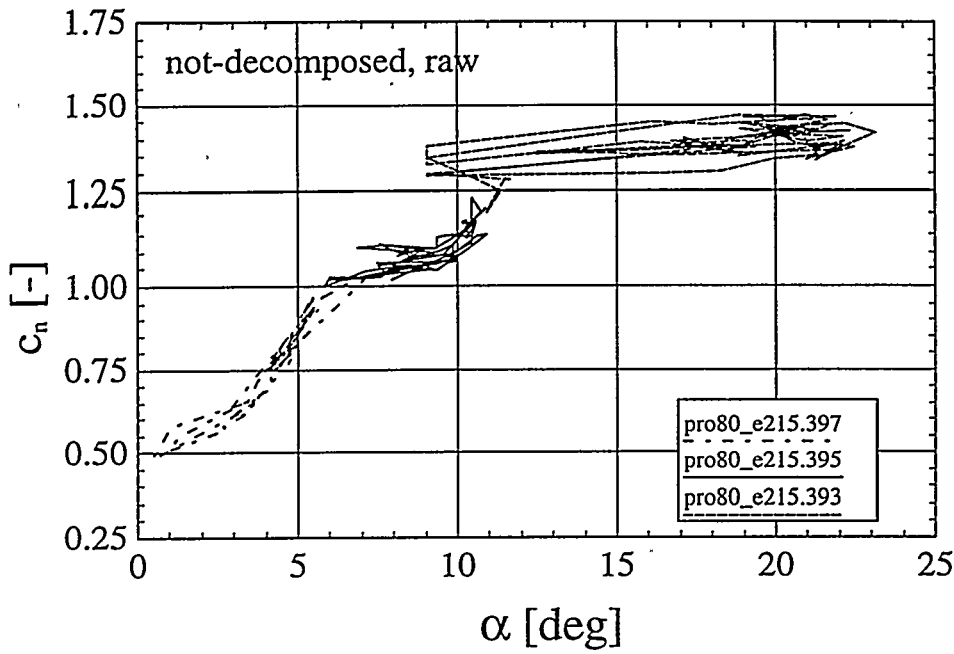
Figure 3-28 Plot of three not-decomposed 3 s records of not-filtered c_n and α.

Table 1: Statistics of the datafile 'pro80_e215.397'

	α [deg]	W [m/s]	c_n [-]	c_t [-]
average	3.7	50.9	0.72	-0.042
st. deviation	1.8	66.6	0.17	0.028
minimum	-2.1	41.0	0.23	-0.145
maximum	10.1	*	1.12	0.011

Table 2: Statistics of the datafile 'pro80_e215.395'

	α [deg]	W [m/s]	c_n [-]	c_t [-]
average	9.2	45.9	1.12	-0.147
st. deviation	2.0	1.9	0.13	0.048
minimum	3.8	38.4	0.70	-0.297
maximum	20.4	51.6	1.52	-0.036

Table 3: Statistics of the datafile 'pro80_e215.393'

	α [deg]	W [m/s]	c_n [-]	c_t [-]
average	18.3	45.0	1.36	-0.276
st. deviation	5.1	1.9	0.10	0.042
minimum	9.1	39.3	0.95	-0.395
maximum	26.4	50.8	1.61	-0.135

4 Data from Delft

4.1 Introduction

This chapter describes the applied methods for the analyses of the Delft field rotor data and the results. The data was digital filtered with different adjusted low pass filters, even below the rotational rotor frequency (1_P). Such a very low pass filter frequency can make visible basic trends (steady aerodynamics) in the measurements. From these filtered data, power spectra functions, coherence functions and transfer functions have been determined between the most relevant aerodynamic parameters. This has been performed for the 70% radial spanwise station of the rotor blade, because it was considered as the most relevant station to investigate the stall induced vibrations on the rotor blade.

4.2 Rotor research facility, blade and instrumentation

Bruining 1997 [4-1] gives a detailed description of the facility, blade and instrumentation.

4.3 Data processing and data analyses

Common Stallvib processing methods

A *common data processing method* was agreed for a consistent evaluation of the field rotor measurements by the four participants, which have contributed to the experimental part of the project. From all the available experimental data, a few data sets are selected, which are typical for the operational conditions. The measurements have been processed in such a way that they are directly suitable in the engineering models, which include the *stall hysteresis* effects.

For the common processing, Risø distributed to the participants their Data Analysis Package for Spectral Analysis (*DAP*). Madsen, 1987 [4-6] describes the background and use of the DAP software. After competitive calculations of the DAP software with the signal processing toolbox of *Matlab*, the Delft University selected for further processing the Matlab software, Krauss [4-4] instead of the DAP software. Both software packages generate the same results for a selected test measurement campaign. The Matlab software offers additional features to filter, to plot the data, and to automate the data processing with scripts.

The following data analyses have been performed:

- Power Spectra Density (PSD) of the angle of attack α measured with the three-hole flow direction probe, the relative velocity w at the 70% span station, and the normal force coefficient c_n
- Coherence function between α and the normal force coefficient c_n
- Transfer function between α and the normal force coefficient c_n

The *transfer function* characterizes the relation between two data channels as a function of the frequencies in the signal. This relation is made visible as the behaviour of the *magnitude (amplitude)* and *phase*, as function of the fre-

quency. When the phase differs from zero, the *loops* become visible in a x vs. y plot.

Risø determines for their *stall hysteresis model* the so-called f, g and h parameters. The assumption is that stall hystereris loops can be derived from the quasi steady $c_n(\alpha)$ curve and terms based on the derivatives of α and the relative velocity w. The f, g, and h parameters are functions of α, f is respectively related to the first derivative of α, g is related to the second derivative of α and h is finally related to the first derivative of w. This method is used to parameterise the dynamic loop behaviour of α vs. c_n; see. Petersen, [4-7] and Petersen and Madsen, 1997 [4-8].

Especially the phase relation is sensitive for the response of the pressure instrumentation equipment. The length of the tubes of each pressure tap is the same to insure the same response for each pressure tap. The signals of the three-hole flow direction probe were exactly delayed one sample to correct for the travel time between the probe head and the rotating blade. The probe head sees the flow earlier than the pressure taps.

Processing steps Delft data

The following four main steps were performed to process the Delft data:

1. Data acquisition with the special designed *W4* software at every six degrees azimuth angle. These six-degree measurements contained already values that were averaged from data samples, which were obtained at 333 Hz sampling rate within one six degrees azimuth interval. In addition, the outliers in the data are removed here. No other filtering is performed. The raw data is stored in binary format and can be replayed with several options for selecting and analysing.

2. Conversion of the raw binary data to ASCII tables in time series format by the *WC* program. The dynamic pressure, which is used for the normalisation of the pressures, is calculated by linear interpolation from the readings of two blade pitot probes. In this step is also done the altitude harmonic correction on the pressure data and the calculation of the aerodynamic coefficients by direct integration of the pressure distribution.

3. Calculation of the stagnation point angle-of-attack, angle-of-attack from the three-hole probe with two special separate Fortran programs by using the ASCII tables as input. The probe angle-of-attack is corrected for the two-dimensional upwash and three-dimensional induced velocities. A geometrical correction is made for the difference in radial position of the probe head and pressure taps. The probe data is delayed one sample to correct for the travel time, because the probe head sees earlier the air than the pressure taps. Results are stored in separate ASCII tables.

4. Data filtering with the Matlab signal toolbox routines. The ASCII tables of the previous step are the input. Low pass filtering and combination with 1_P band suppression were done in this step as well as the production of several plots and resampling of the data to 25 Hz. This was automated with Matlab script files.

Settings for Power Spectrum Density, coherence function and transfer function calculations

Every Delft campaign contains data of approximately 50 rotor revolutions. One rotor revolution holds 60 samples of each data channel, collected at every 6-degree azimuth angle of the instrumented blade. This makes about 3000 samples for each data channel. Due to the data sampling at every 6-degree azimuth angle, the sample frequency depends on the rotational rotor speed. The sample frequency was determined from the time stamps of the data samples. The sample frequency expressed in Hz is very close to the rotational speed in rpm, because of the 60 samples in revolution. The *PSD* (Power Spectrum Density) was calculated with a FFT (Fast Fourier Transform) length of 512 samples, an overlap of 256 samples, and a hanning window. The hanning window describes how the overlap is made, see also Krauss, 1994 [4-4].

Before the PSD calculation, the signal is *detrended* by removal of a best straight-line fit from the signal to prevent distortion of the spectrum. The PSD are scaled in such a way that the last value of the integrated Power Spectrum corresponds with squared value of the standard deviation of the signal (Parseval's Relation). Due to gradual variation of the signals a linear detrend is necessary, removal of the mean of the signal only is not in agreement with the Parseval's Relation.

The same settings have been applied to determine the coherence function and transfer function as used for the PSD calculation.

Deterministic and stochastic signal

The data *time series* – which corresponds to one measurement campaign - were split in a *deterministic* part and a *stochastic* part. The reason to do this is that the deterministic part of the signal might be more dependent on the specific experimental setup (for example the tower shadow, yaw or wind gradient) than the stochastic part. The idea behind this decomposition of a measured signal is that one extracts the real signal (is the stochastic part) from the noise signals (is the deterministic part). The deterministic part of the signal is equivalent to the phase average, and the stochastic part is equivalent to the random component of the signal, see also Brand, 1997 [4-1].

For the Stallvib common approach, the deterministic part was constructed from the time series of the original signal by binning on the azimuthal position of the instrumented rotor blade. In this way, the original time series of the data were compressed to a time series of one rotor revolution. This very short time series of 60 samples was artificially extended to the original signal length by concatenation several times of this single 60-sample time series.

One should be aware that when the flow conditions did change during the acquisition of such a time series the data for high angles of attack and low angles of attack are both in one bin. This is normal for some time series (measurement campaigns) of the Delft data, because the wind speed increased or decreased during the measurement campaign (see Figure 4-1). The angle of attack will of course be affected by a change of the incoming wind velocity. Each measurement campaign had a nearly constant rotational rotor speed during the data sampling.

Digital data filtering

The data has been digitally filtered with different low pass frequencies to investigate the quasi-steady behaviour. The low pass filter can remove for example the higher harmonics in the signals, which is caused by yaw and wind shear.

Alternatively, the filter can remove only the higher frequencies, which originate from the unsteady wind conditions for example, if a higher cut-off frequency is selected. For the graphs presented in this chapter from the measurements only 4 Hz and 25 Hz have been used.

Special *digital filtering* techniques are possible, because of the off-line post processing process. The entire data sequence is available prior to filtering, which allows for a non-causal, *zero-phase* filtering approach of the time series. Therefore, the method filters also the time series in reversed order. For the digital filtering, the elliptical Infinite Impulse Response filter (IIR) was selected. The zero-phase filter has been implemented with help of the filtfilt function and ellip function of the Matlab Signal Processing toolbox (see Krauss 1994 [4-4]. The elliptical filter suppression is adjusted to –125dB, which reduces almost completely the signal above the low pass frequency. The applied order depends from the low pass frequency and is the maximum of what could be achieved without numerical convergence problems:

Low pass filter frequency	Filter order
0.45 1_P	8
1.5 1_P	10
2.5 1_P	12
3.3 1_P	13
3.5 1_P	14
>4 1_P	15

Table 4-1 Used filter order of digital elliptic filter for different low pass frequencies

In table Table 4-1, the filter frequency is expressed as fractions of the rotational frequency.

Band suppression filtering has been applied too to remove the 1_P component in the signal. The 1_P component may be affected by an incorrect altitude harmonic removal of the pressure signals. The final data files were digitally resampled at 25 Hz to make the data consistent with the data of the other participants.

Figure 4-2 through Figure 4-4 show the filter characteristics and filter effects upon an artificially generated test signal with a few harmonics and noise.

Concluded, digital resampled time series

Finally, the time series were resampled with the Matlab signal processing toolbox routines at 25 Hz to overcome the problems of different sampling rates in the common Stallvib approach. Remember that the original sampling rate of the Delft time series are depending on the rotational rotor speed, because only six-degree azimuth samples were collected.

The selected 25 Hz resampled measurement campaigns that have been delivered to the project are *pc060712.'94*, *pc290722.'94*, *pc380708.'94* and *pc510901.'94*. All four campaigns were sent twice: one copy was low pass filtered at 4 Hz and the other at 25Hz. In addition, pc380708.'94 was also sent with low pass filtered at 4 Hz and 1_P band suppression. The files are time series and have eight columns that containing respectively: time, blade azimuth position, wind, alfa_three-hole probe, relative velocity 70% station, c_n value, c_t value, and yaw misalignment angle.

4.4 Results 70% spanwise station

Filtered time series

The original raw signals have been filtered with the low pass elliptic filter with cut off settings of 25 Hz and 4 Hz. respectively. These two cut off settings were agreed by the project coordinator. The filter order was as high as possible, see Table 4-1. Above 25 Hz the signals contain mainly noise from the instrumentation equipment. The 4 Hz cut off frequency was considered as representative for the low frequency behavior.

No time delay correction was applied for the wind signals, which were acquired one rotor diameter upwind at the mobile tower. Time traces for the campaign *pc380708.'94* using the different filters are shown in Figure 4-5 through Figure 4-7.

Results of 25 Hz digital low pass filtered

The Power Spectrum Density (PSD) function, Figure 4-8 and Figure 4-10, shows that the dominant frequencies in the signals are at 1_P and at the higher harmonics. This is mainly caused by yaw and wind shear and the remains of the altitude harmonic in the pressure signals.

Results of 4 Hz low pass filtered

The *coherence* function
Figure 4-11 reflects the correlation between the angle of attack and the normal force coefficient c_n as function of the signal *frequency*. The function values are real numbers between 0 (no correlation) and 1(100% correlation).

The *transfer* function
Figure 4-11 function gives information about the magnitude of the lift gradient ($dc_n / d\alpha$) and the phase between the angle of attack and c_n, also as function of the signal frequency. For the steady wind tunnel case, the magnitude of the lift gradient is in the order of a 0.1 for the pre stall conditions, which corresponds with a zero normalized frequency. This can be observed for the field measurements too, with a small decreasing trend at increasing frequency. The magnitude (amplitude) function shows some kind of resonance peak at 1_P and 2P. Remember that a zero phase means that there is no hysteresis loop in the α vs. c_n plot.

Results of band suppression and 4 Hz low pass filtering

Results of this analysis are shown in Figure 4-12 through Figure 4-14. The band around 1_P was suppressed to exclude the influence of the eventual remains of the altitude harmonics in the signal. The altitude harmonics originated from the dynamic behaviour of the pressure measure equipment (transducers and tube system). This harmonic was already removed as good as possible before all filter steps. When the band around 1_P is suppressed, the phase function shows a more linear behaviour than the magnitude (amplitude) function in comparison with no 1_P-band suppression.

4.5 Symbol list

The conventions of Schepers, 1994 [4-9] and Bruining, 1997 [4-1] are followed.

4.6 References

[4-1]
Bruining, Aerodynamic Characteristics of a 10 m Diameter Rotating Wind Turbine Blade; Experimental Results from the Delft University of Technology for the "Dynamic Stall and 3D Effects Project", Delft University of Technology, IW95-084R, ISBN 90-9011126-3, September 1997

[4-2]
Brand, Second ECN progress report work package #1 EC "Stallvib" project, actions M-1,M-4 and M-5, ECN-DE Memo-97-034, August 1997

[4-3]
Brand, Second ECN progress report work package #1 EC "Stallvib" project, actions M-1,M-4 and M-5, ECN-DE Memo-97-034, August 1997

[4-4]
T.P. Krauss, L Shure, J.N. Little, Signal Processing Toolbox; For Use with Matlab, User Guide, The MathWorks Inc. USA, June 1994

[4-5]
H.A. Madsen, J.T. Petersen, Proposal for the EC Programme Non Nuclear Energy Joule 1994-1998; Prediction of Dynamic Loads and Induced Vibrations in Stall, Roskilde Denmark, March 22 1995

[4-6]
P.M. Madsen, DAP – 1, A data Analysis Package for Spectral Analysis, Version 1.2, Wind Energy Research Center, Solar Energy Research Institute Golden Colorado, draft November 87

[4-7]
J.T. Petersen, Prediction of Dynamic Loads and Induced Vibrations in Stall; First Periodic Report 01.01.1996 to 30.06.1996, Contract JOR3-CT95-0047, Riso National Laboratory, February 1996

[4-8]
J.T. Petersen (ed.), H.A. Madsen (ed.), Prediction of Dynamic Loads and Induced Vibrations in Stall (StallVib); first Twelve-monthly progress report January 1st 1996 – December 31st 1996, CONTRACT jor3-ct95-0047 (DG12-WSME), Riso National Laboratory, February 1997

[4-9]
J.G. Schepers, Reference system, terminology and conventions, to be used within the Joule II project "Dynamic Stall and 3D Effects", FFAP-A-1030, June 1994

4.7 Figures

Campaign: pc380708.'94;   Sample Frequency ca.: 70.78 Hz;   25.00 Hz dig. filter
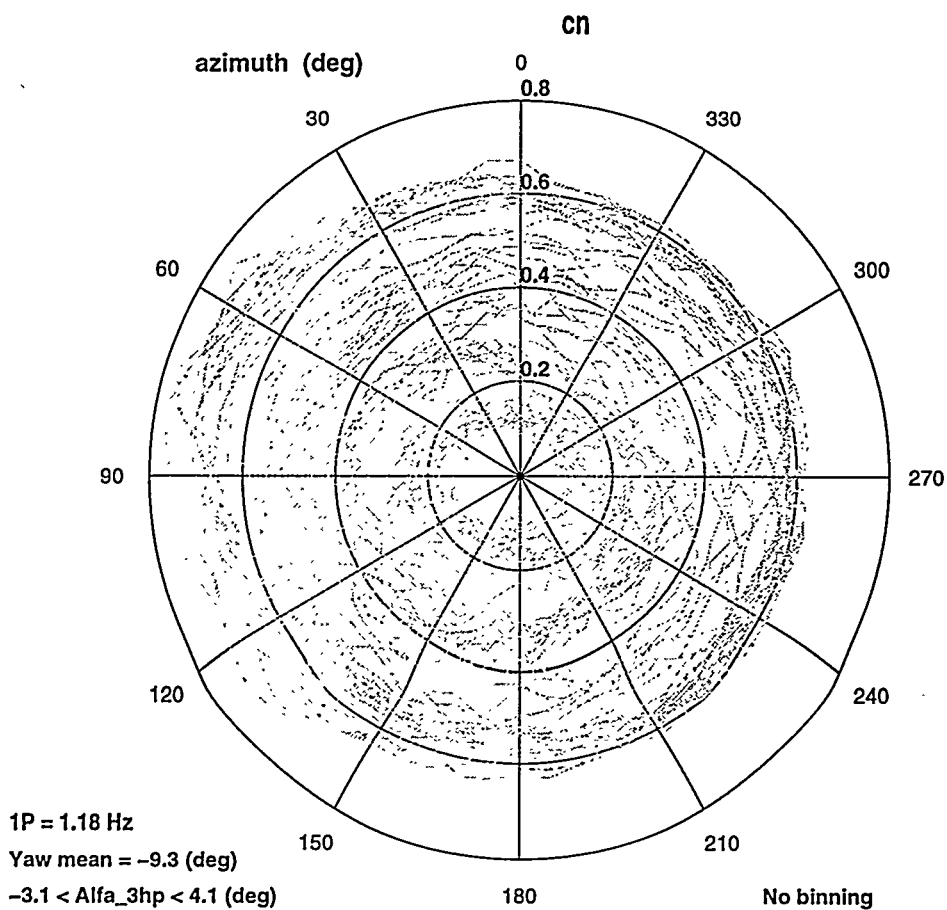
Figure 4-1 Time series of c_n, *plotted as function of the azimuthal angle, low pass filtered as 25 Hz.*
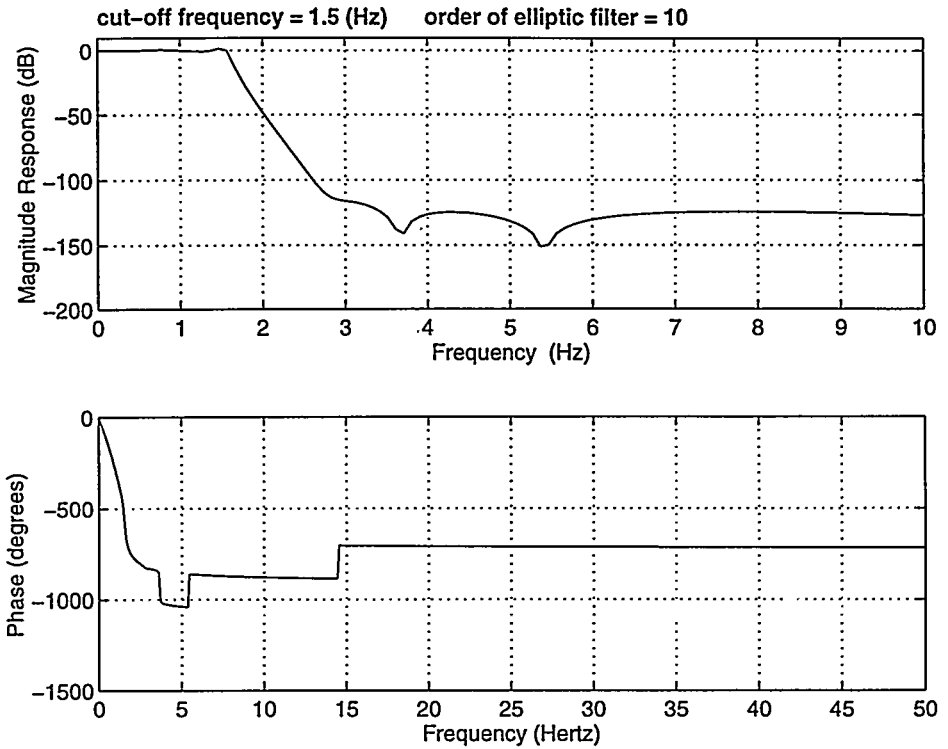
Figure 4-2 Magnitude response and phase of the applied elliptic filter with -125 dB damping, here shown with a cut-off frequency af 1.5 hz.
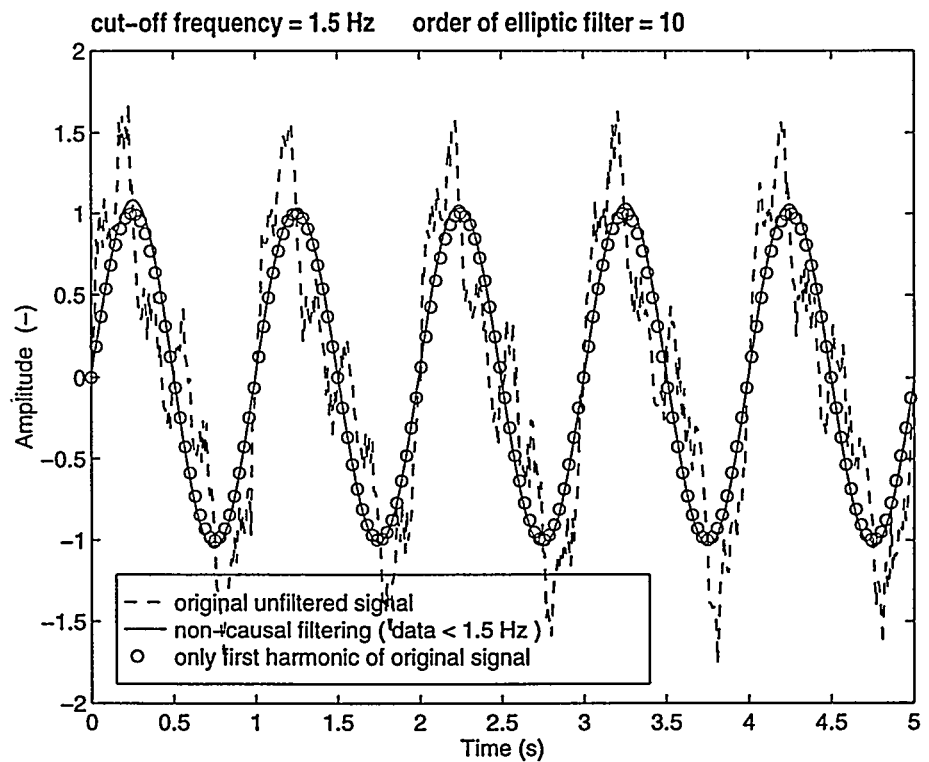
Figure 4-3 Effects of filtering methods on an artificially generated signal, which is composed from three harmonics and noise.

cut-off frequency = 1.5 (Hz)   order of elliptic filter = 10
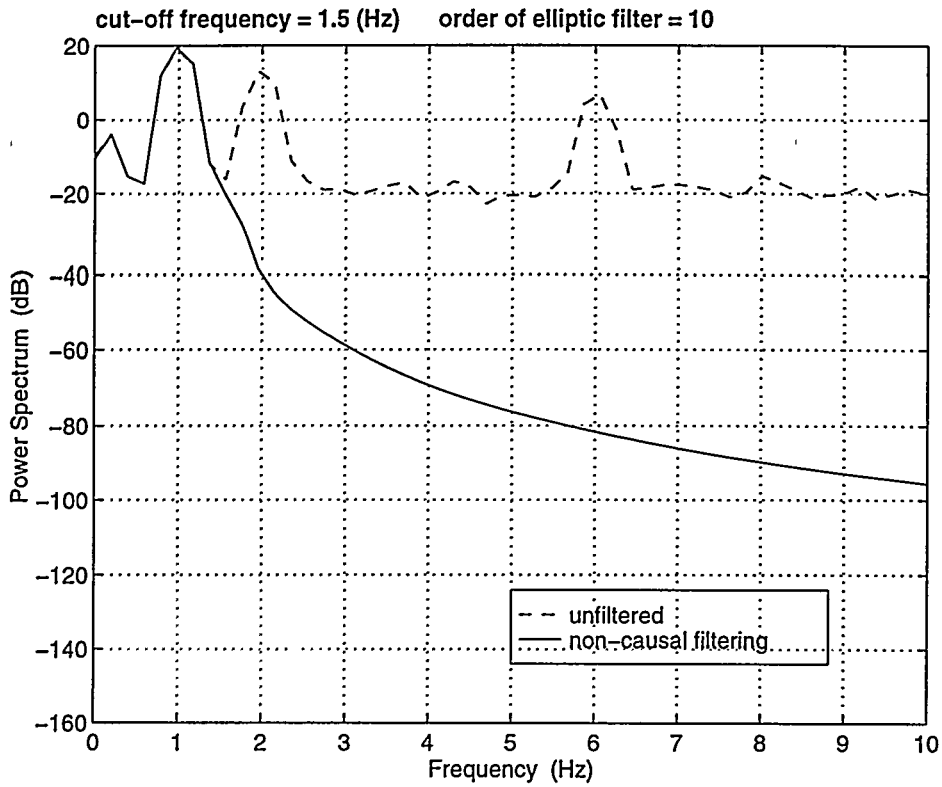
Figure 4-4 Corresponding power spectra of the artificially generated signal in Figure 4-1; unfiltered+- and filtered.
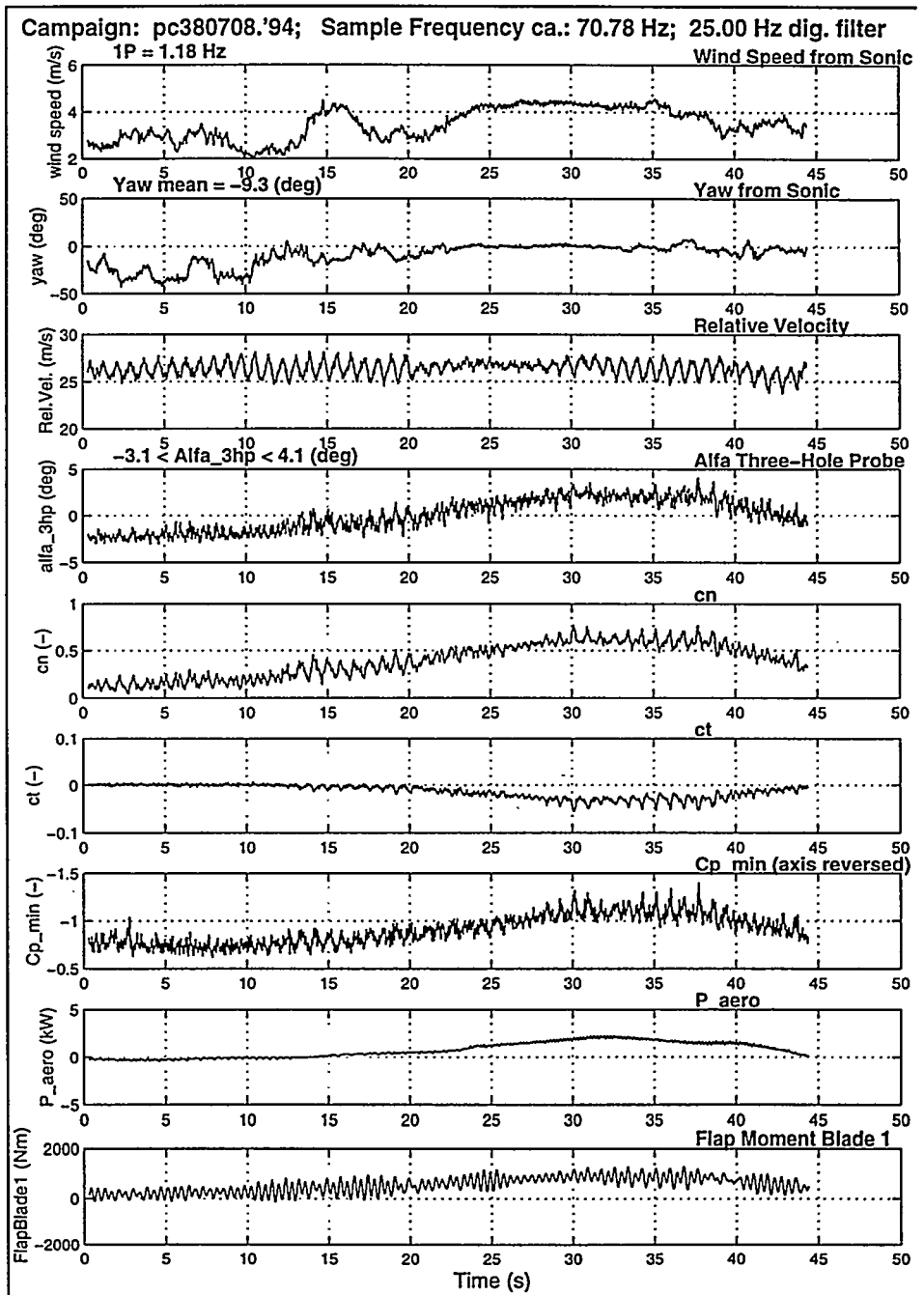
Figure 4-5 Nine signal time-series filtered at 25 Hz low pass campaign pc380708.'94.

Campaign: pc380708.'94; Sample Frequency ca.: 70.78 Hz; 4.00 Hz dig. filter
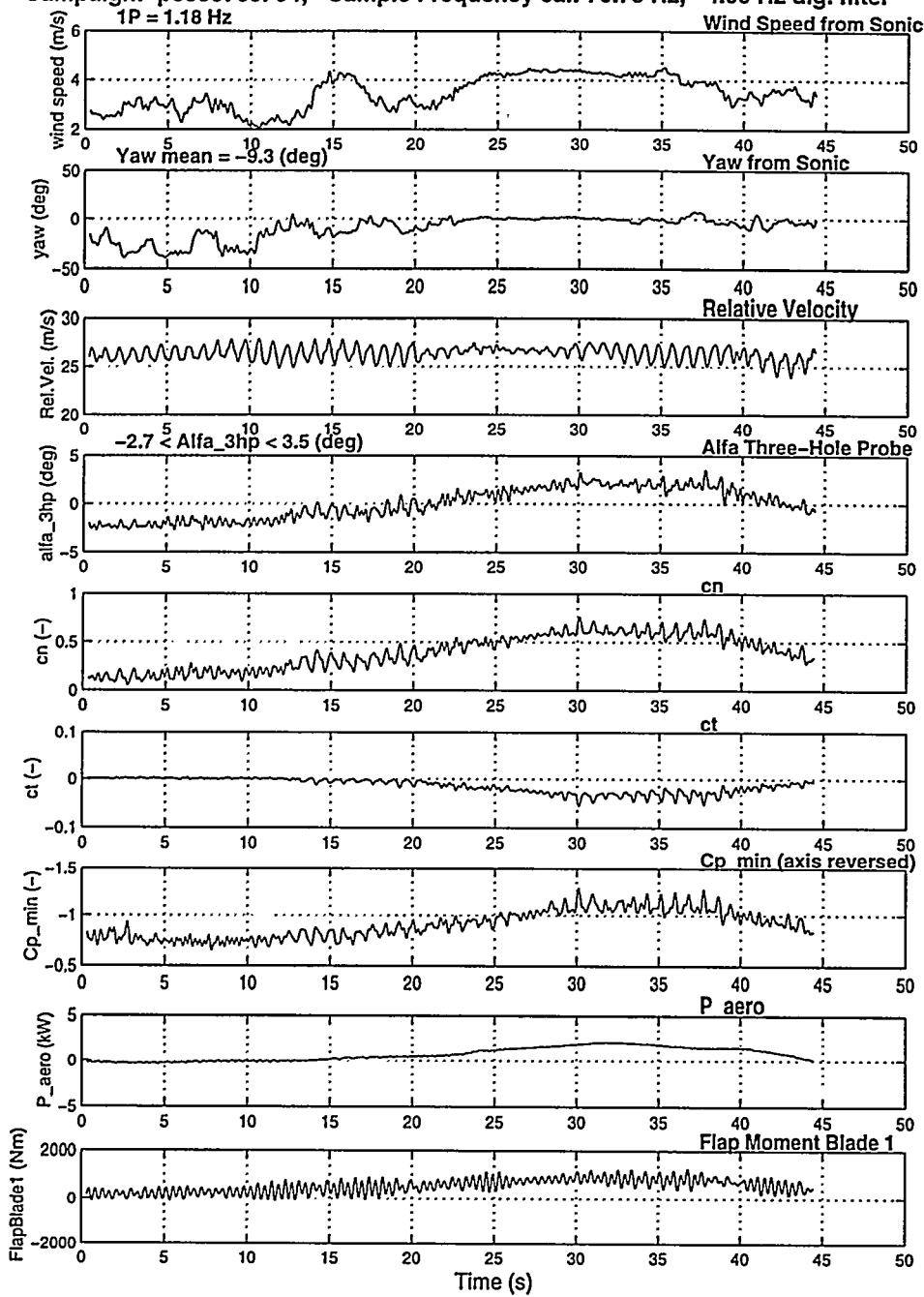
Figure 4-6   Nine signal time series at 4 Hz low pass filtered of campaign
pc380708.'94
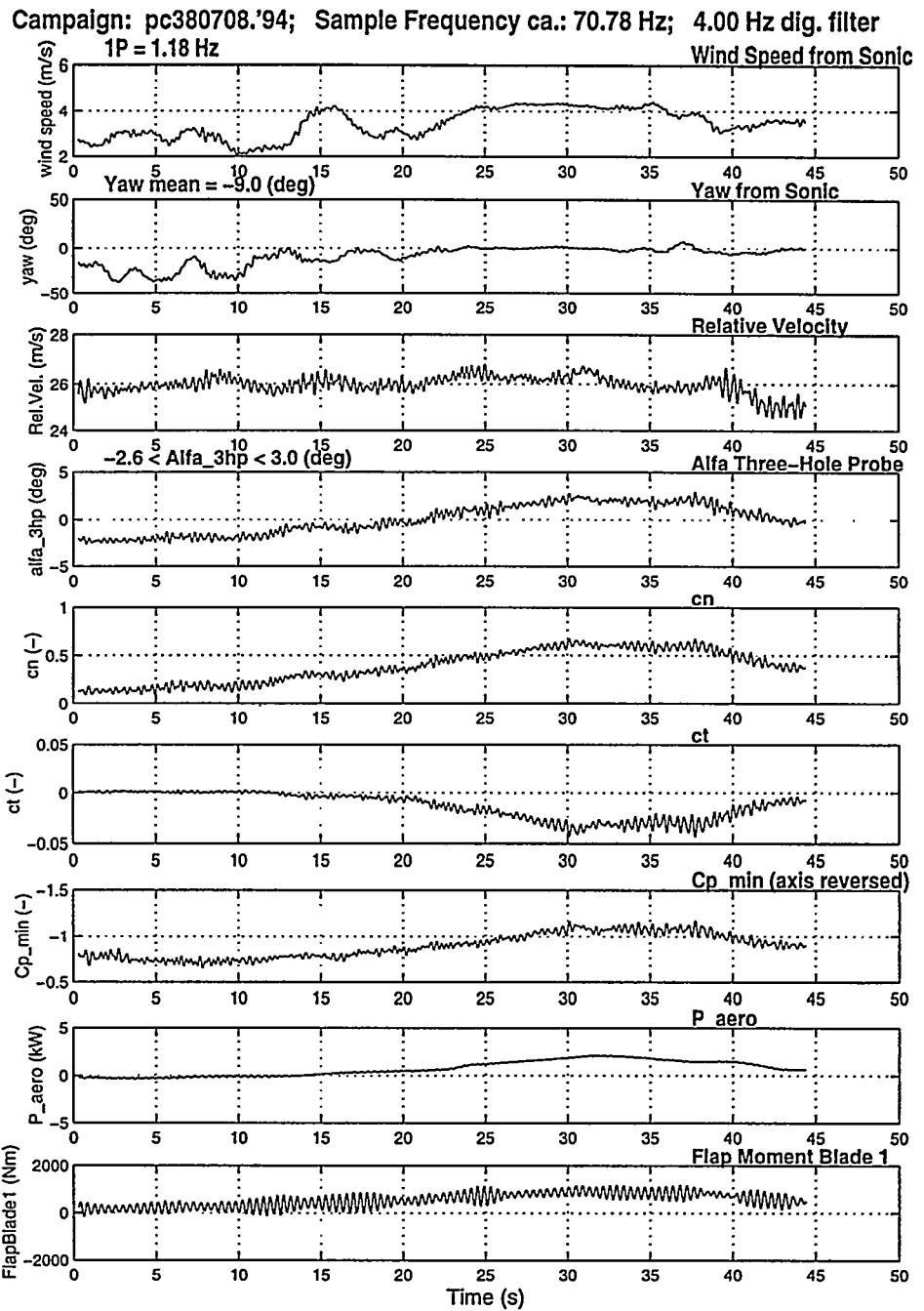
Figure 4-7   Nine signal time series with the 4 Hz low pass filter and additional 1_P band suppression (between 0.45_P and 1.5_P) of campaign pc380708.'94
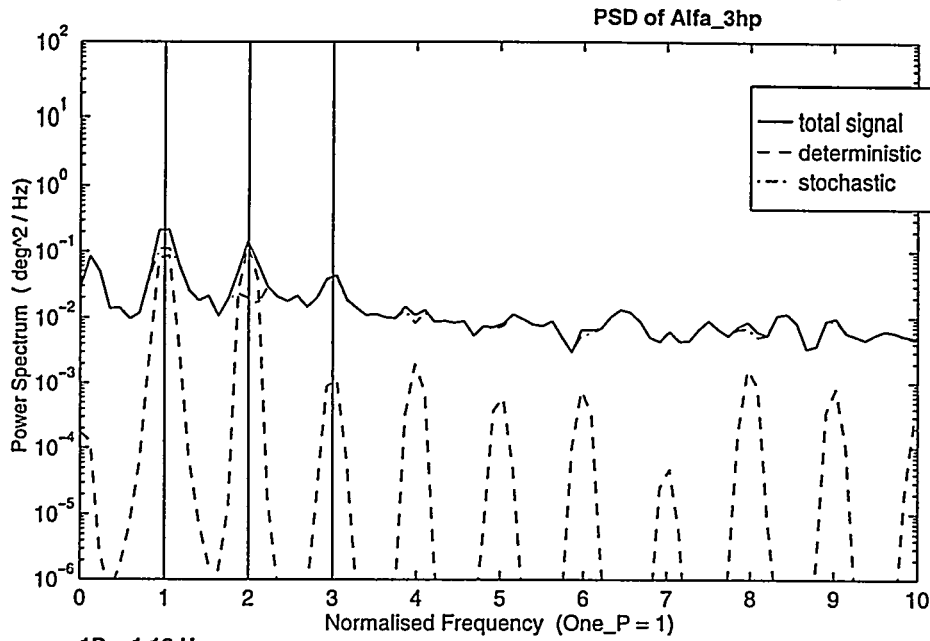
PSD of Alfa_3hp

1P = 1.18 Hz

Yaw mean = –9.3 (deg)

–3.1 < Alfa_3hp < 4.1 (deg)

PSD Integrated of Alfa_3hp
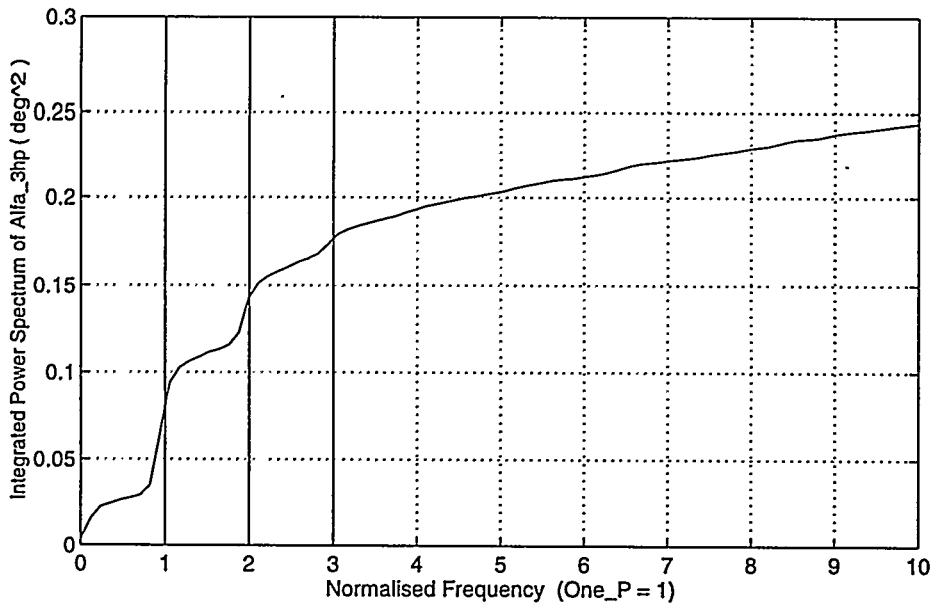
Figure 4-8 Power spectrum of the angle of attack, obtained from the three-hole probe, with the deterministic, stochastic and total part

Azimuth binning (6 deg bins) cn

1P = 1.18 Hz
Yaw mean = -9.3 (deg)
-3.1 < Alfa_3hp < 4.1 (deg)   Azimuth binning (6 deg bins) Alfa_3hp
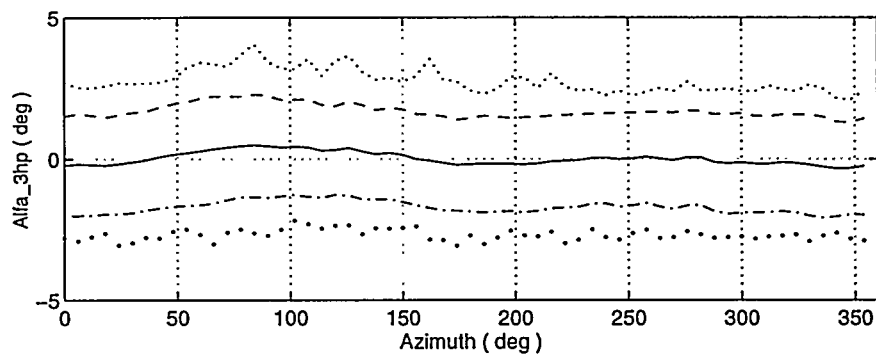
Azimuth binning (6 deg bins) WW (rel. Vel.)
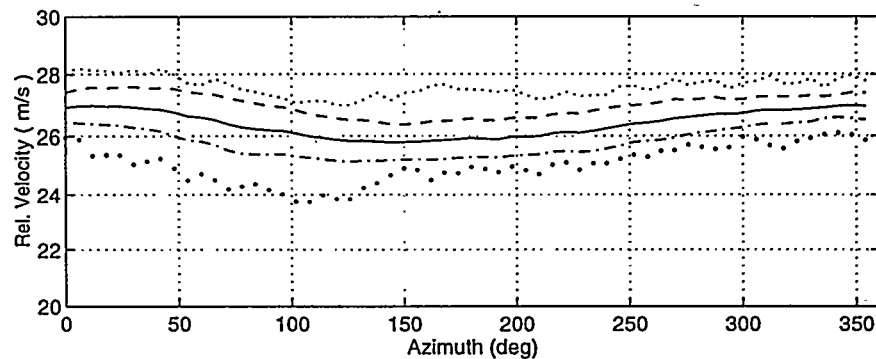
Figure 4-9 Azimuthal binned results for c_n, the angle of attack obtained from three-hole probe and the relative velocity at the 70% span station. Average and standard deviation are shown as well as the maximum and the minimum values in each bin. A azimuth position of zero degrees corresponds to the top position of the blade.
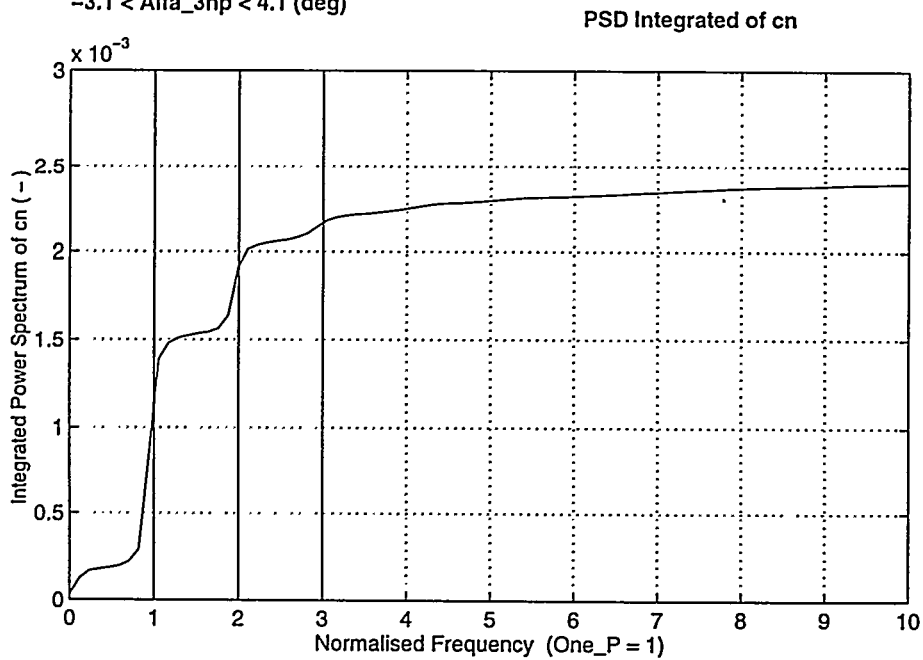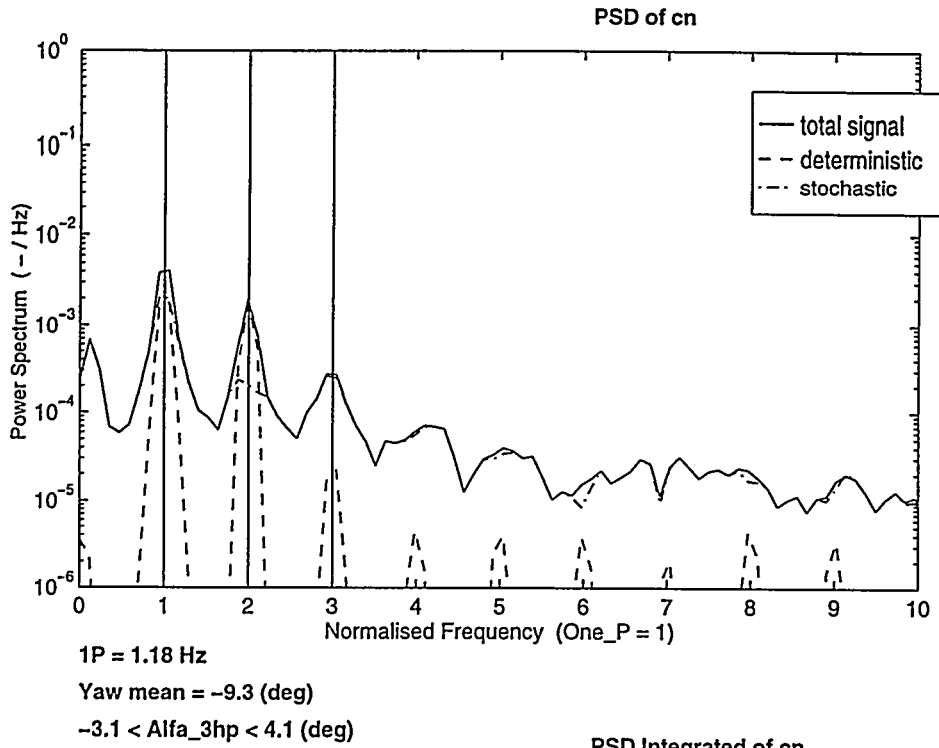
Figure 4-10 Power spectrum of c_n with the deterministic, stochastic and total part.

Campaign: pc380708.'94;   Sample Frequency ca.: 70.78 Hz;   4 Hz dig. filter
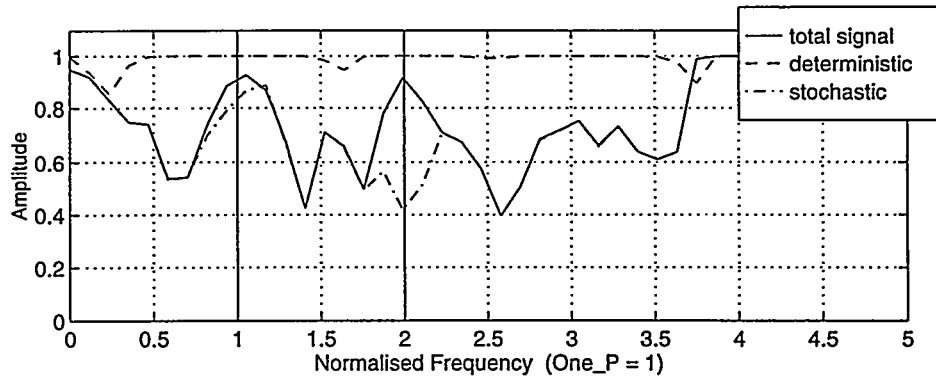
Coherence Alfa – cn

1P = 1.18 Hz
Yaw mean = –9.3 (deg)
–2.7 < Alfa_3hp < 3.5 (deg)

Transfer Function Alfa – cn
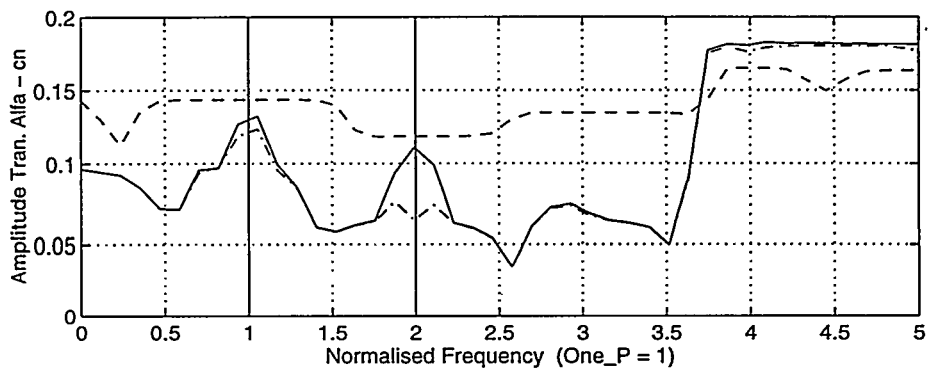
Phase (Transfer Func.) Alfa – cn
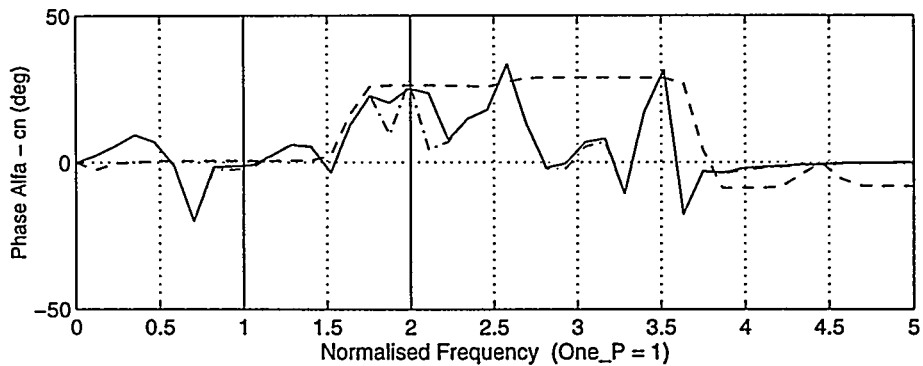
Figure 4-11 Coherence and transfer function between c_n and the angle of attack obtained from the three-hole probe

PSD of cn

1P = 1.18 Hz

Yaw mean = -9.0 (deg)

-2.6 < Alfa_3hp < 3.0 (deg)

PSD Integrated of cn
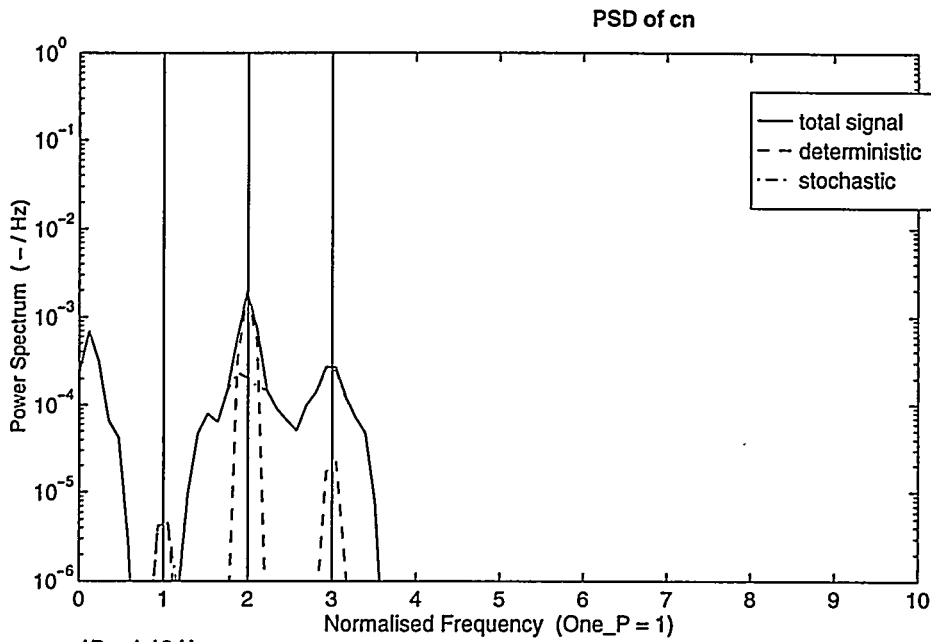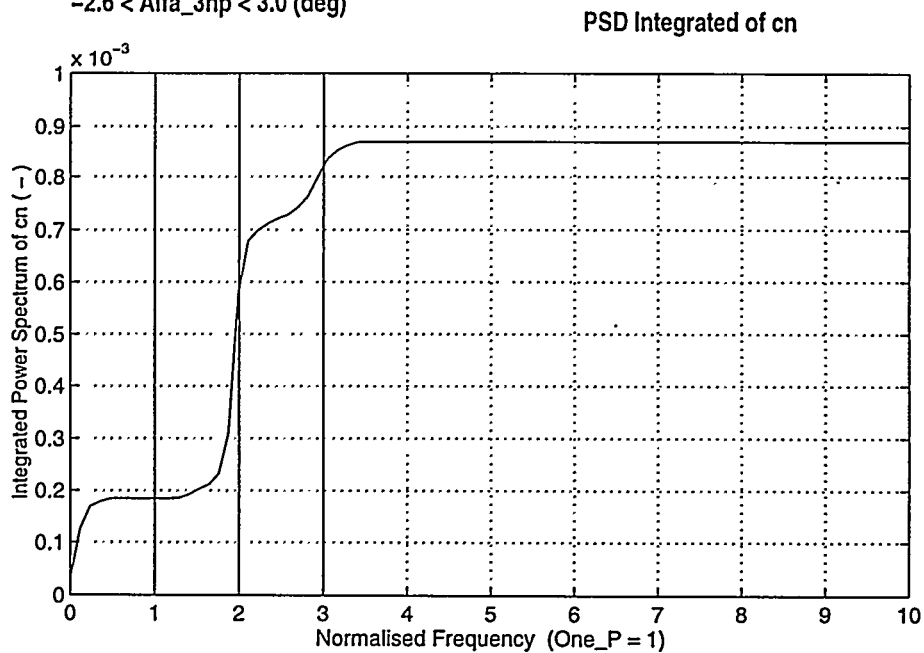
Figure 4-12 Power spectrum of c_n with low pass filtering and band pass filtering: all frequencies beyond 4 Hz and the band between 0.45 1_P and 1.5 1_P are suppressed.

Campaign: pc380708.'94; Sample Frequency ca.: 70.78 Hz; 4.00 Hz dig. filter

Figure 4-13 Azimuthal binned results of c_n, the angle of attack obtained from three-hole probe and the relative velocity of the 70% span station. Average and standard deviation are shown as well as the maximum and the minimum values in each bin. Low pass filtering and band suppression filtering: all frequencies beyond 4 Hz and the band between 0.45 1_P and 1.5 1_P are suppressed

Campaign: pc380708.'94; Sample Frequency ca.: 70.78 Hz; 4 Hz dig. filter
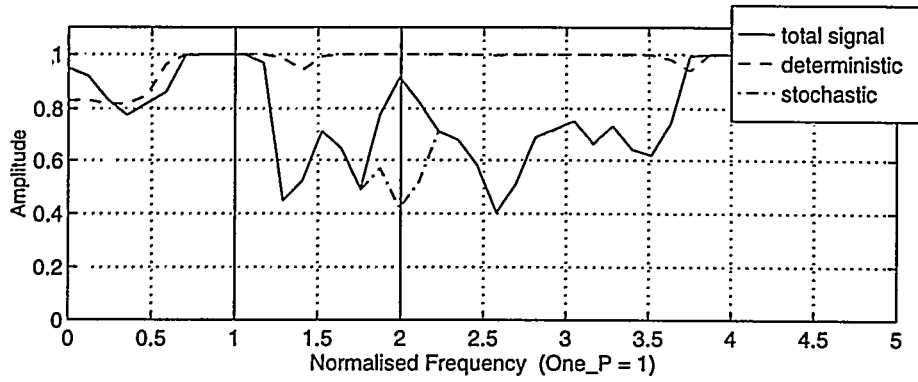
Coherence Alfa – cn

1P = 1.18 Hz
Yaw mean = –9.0 (deg)
–2.6 < Alfa_3hp < 3.0 (deg)

Transfer Function Alfa – cn

Phase (Transfer Func.) Alfa – cn
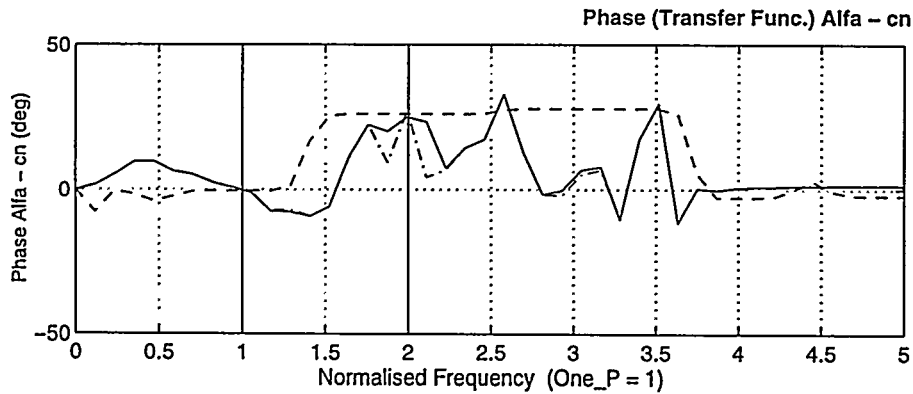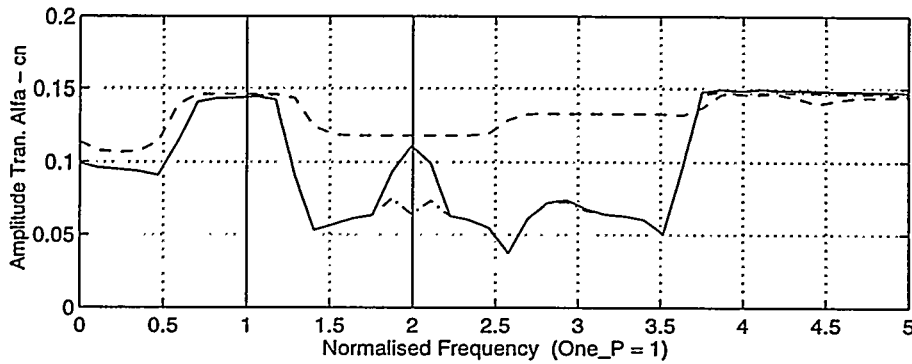
Figure 4-14 Coherence and transfer function of c_n and the angle of attack with low pass filtering and band suppression filtering: all frequencies beyond 4 Hz and the band between 0.45 1_P and 1.5 1_P are suppressed

5 Data from Imperial College

5.1 Introduction

The contribution from Imperial College to the project has been to carry out further analysis of existing aerodynamic data obtained from field tests and supply information on rotor blade section characteristics in order to assist the development of the engineering codes. The behaviour of the aerodynamic loads, and in particular the edgewise loading, through the stall were of interest. Previous work under the EC Joule research programme had established the strong three-dimensional behaviour of inboard blade stall on a rotor, covering field measurements, laboratory experiments and theoretical development, see for example, references [5-1] and [5-2] (field test data including that from the Rutherford Appleton Laboratory, Graham and Paynter) and [5-3] (laboratory scale data). The present programme was directed at improving the prediction of the contributions to unsteady rotor blade loading, particularly the unsteady loads arising from the stalling of the outboard part of the blade.

The data used in the present work was taken on the same wind-turbine as was used for the previous tests [5-1], [5-2] and consisted of blade surface pressure distributions sampled at 50Hz at 6 sections along the span of one blade of the 17m diameter, 3 bladed, fixed pitch, upwind H.A.W.T.

5.2 Experimental Details

The test rotor, sited at the Rutherford Appleton Laboratory was fitted with LM blades of NACA63200 section. Figure 5-1 indicates the geometry of the instrumented blade and the pressure sections. Each test section had 25 pressure tappings connected by 500 mm length tubes to 32 channel electronically scanned pressure blocks sited midway between adjacent sections in pairs. Each block could read one or other of the two sections to which it was connected at any one time. The time constant of the pressure system was found to be about 40ms. Incident velocity, angle of attack (AoA) and out of (section) plane angle were obtained from the readings of a three five hole Rosemount pressure probes, Figure 5-2. Each probe which was also fitted with static holes some way back along its shaft was mounted on the windward side of the blade midway between pairs of pressure sections, projecting about 1/2 chord ahead of the leading edge. The probes were connected to their corresponding pressure blocks by tubes of about ¾m in length giving a slightly longer time constant. The 32nd channel of each pressure block was connected to the reference port in the hub of the rotor by a long tube fitted with a fluid dynamic damper (reservoir plus restrictor). The purpose of this damper was to control the oscillations of pressure resulting from the cyclic changes in gravitational head as the rotor rotated. The wind turbine used for the tests is a 50kW Wind Harvester which has been downrated to a rotation speed of just less than 40 RPM in order to enhance the probability of obtaining high AoA for the incident flow onto the blades. In addition to precalibration, the pressure system was designed to be

calibrated for slope and zero reading during the course of a measurement sequence to compensate for temperature and other drift effects. Temperature effects were further kept to a minimum by operating the transducer blocks enclosed within temperature control jackets maintained at a constant temperature slightly above ambient in order, in addition, to avoid vapour condensation in the system. The 5-hole probes had also been precalibrated for incidence and dynamic pressure in a wind tunnel prior to the measurement campaigns, see for example Figure 5-3. When used on the rotor blade the probe output was first converted to uncorrected angle of attack and dynamic pressure using the wind tunnel calibration obtained for the probe in isolation. These results were then further corrected for the influence of the pressure field of the blade. This correction was carried out by computing the local circulation of the section from the measured pressure distributions and then calculating theoretically the correction due to this circulation placed at the quarter chord. All probe data was corrected in this way. Further details of the instrumentation and of the whole system are given in [5-4] and [5-5].

Calculation of angle of attack was probably the most difficult measurement in the whole programme of acquiring field data. As a result numbers of different procedures - pressure probes as reported here, angle of attack 'flag' probes, section stagnation point location and estimation from normal C_N and edgewise C_T force coefficients, see [5-6], were used by different groups in the programme and by the group carrying out similar field rotor measurements at NREL, see for example, [5-7] and [5-8]. For the present data AoA (α) was usually computed from the 5-hole probes, but in some cases estimates were also made from the relationship: $\alpha = \tan^{-1}(C_T / C_N)$ which assumes that the drag is very small and therefore only applies for pre-stall conditions. Most of the methods used are for different reasons considerably less accurate in the post-stall regime.

In addition to the pressure data, wind speed and direction were continually sampled at hub height at anemometer masts sited approximately two diameters from the rotor and upwind of it for the prevailing (westerly) wind direction, in-plane and out-of-plane bending was recorded from strain gauges in the root of the blade and nacelle direction, rotor power and azimuth angle were also monitored.

5.3 Data Analysis

Since the aim of the project was to study blade vibration effects due to stall the work reported here concentrates on analysis of data from the outboard stations on the blade (at 65% and 80% tip radius) which contribute most to the blade vibration. Results of the analysis of data from the more inboard stations have been reported previously, for example in [5-1] and [5-2].

Raw data sets (typically representing time histories from two sections each for from 1 min. to 10 mins. duration) were obtained during several measurement campaigns and stored as digital pressure counts. The first pass of data processing was to examine each file and remove those which contained severe contamination in the form of large numbers of significantly erroneous readings, typically spikes or patches of zeros caused by transducer or sampling errors (for example caused by water in a pressure tapping or contamination from external electronic noise). The remaining files, consisting of some reference and calibration sets and in the main operational data were now deemed to be 'good' in the sense of not containing large, obvious errors, with the exception of numbers

of isolated spikes resulting from a single defective reading or in some cases sequence of readings from a single channel at any one time. These errors were able to be approximately corrected by an interpolation procedure. The data was scanned automatically for errors of this type using a test routine. When located the erroneous value was removed and replaced by an interpolated value obtained from the readings on either side of it in either time or space.

Figure 5-4 shows a pressure distribution (still in digital count form) at a single sampling time for the most outboard section after the automated cleaning up process. This is an example in which a single reading, almost certainly in error but not of large magnitude, has passed through the error removal system because it fell below the removal criterion. Such readings contribute some errors to the data but are not easily removable by means other than very time consuming inspection. A short example (3 cycles) of a time series of the cleaned up pressure data, converted to engineering units, is presented as a sequence of distributions for one section of the blade in Figure 5-5. These sequences of data were then integrated over the chord of the blade section to generate time series of normal force coefficient C_N and edgewise force coefficient C_T. For the latter, it must be remembered, that the force is due to pressure only and does not include the skin friction contribution which is significant for the total edgewise force. C_N similarly does not include this component but it is less significant for that case. Figure 5-6 shows corresponding time series of normal force, angle of attack (radians) and centre of lift on the section. The last of these shows that the centre of lift is mostly in the region between the quarter and one-third chord which would be expected for this section in an attached flow regime as corresponds to this data sequence. Figure 5-7 shows corresponding time series of normal force coefficient and edgewise force coefficient. The time series of the data show clearly that all the force and incidence data cycles through a range of values with the rotor rotational frequency. This effect can be due to either the effect of a strong mean vertical shear or a mean horizontal shear (very unusual) or the effects of yaw between the rotor and the wind. In fact, as shown in Figure 5-8 which presents series of wind speeds at the two masts, direction, nacelle yaw angle and electrical power, it is clear that the rotor is always offset from the wind direction by an angle of about 5 to 10 degrees. This is due to the slow response of the highly damped fan tail yaw drive fitted to the nacelle and is sufficient to explain the major part of the once per revolution cycling of the angle of attack and forces on the blade. The normal force coefficient for a complete data set is shown plotted as a set of points against the angle of attack for the outboard most station in Figure 5-9. The distribution of these points correspond to samples on continuous loops formed by the normal force - angle of attack curves. Such curves cover a fairly extensive region from any one data set as shown in Figure 5-10, for the 65% station. This is due to the low frequency variations of the wind speed (and direction). The noisiness of the curves is due to higher frequencies in the wind turbulence and the flexible blade response. The mean line through the data in Figure 5-9 is compared with the steady normal force characteristic for the section (thinner line), obtained here by a viscous-inviscid matched computational prediction (XFOIL). The measured data is below the theoretical two-dimensional data and exhibits a lower slope. These effects are due to the proximity of the section at 80% to the tip of the blade and hence the influence of tip downwash and three-dimensionality. An alternative to straight presentation of the data is to bin it according to angle of attack averaging the binned data. Curves resulting from this are shown in figure 11 and compared with the XFOIL prediction. The agreement between the binned average and the 2-dimensional theoretical prediction for the 65% station shown here is improved.

Because of the difficulty in further interpretation of the data as time series directly spectral analysis has been carried out together with filtering of the data. The data was low pass filtered digitally at 25 Hz and then transformed into power spectral densities (PSD) using Fast Fourier Transform routines. An example of a power spectrum of the edgewise force for the 80% station is shown in Figure 5-12. The large peak at the once per revolution frequency (0.645 Hz) is clearly visible.

By taking ratios of PSD of normal force and angle of attack transfer functions can be obtained which should show the range of frequency over which the C_N - AoA relation approximates in gradient to the steady flow result for the section. Figure 5-13 shows examples of transfer functions between C_N and AoA for different sections and data sets. It can be seen that at very low frequency there is some large variation almost certainly due to wind variation and insufficient length of data sequences and at the high frequency end the transfer function rapidly decreases as would be expected from the unsteady aerodynamic effect. Between the frequencies of about 1 Hz and 4 Hz however the value of the transfer function is reasonably constant at a value equivalent to the ratio just greater than 6 (shown in the figures as a dashed line) for the normal force coefficient - AoA gradient. This is the value for the section in steady flow prior to the stall. In this same region the coherence of the two data series is high (~0.8) but significantly less than one, Figure 5-14, and the phase difference between the signals is reasonably small (less than $\pi/4$ radians), Figure 5-15. The explanation of why the coherence and phase are not fully correlated may arise partly from the greater time lag in the pressure data from the AoA probes caused by the longer tubes from pressure tapping to transducer block.

In order to study the effects of fluctuating force on blade excitation (and in particular edgewise vibration) the normal force time series have been digitally band pass filtered between 1.5 Hz and 4 Hz using Butterworth filters. The resulting normal force and angle of attack time series are then plotted against each other as continuous loops. Examples of these are shown in Figure 5-16. The loops cover a much smaller range than the unfiltered data and the slopes of their major axes are approximately determined. The absolute values of the filtered values of C_N and AoA are around zero in the lower figure because of the high pass element of the filtering which has removed the mean values of the data. In the upper figure, taken for a shorter sequence, the mean values of C_N and α have been added back in to give a more representative value. The slopes of the major axes of individual loops are less than the apparent slope for the whole distribution and are estimated to be, on average, about 0.05 / degree or 2.9 / radian.

5.4 Conclusion

This section presents the results of the analysis of blade surface pressure data taken on sections of a rotor blade on a Wind Harvester 17m HAWT. in the field. The data has been cleaned up to remove errors occurring in acquisition of the data and then integrated to obtain normal and tangential force coefficients for the blade sections. The resulting data has been plotted as individual samples, binned and averaged and Fourier transformed to generate spectra. Finally the data has been band pass filtered to obtain force - angle of attack loops in the frequency range in which the transfer function is approximately equal to the steady flow gradient of normal force against angle of attack.

5.5 References

[5-1]
Bjoerck A. and Thor S.-E. Dynamic stall and 3-D effects.   Proc. EUWEC. p 683, Goeteborg, 1996

[5-2]
Graham J.M.R. and Paynter R.J.H.   Contribution to Dynamic Stall and Three-dimensional Effects. Final report for EC DGXII Joule II project, JOU2-CT93-0345, by Bjoerck A., FFA TN 1995-31, 1996

[5-3]
Brown C.J. and Graham J.M.R.   The Effect of Turbine Rotation on Maximum Lift Coefficient, Proc. EWEC, p 117, 1989

[5-4]
 Paynter R.J.H., Graham J.M.R. and Infield D.G. Pressure Measurement on a Stall Regulated Wind Turbine Blade,   Proc. EWEC, p 693, Thessaloniki, 1994

[5-5]
Paynter R.J.H. and Graham J.M.R. Blade Surface Pressure Measurement on an Operating Wind Turbine, Proc EUWEC. p 687, Goeteborg, 1996

[5-6]
Petersen J.T., Madsen H.Aa. et al. First 12 monthly progress report on STALLVIB, Contract JOU3-CT95-0047(DG12-WSME) 1996

[5-7]
Simms D.A. and Butterfield C.P. Full Scale Wind Turbine Rotor Aerodynamic Research, Proc. EWEC, p 708, Thessaloniki, 1994

[5-8]
Simms D.A. in Field Rotor Aerodynamics, Proc. IEA R&D WIND Annex XI, Petten NL, (ed. Pedersen B.M.), 1997

5.6 Figures
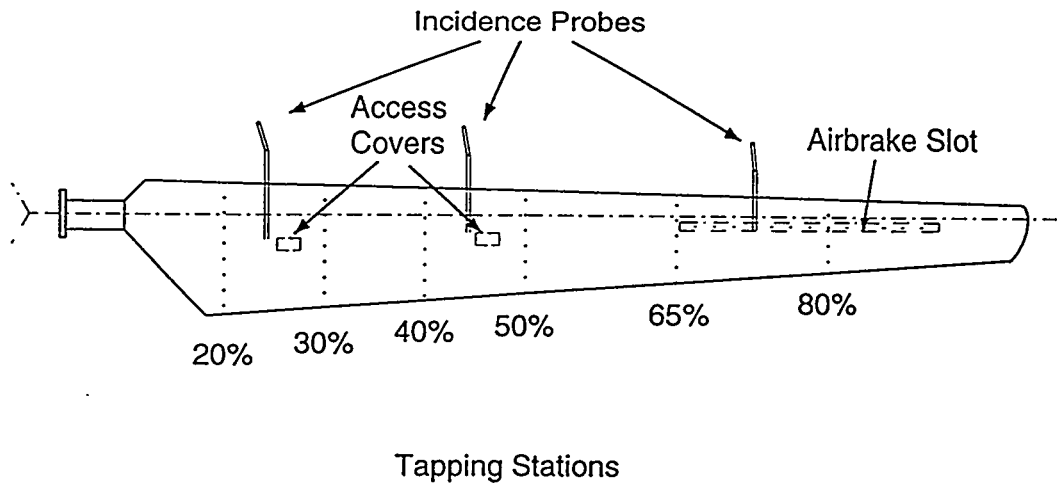
Figure 5-1   Blade Layout
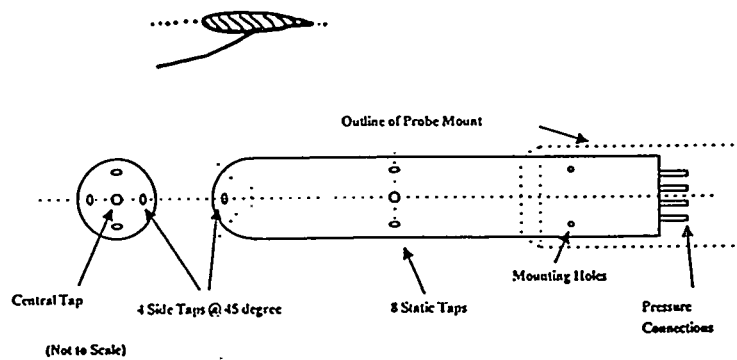
Figure 5-2   Rosemount 5 hole angle of attack and dynamic head probe.
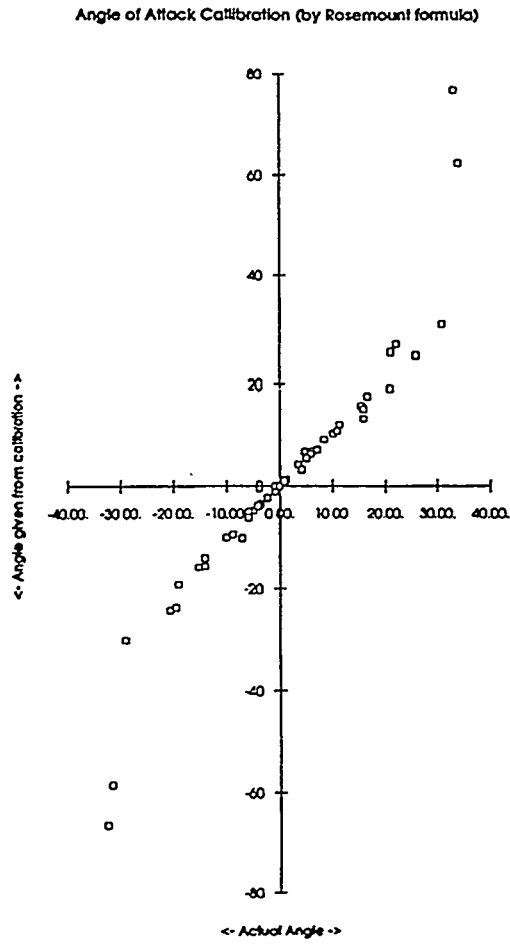
Figure 5-3 Probe calibration.
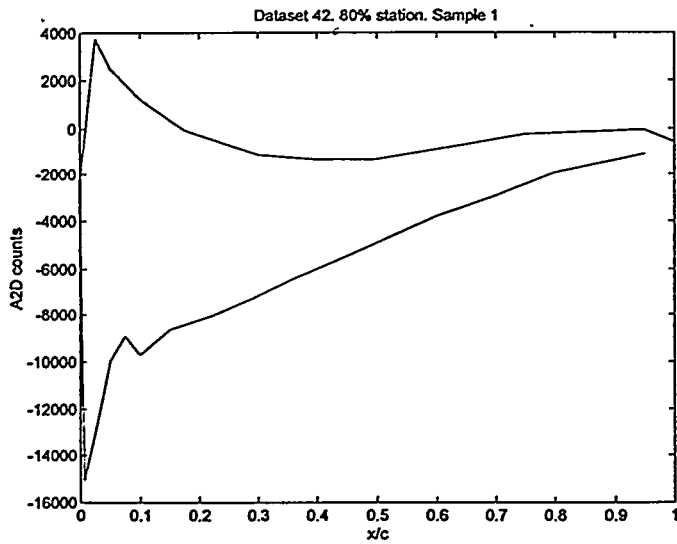
Figure 5-4 Pressure distribution measured around the 80% blade section.
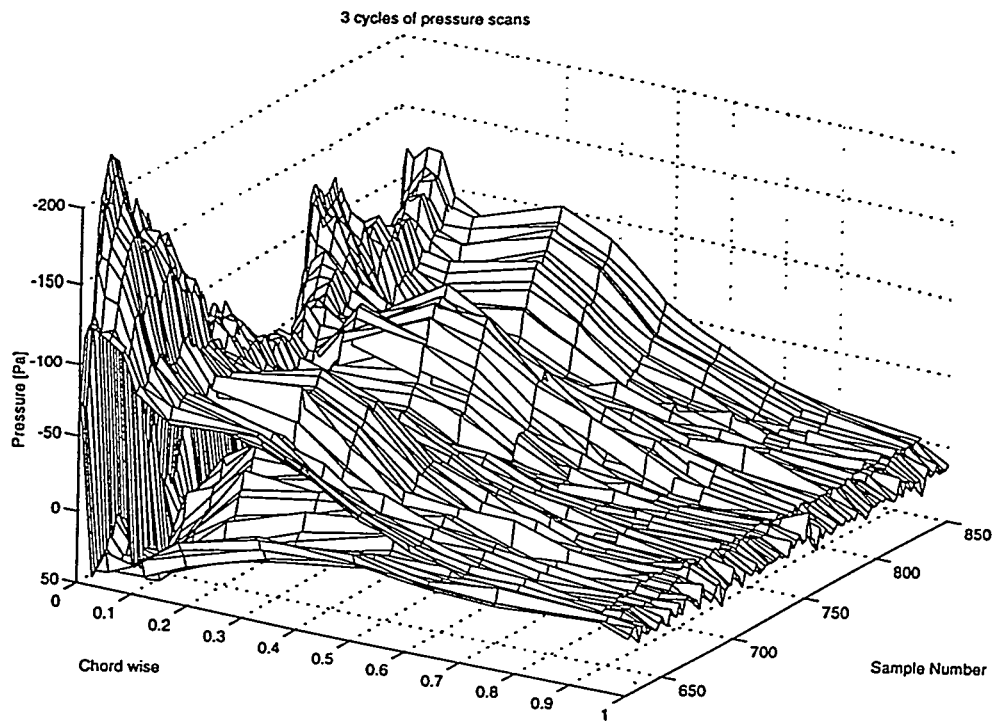
Figure 5-5 Cycles of pressure distribution for the blade section.
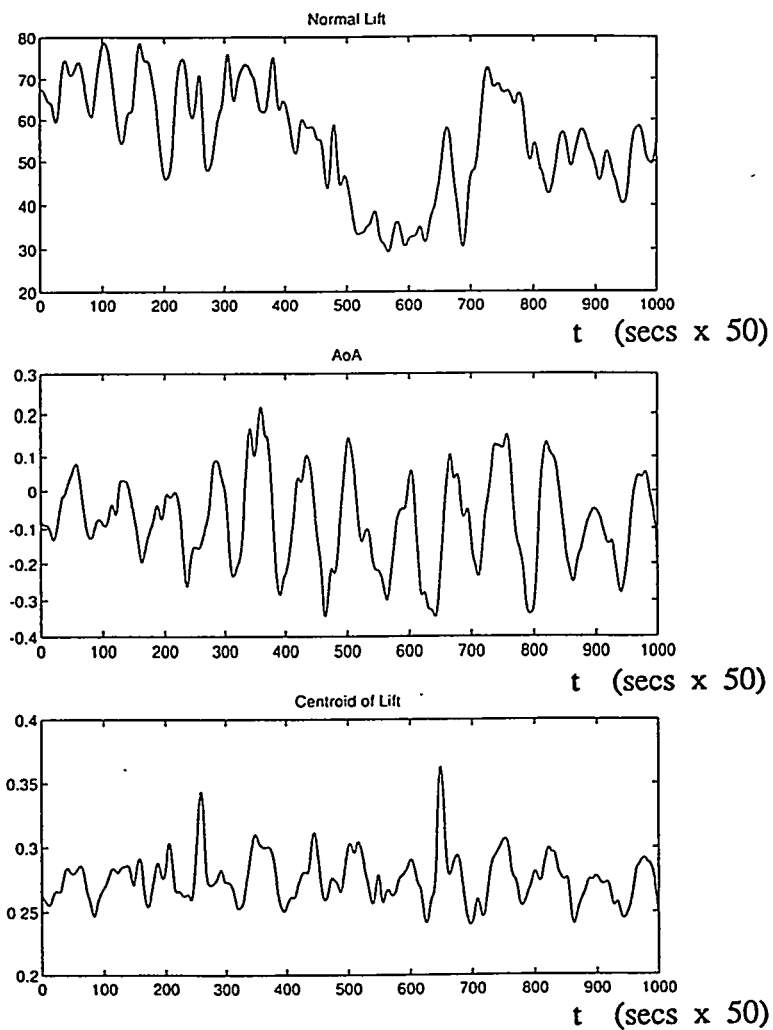
Figure 5-6 Time series of normal force, AoA and centre of lift force.
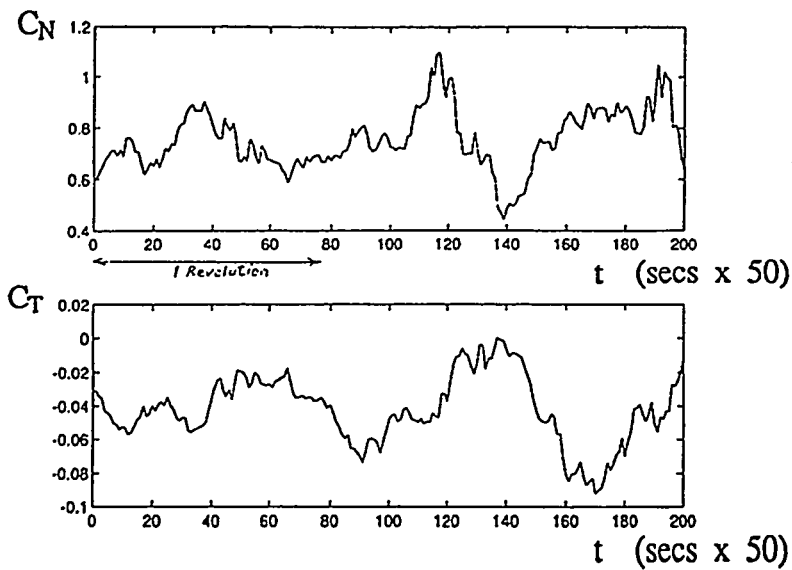
Figure 5-7 Time series of normal and edgewise force coefficients.
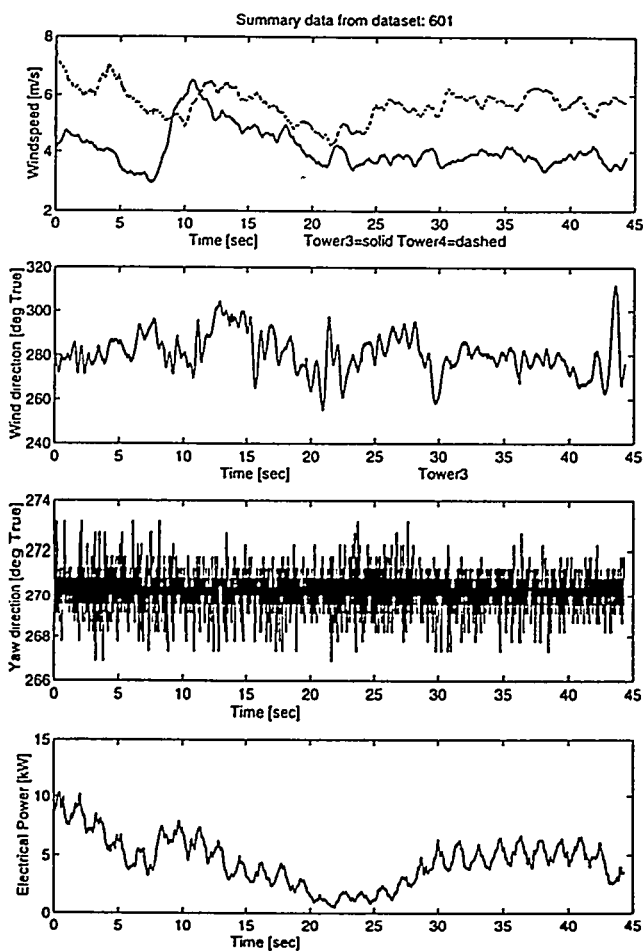
Figure 5-8 Time series of wind speed, wind direction, nacelle yaw angle and power.
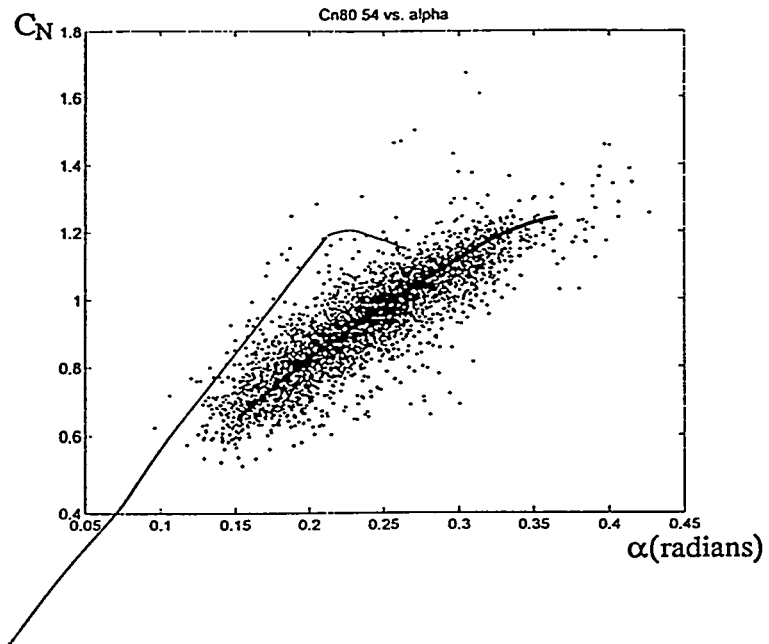
Figure 5-9   Normal force coefficient versus AoA (80% section).
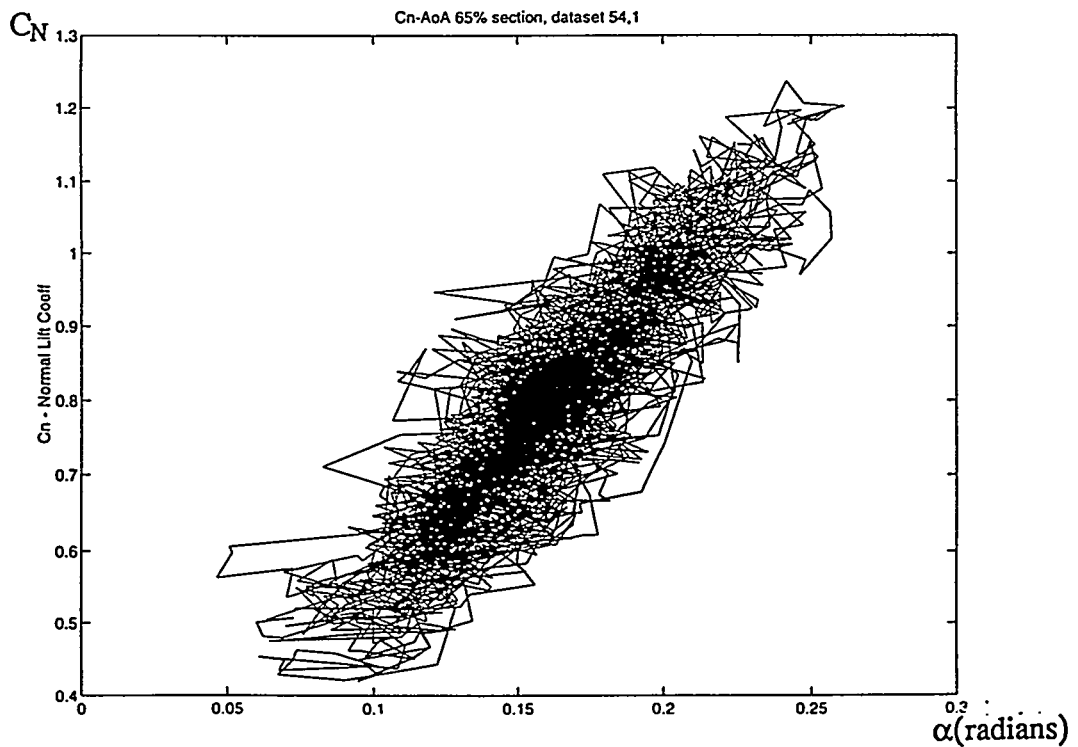
Figure 5-10 Normal force coefficient versus AoA (65% section).
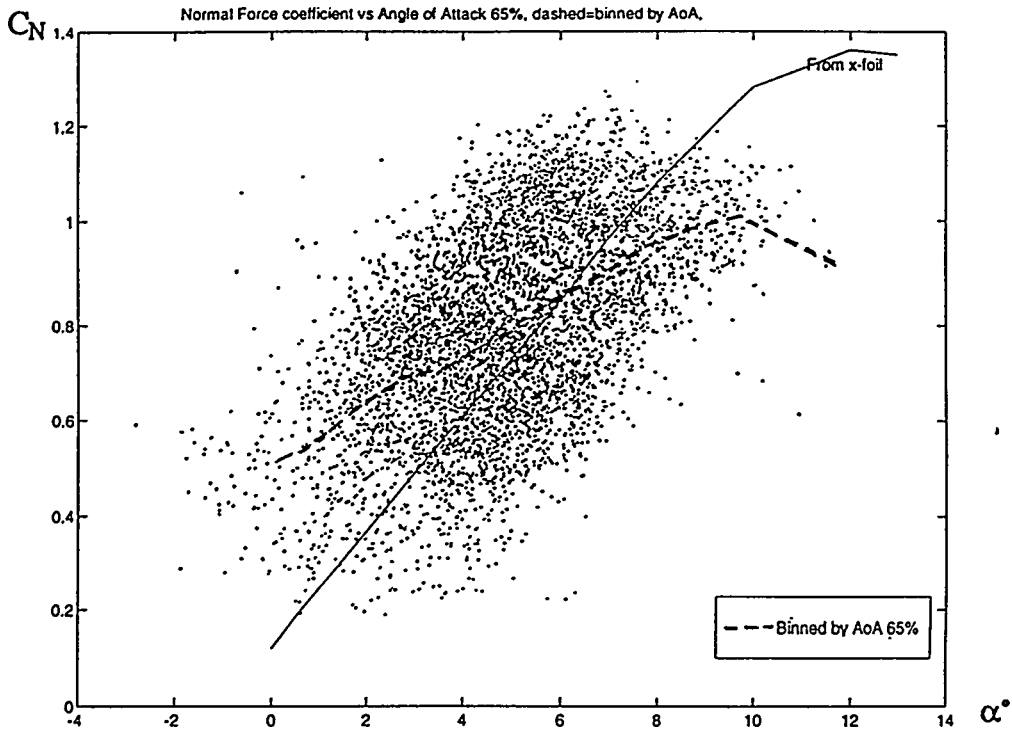
Figure 5-11 Normal force coefficient versus AoA (65% section), binned data.
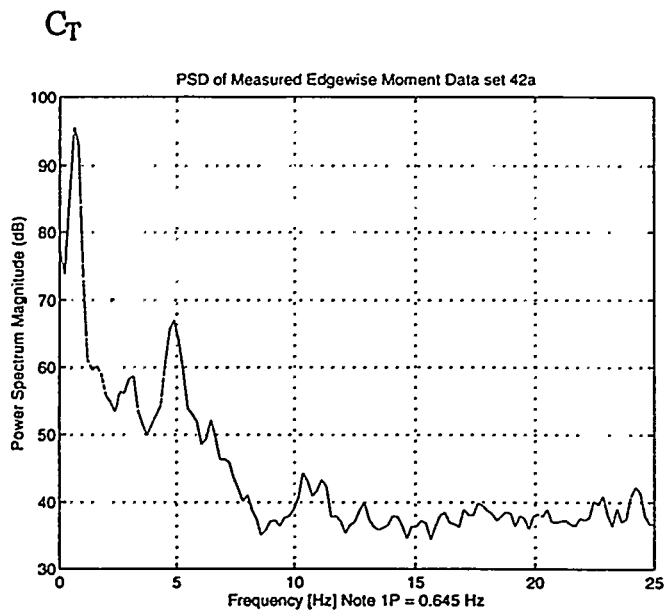
Figure 5-12 Power spectral density of normal force coefficient.
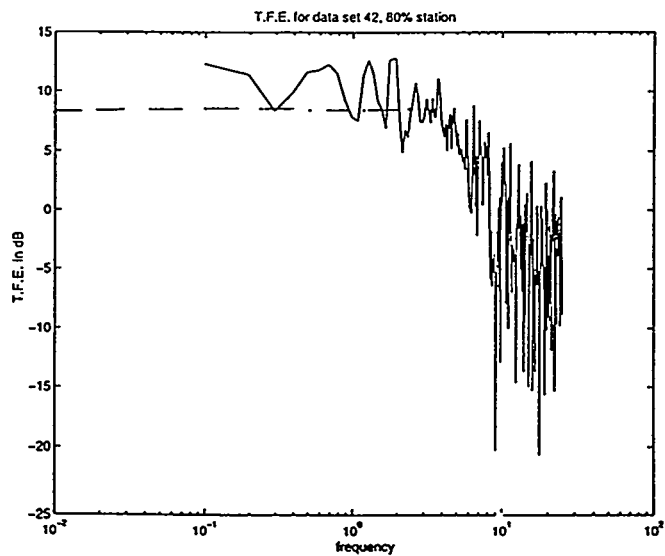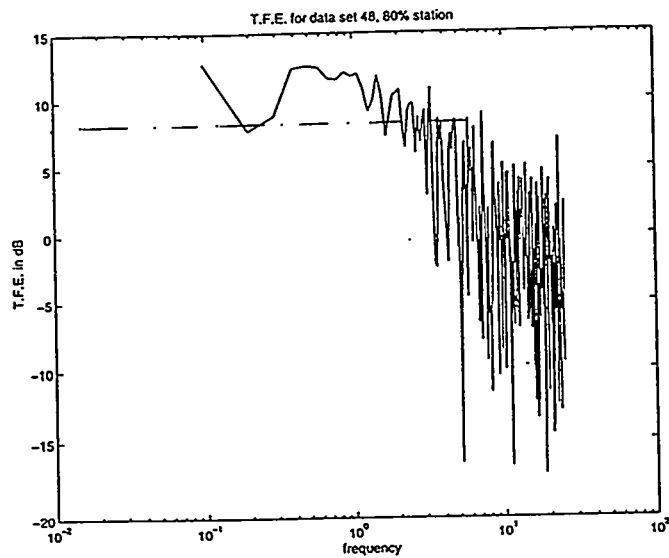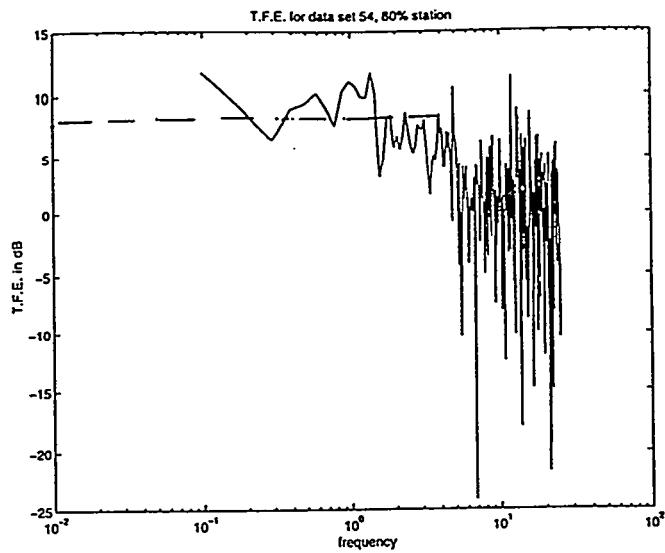
*Figure 5-13 Transfer coefficients between normal force coefficient and AoA
spectra.*
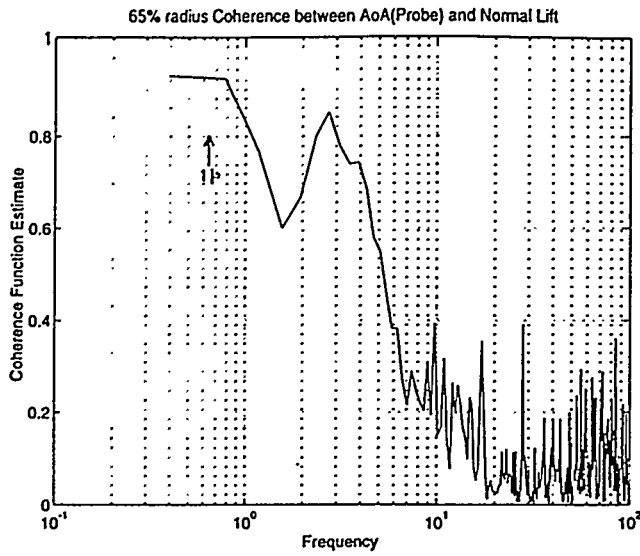
Figure 5-14 Coherence between normal force coefficient and AoA spectra.
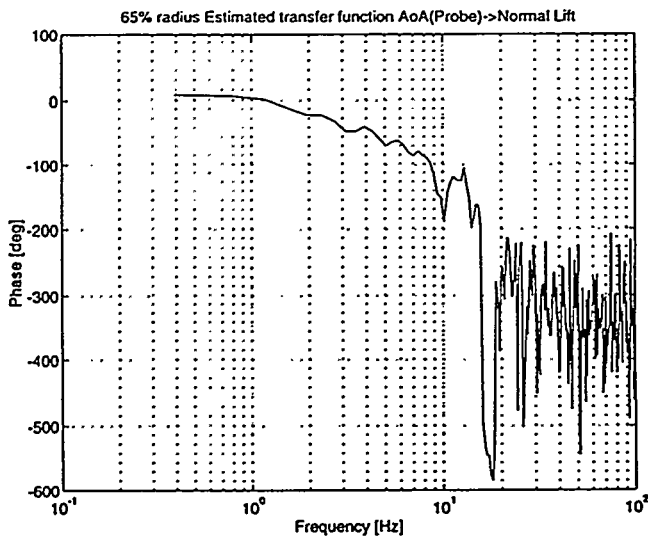
Figure 5-15 Phase difference between normal force coefficient and AoA spectra.
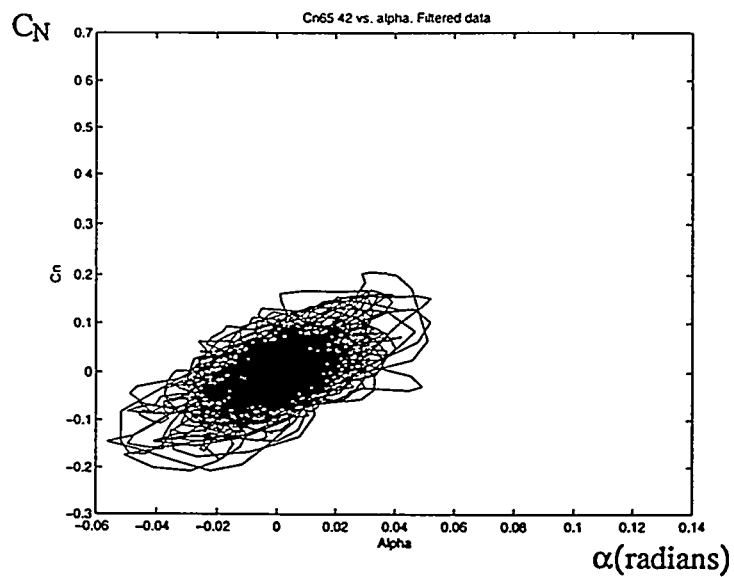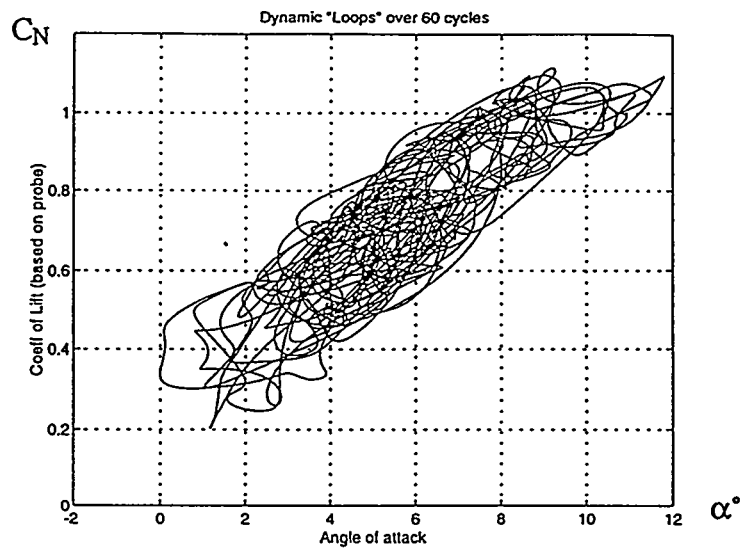
Figure 5-16 Normal force coefficient versus AoA (65% section), band passed data.

6 Data from RISØ

6.1 Background

The data to be used in the present project originate from a measurement proramme carried out in the period from 1987 to 1993 [6-1], [6-2]. In this programme, an experimental facility was developed in order to provide experimental results that could be used to identify the main mechanisms controlling the aerodynamic forces on a rotating HAWT blade in natural conditions. Some of the data have been supplied to the data base developed within the IEA Annex XIV collaboration [6-3] and it is data files from this data base that will be used in the present work.

The experimental facility is described in details in [6-1] and will only be summarised here. A 19 m diameter 100 kW stall regulated turbine with two synchronous rotational speeds, 47.5 and 35.6 rpm., was used as test bed. Blade sectional forces were measured at three radial positions on the blade and correlated with measurements of the inflow to the blade using a five hole pitot tube. Only measurements from the 70 % radial station will be presented here.

6.2 Data overview

The data to be used in the present project comprises two data sets from the IEA ANNEX XIV Data Base [6-3]. It is the files tl200101 and tl210101, each of 10 minutes length. The average wind speed is 7.2 and 14.1 m/s, respectively. Statistics of the data files are shown in Table 6-1 and Table 6-2 and some of the channels are presented as time traces in Figure 6-1 to Figure 6-8.

Table 6-1 Statistics of file tl200101

	W (m/s)	Pow. (kW)	CN2	CT2	alpha (deg)	Vrel (m/s)
Mean	7.23202e+00	2.92860e+01	1.03057e+00	1.16351e-01	6.88999e+00	3.26660e+01
std.	1.39154e+00	1.37830e+01	1.69047e-01	9.56675e-02	2.12681e+00	1.01473e+00
min.	4.27530e+00	-6.48600e-01	4.30540e-01	-1.63020e-01	9.08140e-01	2.86070e+01
max.	1.18270e+01	7.13500e+01	1.47040e+00	4.52560e-01	1.45090e+01	3.67280e+01

Table 6-2 Statistics of file tl200101

	W (m/s)	Pow. (kW)	CN2	CT2	alpha (deg.)	Vrel (m/s)
mean	1.40713e+01	9.14366e+01	1.45555e+00	2.20893e-01	1.69216e+01	3.45977e+01
std.	1.67554e+00	1.21186e+01	1.16107e-01	1.38492e-01	2.43092e+00	1.57395e+00
min.	7.60090e+00	4.22270e+01	1.09180e+00	-5.00430e-01	8.47690e+00	2.94650e+01
max.	1.96070e+01	1.24480e+02	1.90480e+00	7.19580e-01	2.57930e+01	3.93890e+01

6.3 Data processing

The measurements were carried out with a sampling rate of 25 Hz. Before the digital sampling, the signals were passed through an analog anti aliasing filter with a cut off frequency of 20 Hz. Each measurement period is 10 min. and the files are stored as binary files in the form of time series.

The first step in processing the data has been to pass the raw data through a digital Kaiser Window low pass filter. A filter was designed with a cut off frequency between 3 and 3.5 Hz which is well above 3p.

On basis of the filtered signals, derived parameters as e.g. the angle of attack α and C_N which both depend on more channels are computed. The PSD of the filtered and non-filtered angle of attack, Figure 6-10 shows no visible influence on the spectrum below the cut off frequency (in this example a filter with a cut off frequency between 4 and 4.5 Hz was used). In the corresponding time trace of the same signal Figure 6-8 it is clear that high frequency contents is effectively removed.

6.4 Coherence and transfer functions

The coherence between the measured angle of attack α and the normale force coefficient C_N has been computed for the data file tl200101 which covers α variations below stall. The coherence is 1 at the low frequencies and decreases then slowly to 0.7 at 2.5-3 Hz, Figure 6-11. At higher frequencies the coherence is varying rather much and is in general low. The corresponding phase is also shown and is close to zero at low frequencies.

The transfer function between the same two parameters is shown in Figure 6-12. An almost constant amplitude around 0.08 is found which is slightly lower than 0.1 for steady 2D data below stall. The lower values can be due to several reasons: 1) the data file contains data close to stall where the slope of the C_N vs. α curve will decrease; 2) the unsteadiness of α will tend to reduce the slope; and 3) uncertainties in the corrections of the measured α. Although the corresponding phase is varying rather much, Figure 6-12, it seems that C_N in general is lagging α which should be expected for hysteresis loops below stall.

6.5 Stochastic and deterministic parts

By azimuthal binning the determinstic part of α and the relative welocity w has been derived Figure 6-13 and Figure 6-14. Using the azimuthal posistion as pointer the deterministic parts have been subtracted the total signal, leaving back the stochastic part of α and w with an average value equal to zero, Figure 6-15 and Figure 6-16. The azimuthal variations in the deterministic parts of α and w is mainly caused by wind shear (vertical and horizontal) and the upstream effect of the tower in the azimuth interval around 180 deg.

Finally, power spectra have been derived for the two parts where a continues time trace of the deterministic signal has been constructed by concatenation of the results for one revolution. It appears that α is almost completely stochastic whereas w has some deterministic contents, Figure 6-17 to Figure 6-20. The peek around 1p and to some degree at 2p is due to the rotational sampling of the incoming turbulence to the rotor.

6.6 Comparisons with simulations

In order to discover possible major problems in the inflow measurements of α and w, the experimental data have been compared with state of the art simulations of turbulence seen by the rotating blade. A 3D model of the earth boundary layer turbulence, the so-called Mann model [6-4] coupled to an aeroelastic model [6-5] has been used for the simulations.

Some deviations are found in the absolute level of the deterministic part of both α and w, Figure 6-21 and Figure 6-22. However, the power spectra of the stochastic part of α and w show good correlation between measurements and simulations, except at very low frequencies where statistical uncertainty probably is the cause.

6.7 The final data sets

The binned C_N and C_T vs. α curves for the two 10 min. data files selected for the project are shown in Figure 6-27. It is seen that they cover an α interval from well below stall to well above. For a short time period, the instantaneous C_N vs. α is shown in Figure 6-28. Only minor hysteresis is seen below stall whereas considerable loops appear above.

6.8 References

[6-1]
Madsen, H.A. "Aerodynamics of a Horizontal-Axis Wind Turbine in Natural Conditions". Risø-M-2903, Risø National Laboratory, September 1991.

[6-2]
Madsen, H.A. "Aerodynamics of a Horizontal-Axis Wind Turbine in Natural Conditions - Raw Data Overview". Risø-M-2902, Risø National Laboratory, September 1991.
[6-3]
Schepers, J.G. et al. "Final Report of IEA Annex XIV: Field Rotor Aerodynamics". ECN-C-97-027. June 1997.

[6-4]
Mann ,J. "Models in Micrometeorology". Risø-R-727(EN). Risø National Laboratory. March 1994.

[6-5]
Petersen, J.T. "Kinematically Nonlinear Finite Element Model of a Horizontal Axis Wind Turbine. PhD thesis, Risø National Laboratory, DK-4000 Roskilde, July 1990.

6.9 Figures
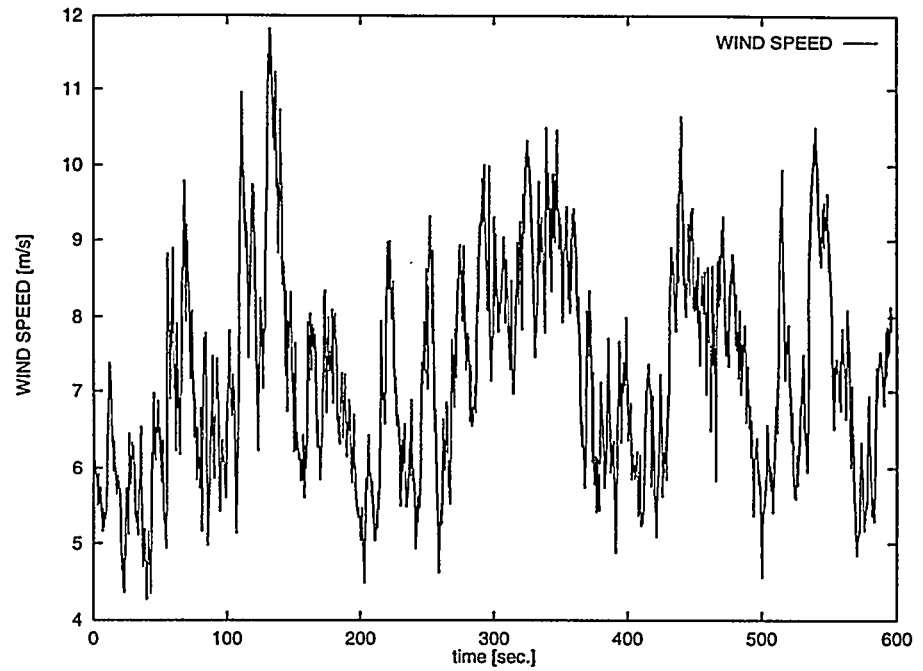
Figure 6-1 Time trace of wind speed, file tl200101.
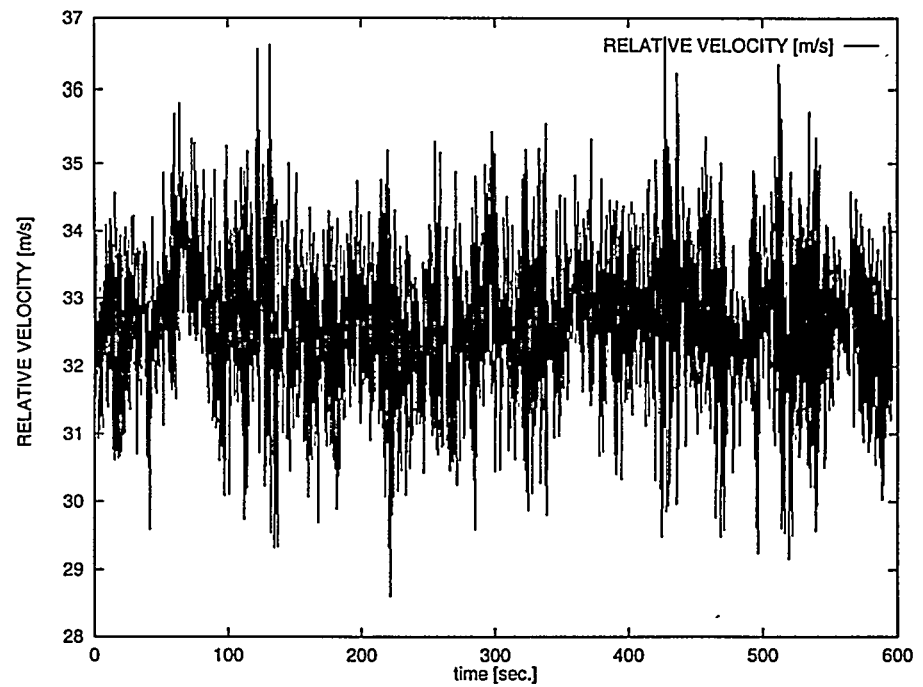
Figure 6-2 Time trace of relative velocity, file tl200101.
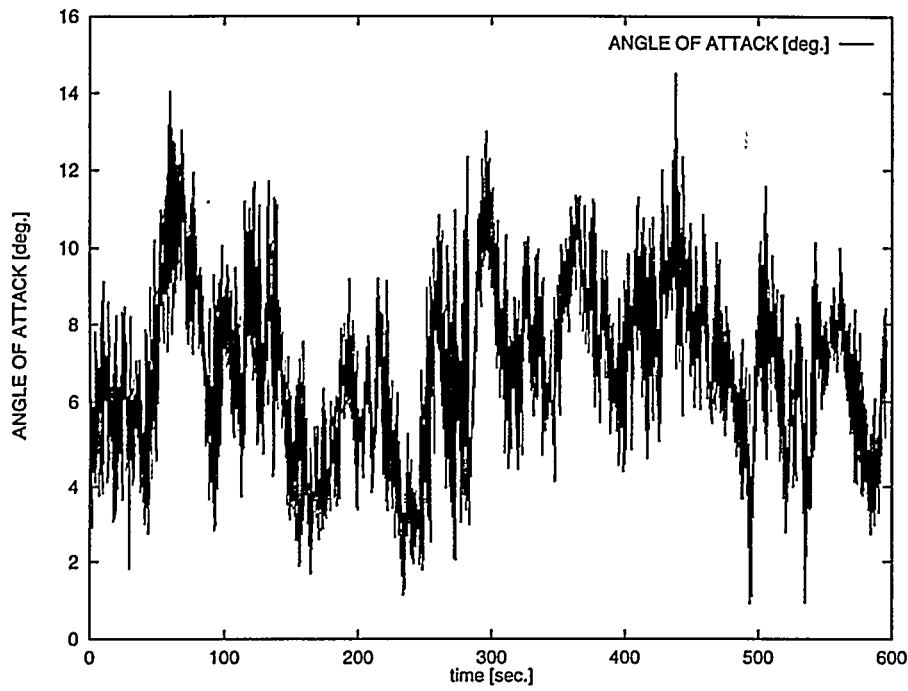
Figure 6-3 Time trace of angle of attack, file tl200101.
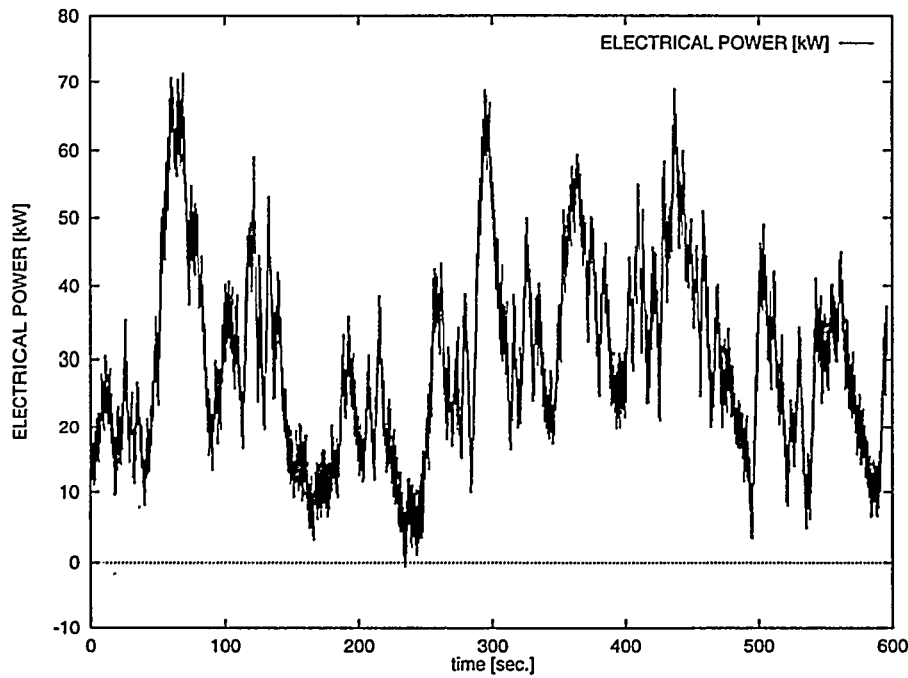
Figure 6-4 Time trace of electrical power, file tl200101.
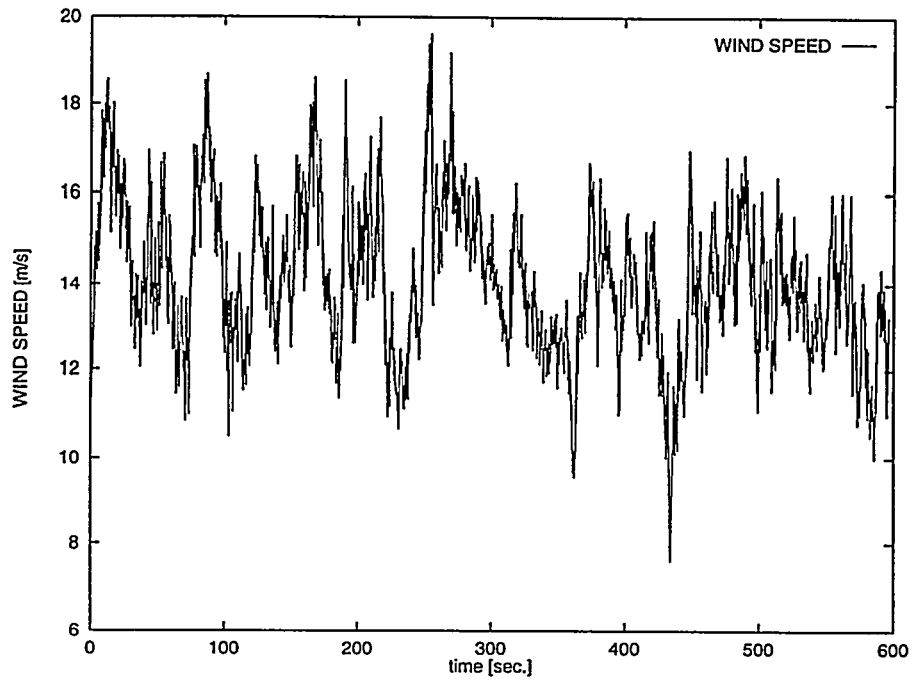
Figure 6-5 Time trace of wind speed, file 210101.
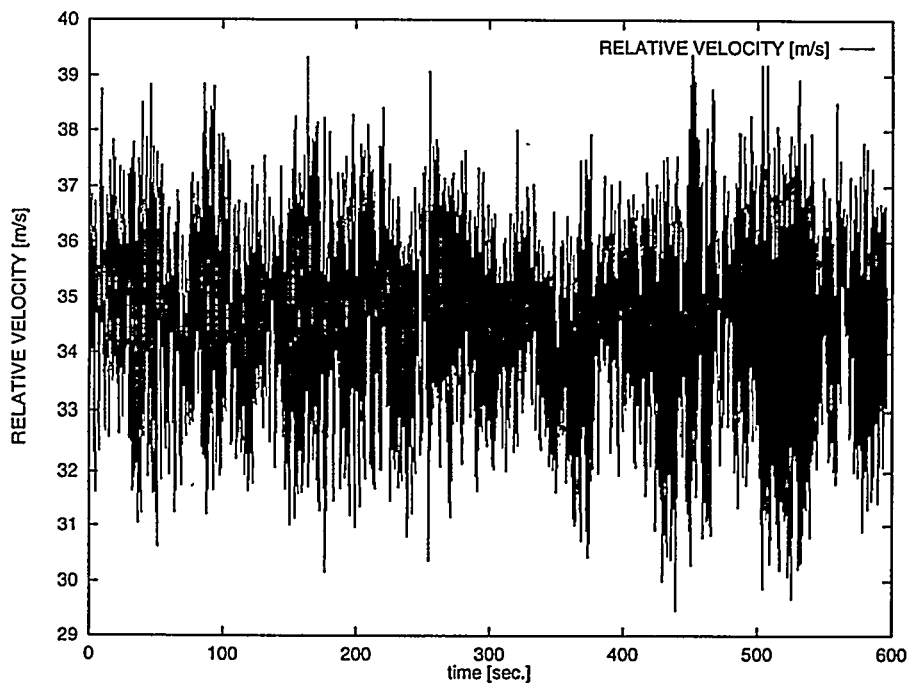
Figure 6-6 Time trace of relative velocity, file tl210101.
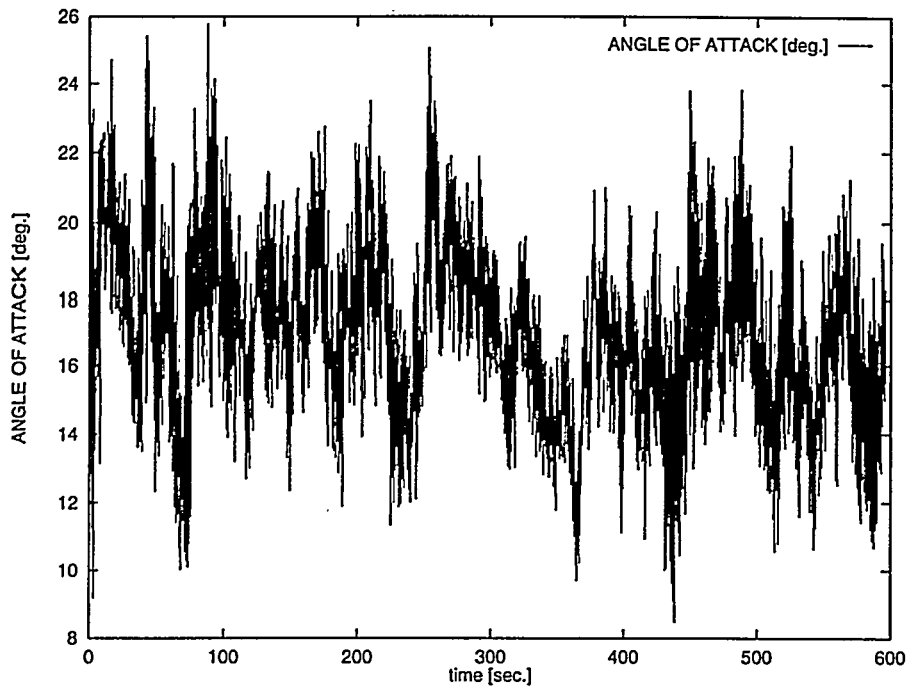
Figure 6-7 Time trace of angle of attack, file tl210101.
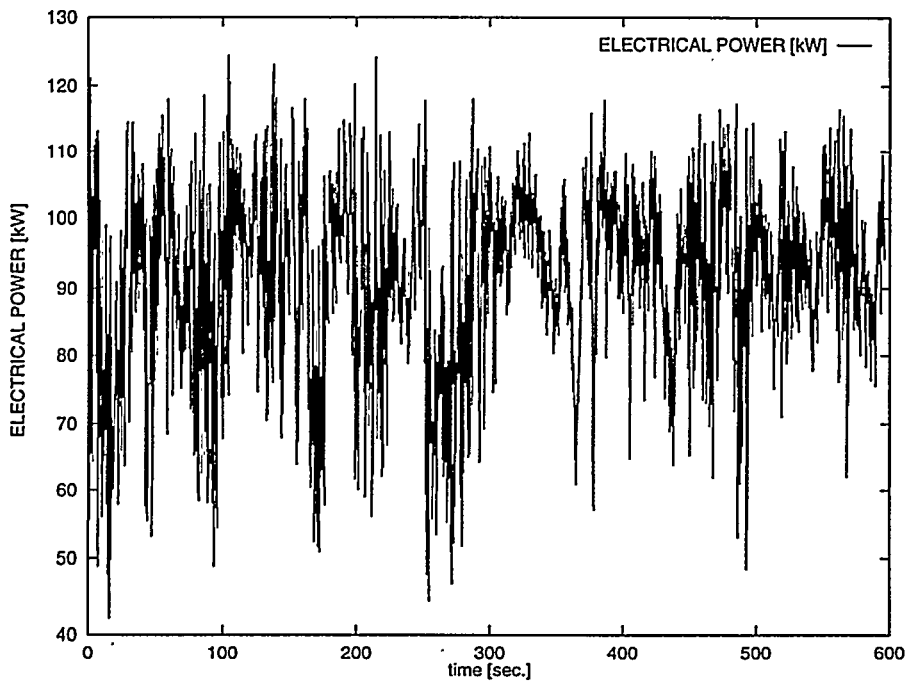
Figure 6-8 Time trace of electrical power, file 210101.
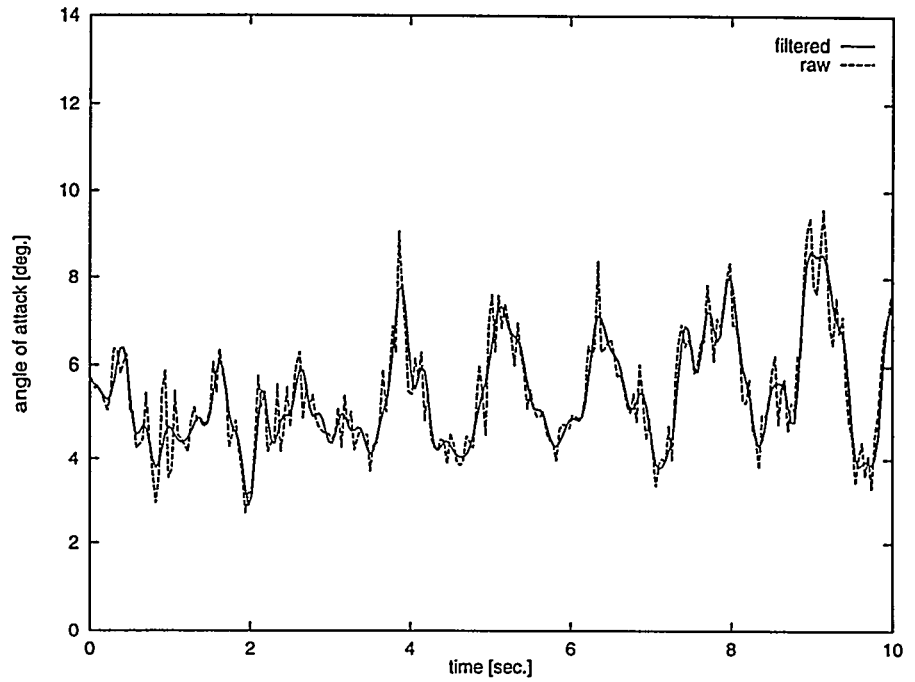
Figure 6-9 Effect of applying the filter seen on a time trace.
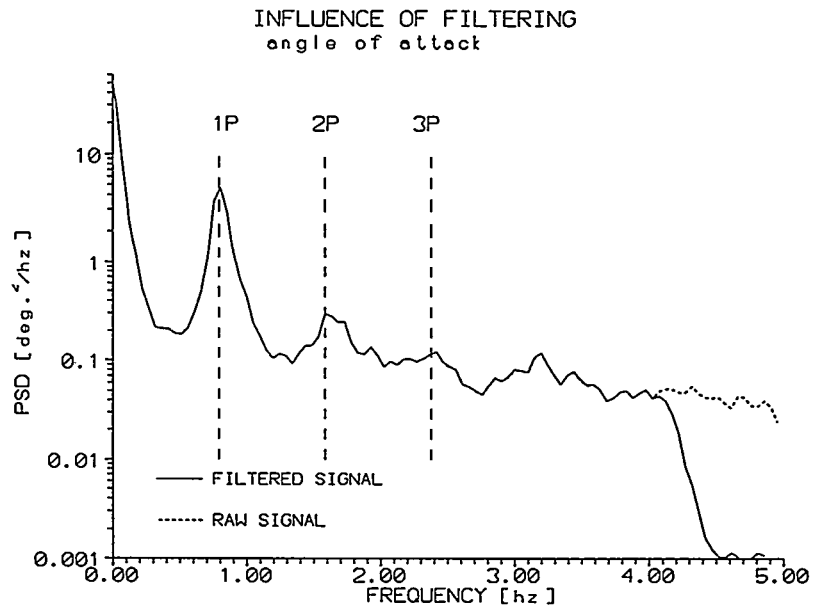
Figure 6-10 Effect of applying the filter seen on a power spectral density plot of angle of attack.

COHERENCE
Attack - CN2
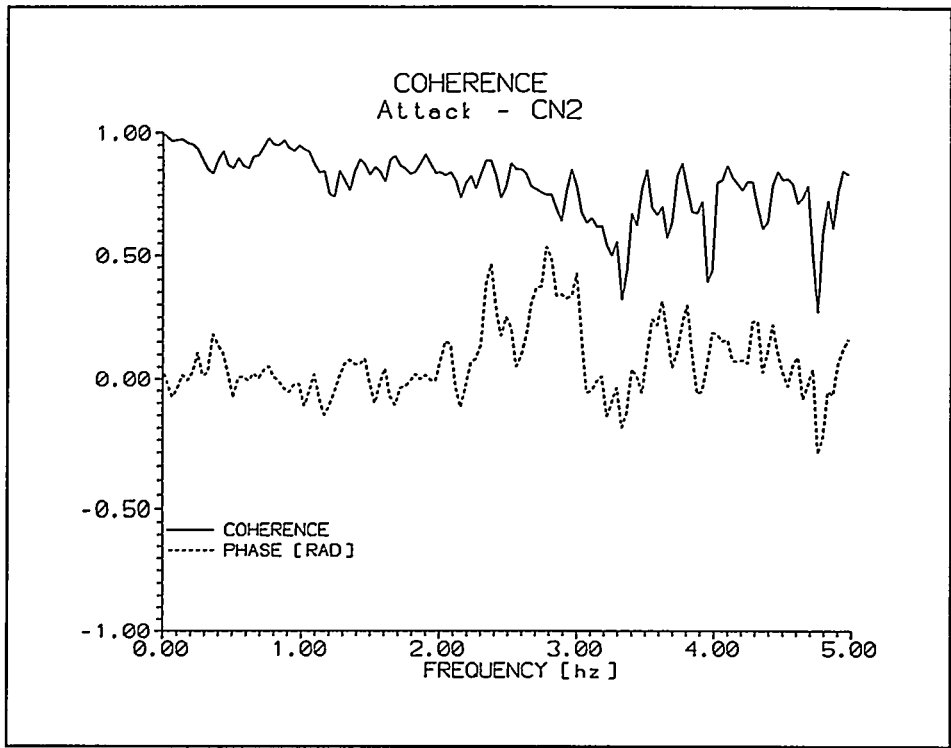
Figure 6-11 The coherence function between angle of attack α and the normale force coefficient C_N.

TRANSFER FCT.
Attack - CN2
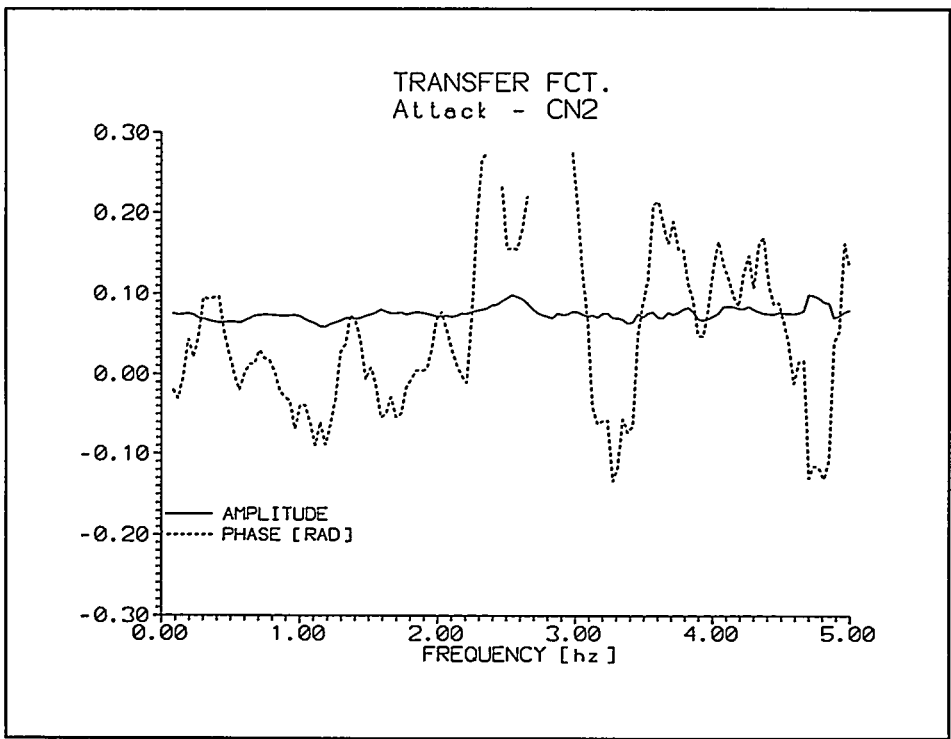
Figure 6-12 Transfer function between α and C_N.
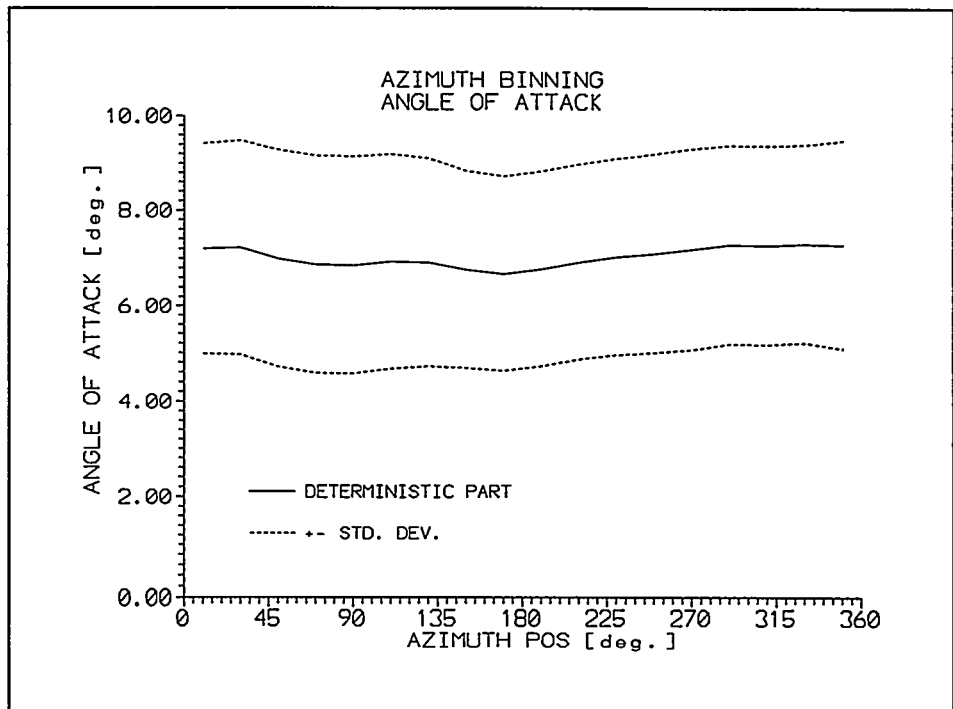
Figure 6-13   Azimuth binning of α.
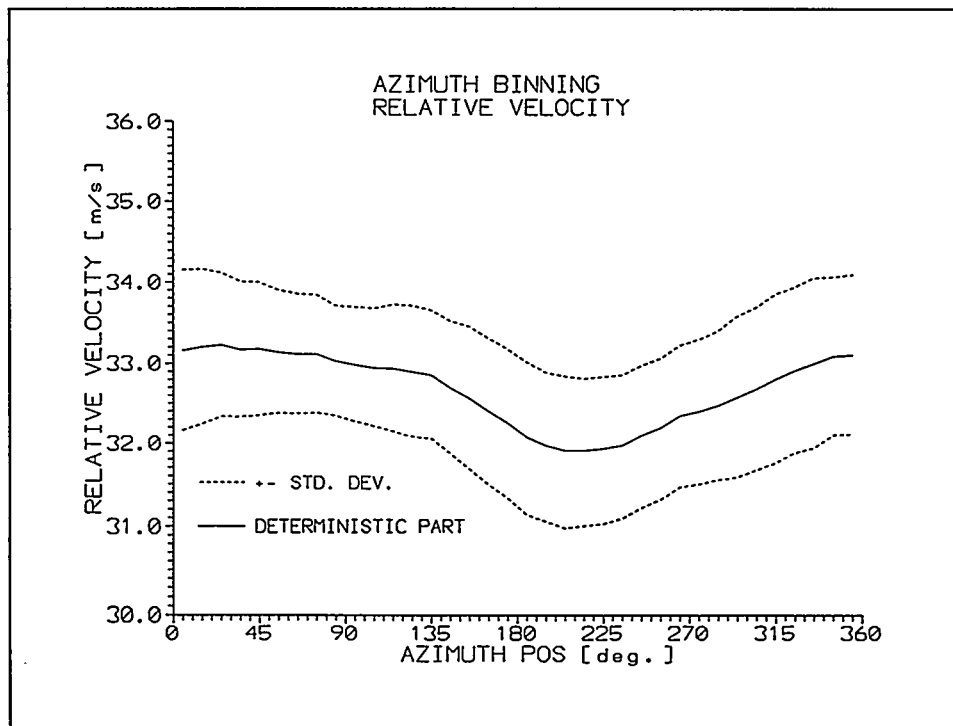
Figure 6-14   Azimuth binning of w.
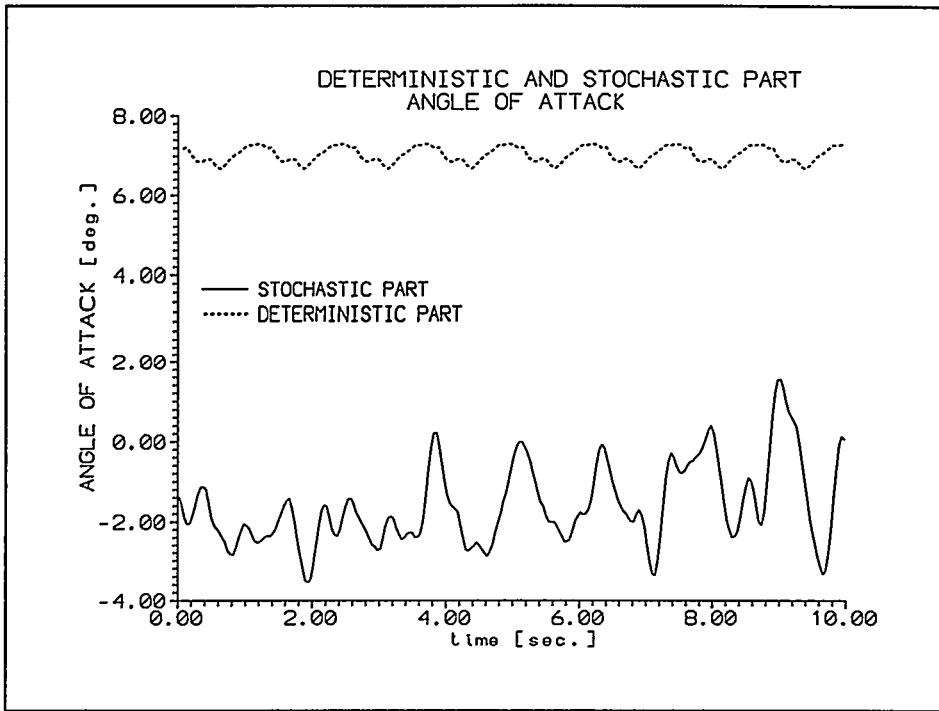
Figure 6-15   Time traces of the deterministic and stochastic parts of α.
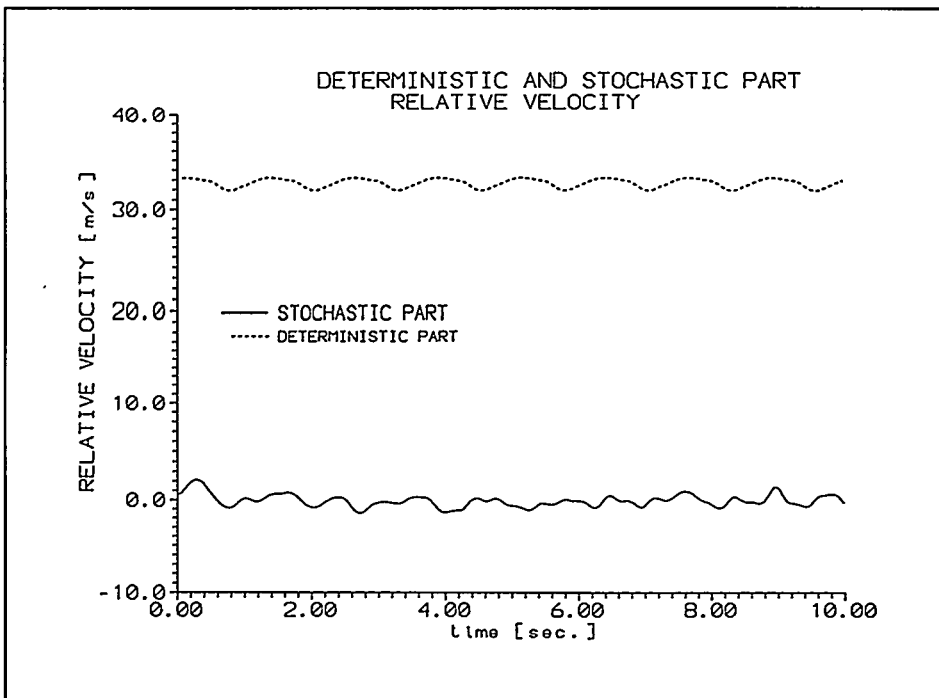
Figure 6-16   Time trace of the deterministic and stochastic parts of w.
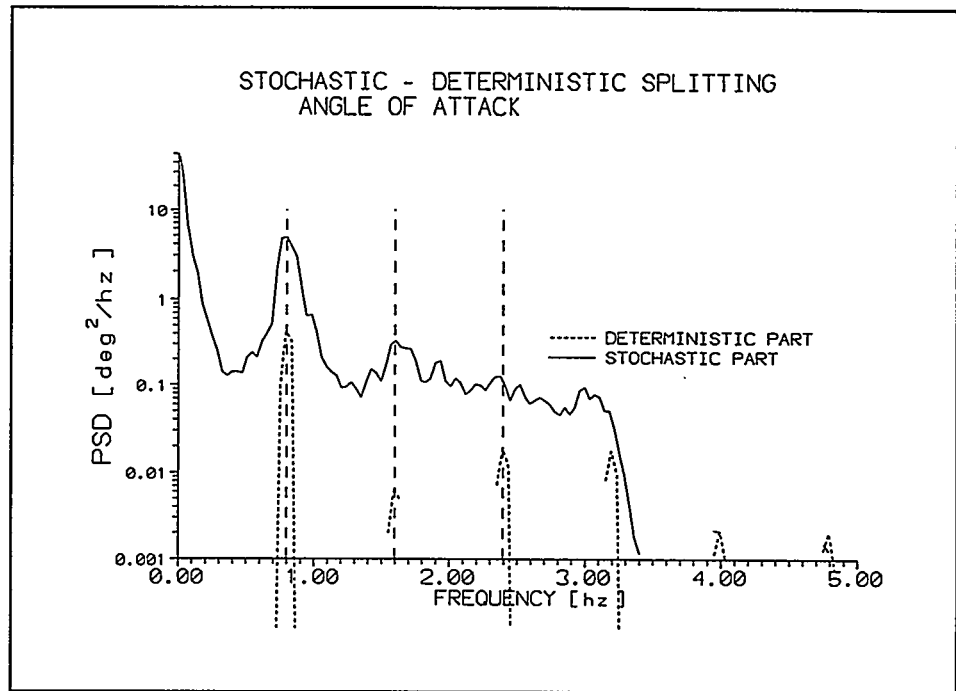
Figure 6-17   Power spectra of the deterministic and stochastic part of α.
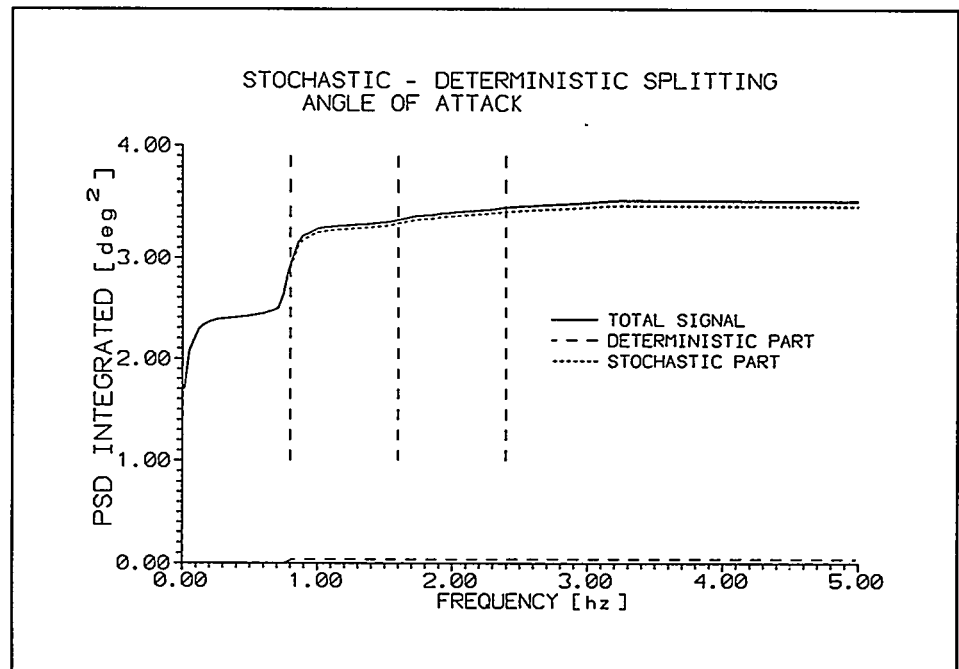
Figure 6-18   Integration of the PSD spectrum in Figure 6-17.
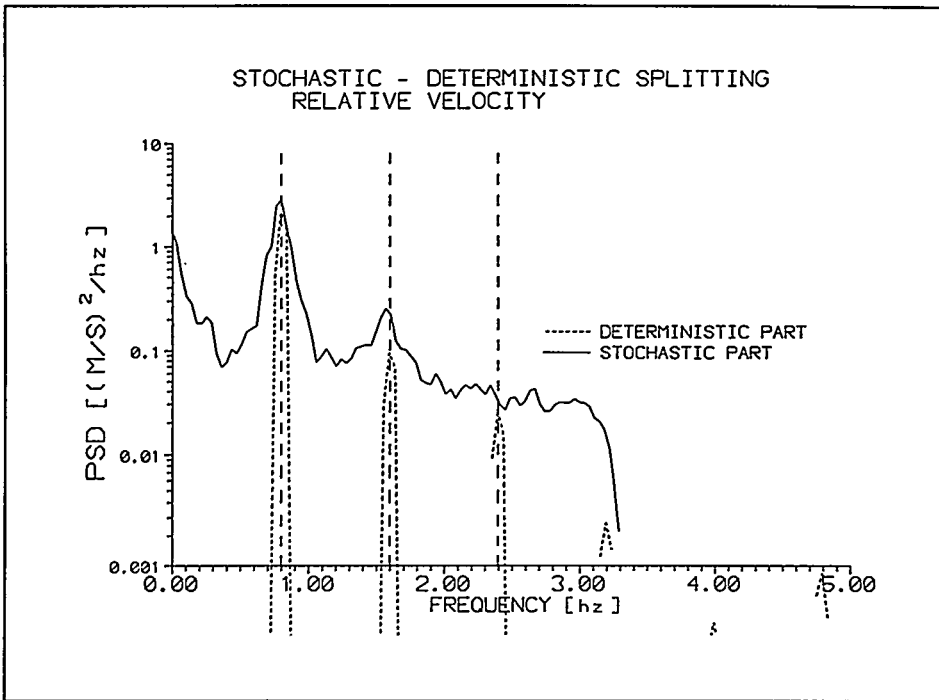
Figure 6-19   Power spectrum of the deterministic and stochastic part of w.
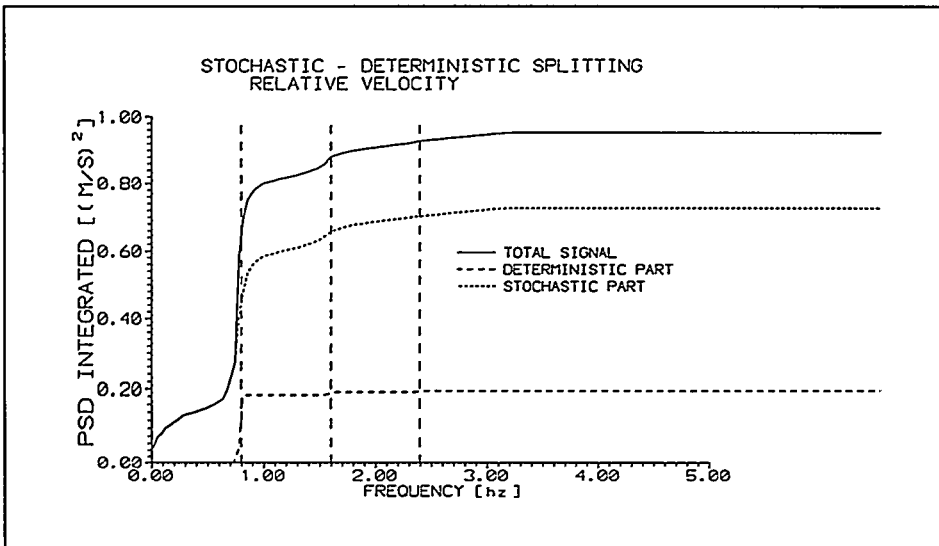
Figure 6-20 ·Integration of the PSD spectrum in Figure 6-19.
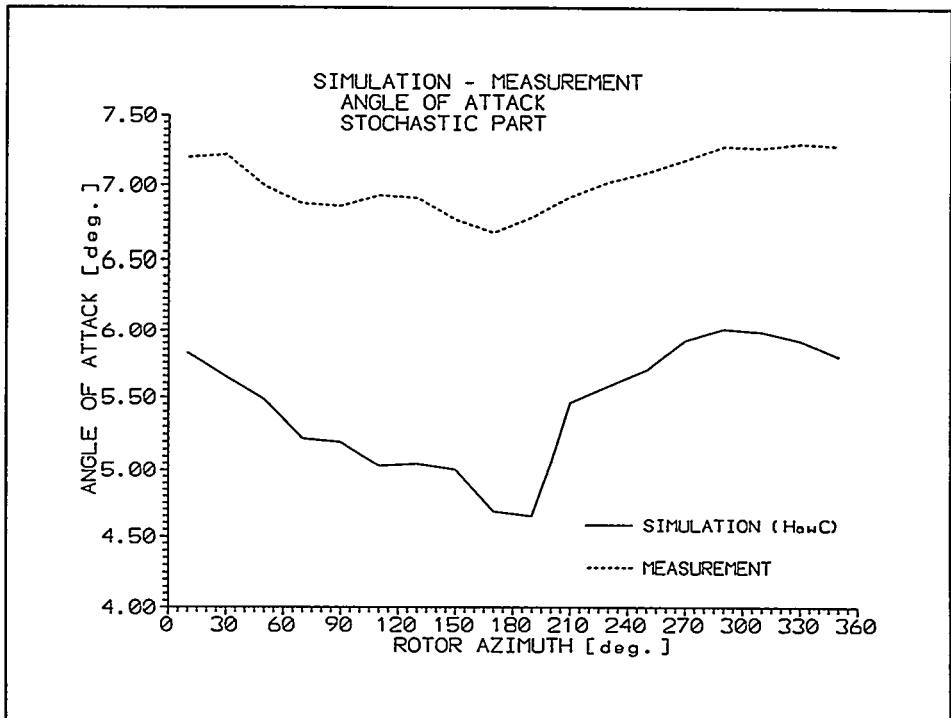
Figure 6-21   Comparison of simulated and measured azimuthal variation of α.
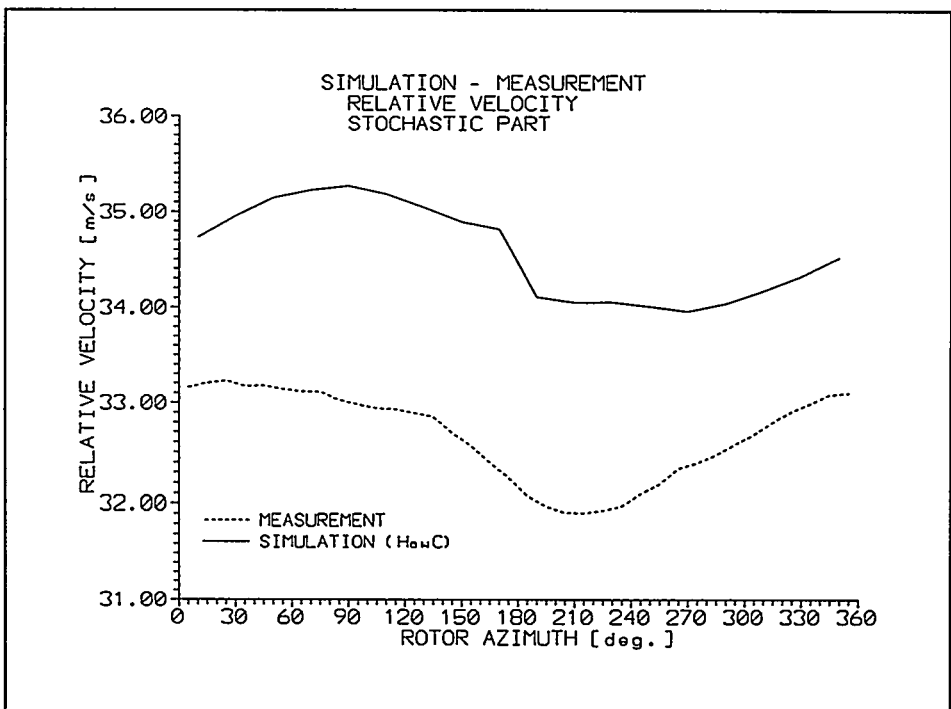
Figure 6-22   Comparison of simulated and measured azimuthal variation of w.
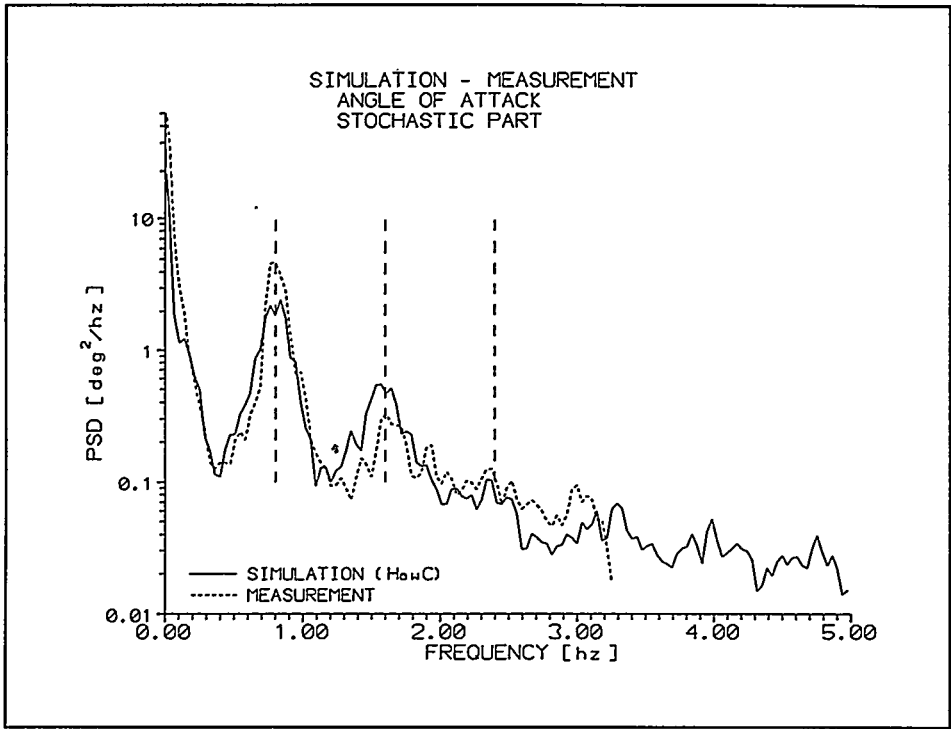
Figure 6-23   Power spectrum of simulated and measured α.
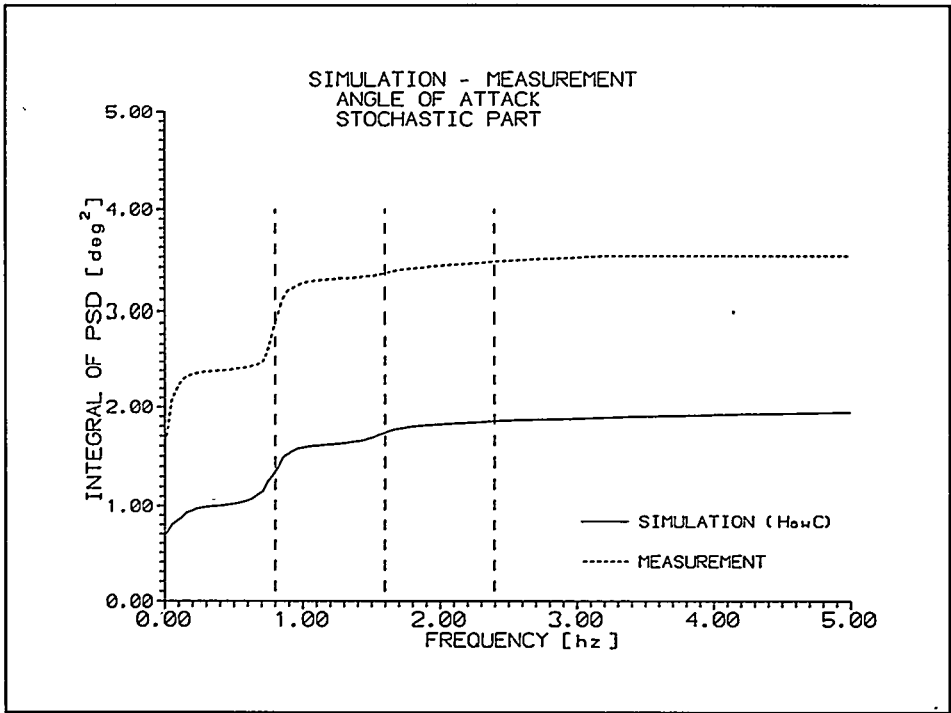
Figure 6-24   Integration of the power spectra in Figure 6-23.
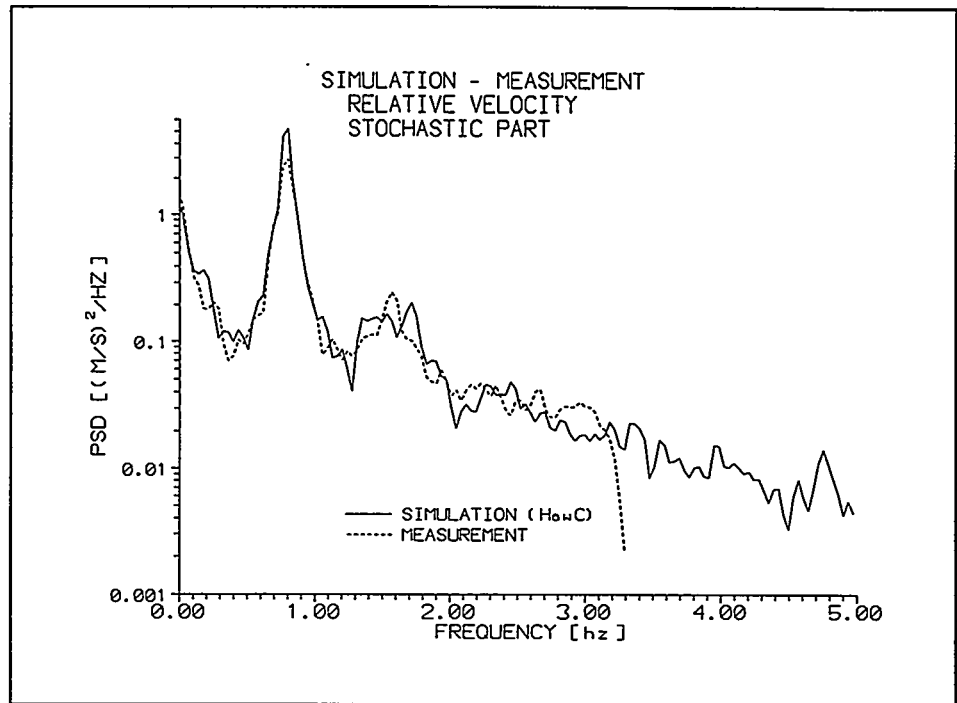
Figure 6-25   Power spectra of simulated and measured w.
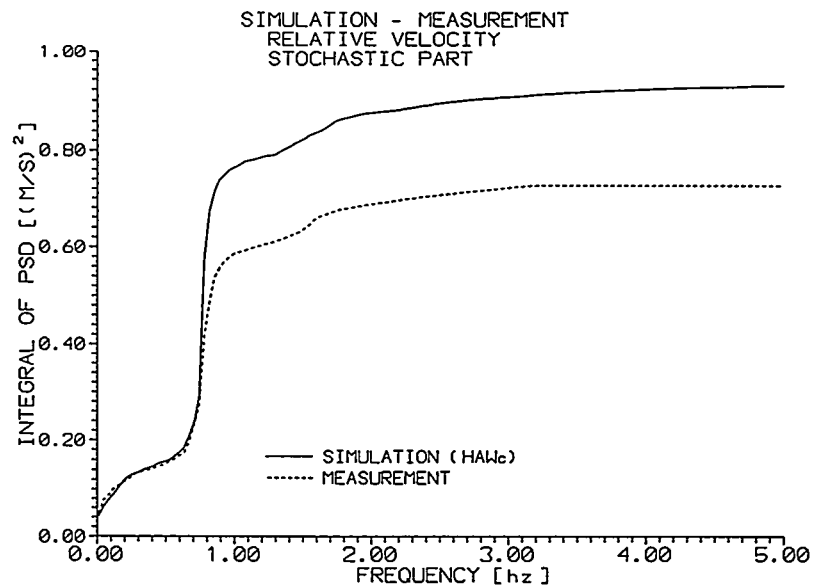
Figure 6-26   Integration of the spectra in Figure 6-25.
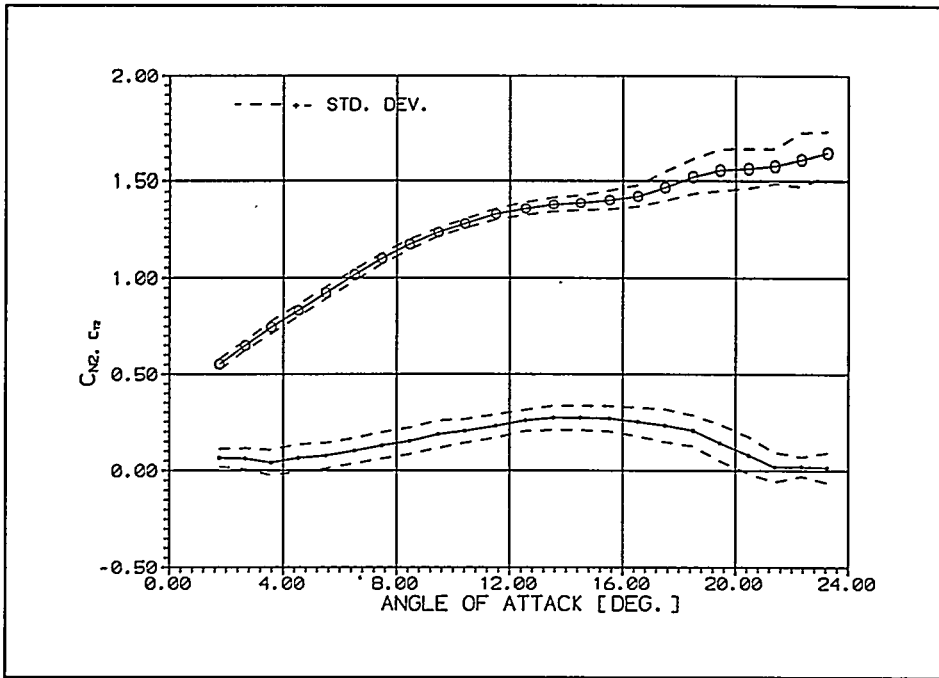
Figure 6-27 C_N and C_T vs. α curves based on the final processed data sets.
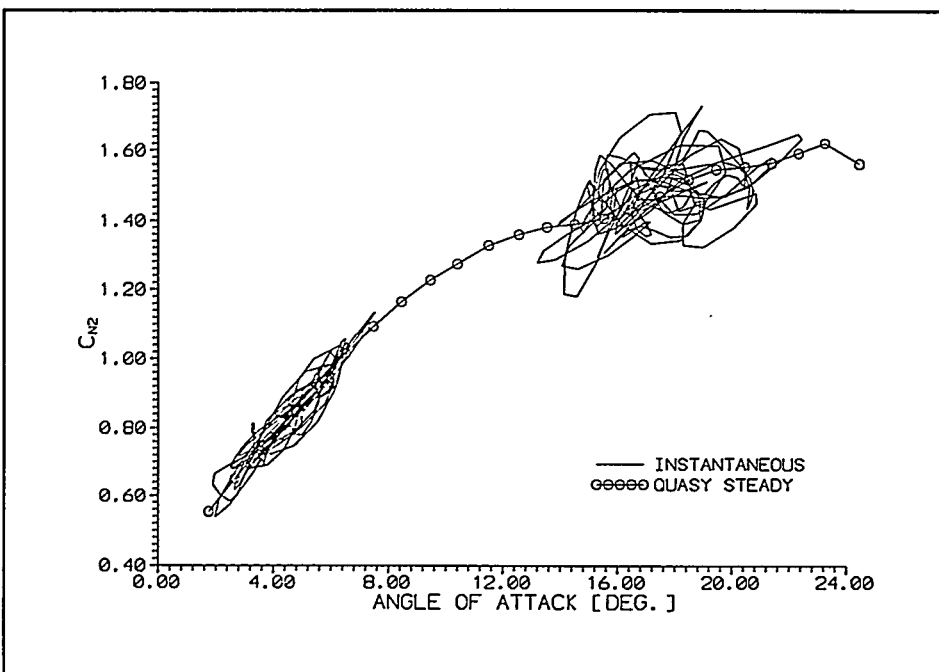
Figure 6-28   Instantaneous C_N vs. α relation below stall and above stall.

7 Data from NREL

7.1 Background

Although NREL has not participated in the present project it was decided to process some of the data they have supplied to the IEA Annex XIV data base. NREL has also participated as observer at some of the STALLVIB meetings and contributed in discussions of the field rotor data sets.

7.2 Experimental set-up

Details about the NREL experiments and an overview of their data con be found in [7-1] so only a brief description of their experimental setup will be presented here.

A 10 m diameter turbine with pitchable blades has been used as test bed. The turbine has been run with different blades during the measurement campaign but the data in the present report from phase IV of the measurements are for a twisted blade with constant chord and using the NREL S809 airfoils. Surface pressure measurements were performed at five radial stations and correlated with inflow measurements from five, five hole pitot tubes.

7.3 Overview of data and data processing

The files in the data base are 60 sec. long and stored with 52 Hz sampling rate. Before the data files have been stored in the data base they have been passed through a 4-pole 10 Hz Butterworth filter. Five data files from the 67 % radial station have been concatenated to one 300 sec long file covering inflow conditions from low angle of attack α to 30-35 deg. Figure 7-1 to Figure 7-3. The turbine is a downwind turbine and the tower shadow is visible in the angle of attack signal, Figure 7-4. It should also be noted that the uncorrected α is used here. In the data base there is also a corrected α where the influence from the upwash is considered.

The data have been further processed for use in the present project. First the sampling rate was reduced to 25 Hz by interpolation of the data. 25 Hz was used by Risø in their measurements and it was found convenient to have the data at the same scan rate for the further processing. Then the data was passed through a low pass filter with a cut off frequency of 4 Hz which let the 3p component almost undamped, Figure 7-5 to Figure 7-7. As the time derivative is needed in one of the stall hysteresis models for which the data files have been used this derivation is illustrated in Figure 7-8. The time derivative is derived using a savitsky-golay filter [7-2] which uses 4 double sided points around the actual point Figure 7-8.

7.4 The final data sets

Using the final processed data the C_N, C_T coefficients and the electrical power have been binned vs. α, Figure 7-9 and Figure 7-10. It is seen that the total data set covers the power interval from zero power to deep stall.

Finally, instantaneous C_N vs. α has been plotted together with the quasy steady C_N curve, Figure 7-11. Even at low α the hysteresis loops are big and this is somewhat surprising when compared with results from simulations with empirical stall hysteresis models in this area with no separation. One reason for the big loops could be that the dynamic pressure used to non-dimenzionalize C_N is not in complete phase with the forces on the airfoil. In the present case the stagnation pressure measured on the airfoil was used as a basis for non-dimenzionalizing. As the dynamic pressure is also measured with the five hole pitot tube a recalculation of C_N using this pressure as a basis was carried out, Figure 7-12. However, the general character of the loops has not changed.

7.5 References

[7-1]
Schepers, J.G. et al. "Final Report of IEA Annex XIV: Field Rotor Aerodynamics". ECN-C-97-027. June 1997
[7-2]
Press, W.H. et al. "Numerical Recipes in C". Cambridge University 1988.

7.6 Figures
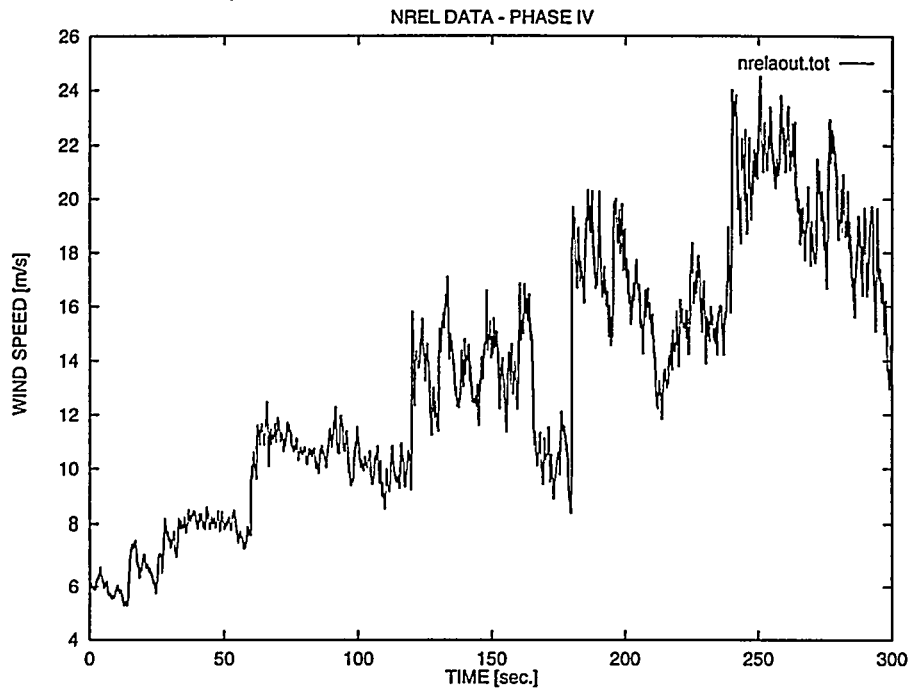
Figure 7-1   The total time series is a concatenation of 5 separate 60 sec. times series.
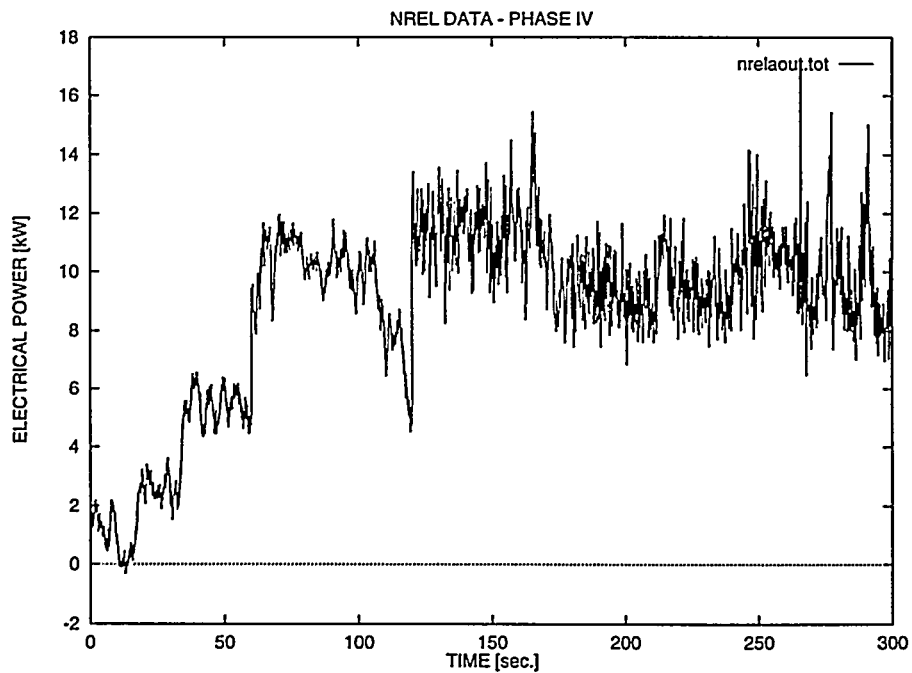
Figure 7-2   The electrical power for the for the total time trace.
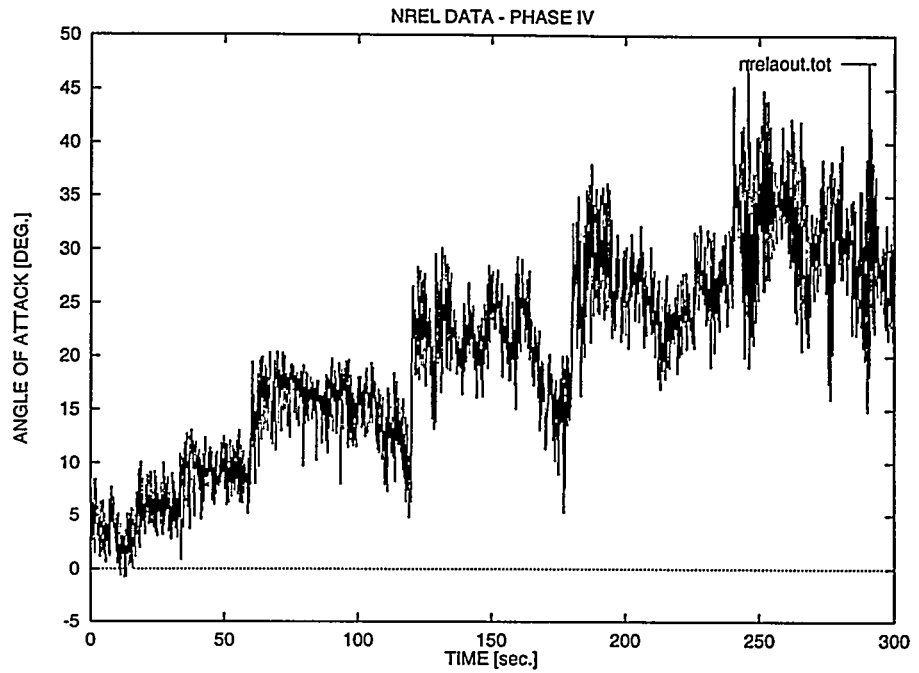
Figure 7-3   The angle of attack (uncorrected) for the total time series.
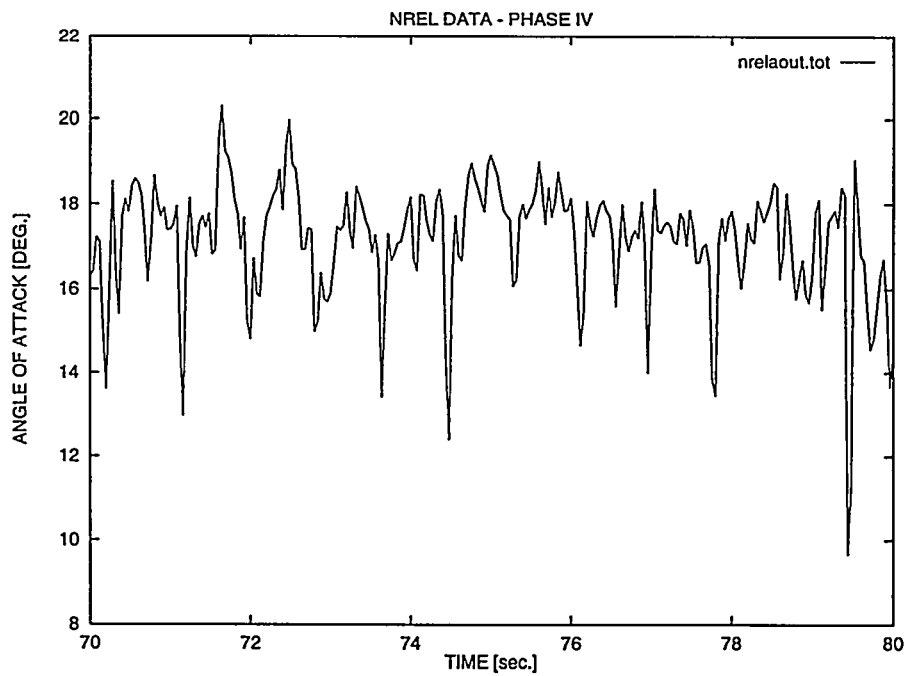
Figure 7-4   A 10 sec. time sequence of the angle of attack where the influence from the tower shadow is visible.
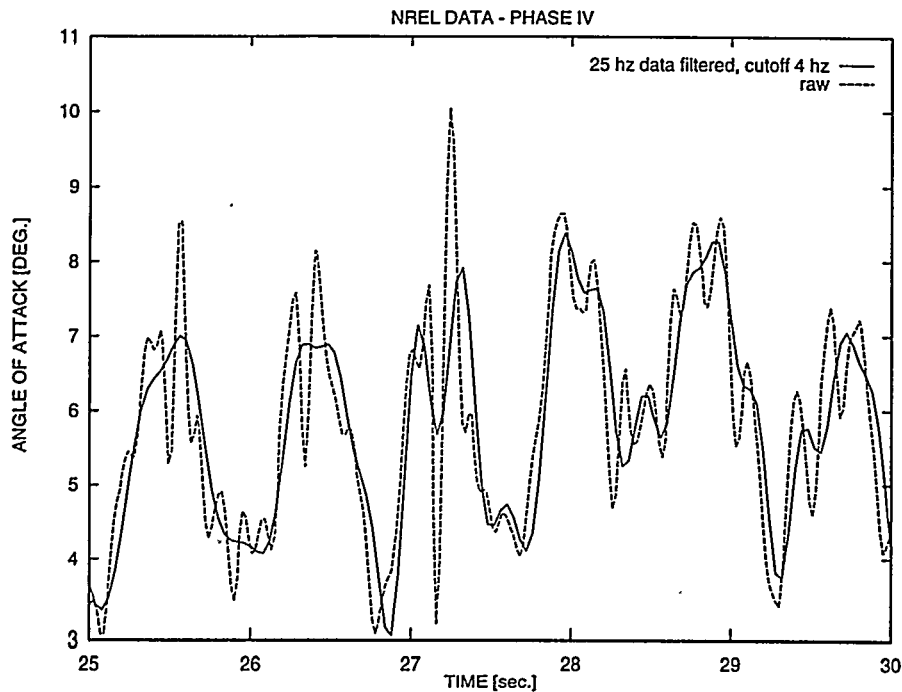
Figure 7-5 The raw data compared with averaged data (first block averaged to 25 Hz and then low pass filtered with a cut off frequency of 4 Hz).
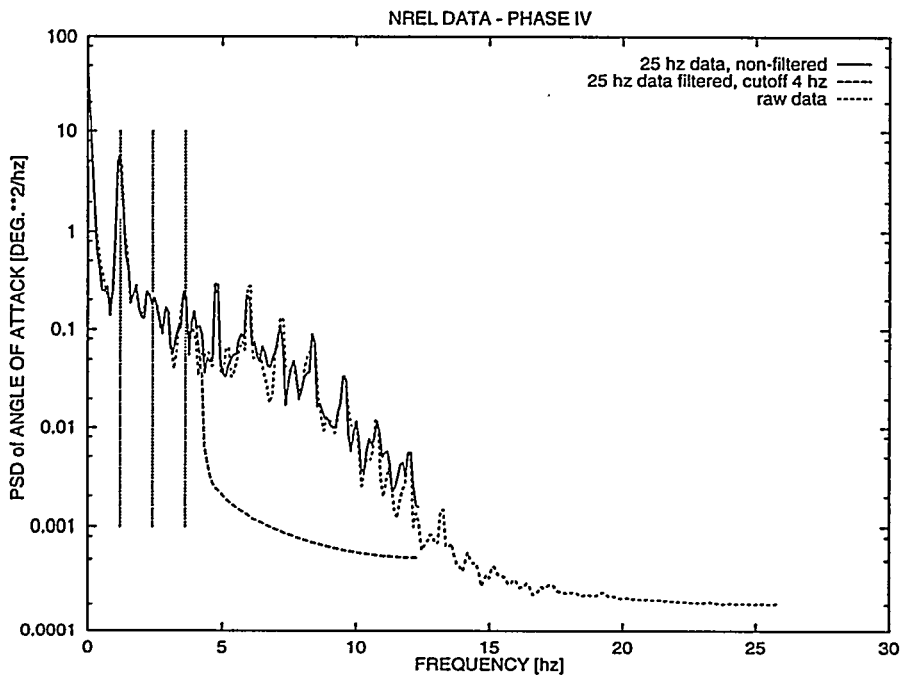
Figure 7-6 Power spectra of the same data as shown in Figure 7-5.
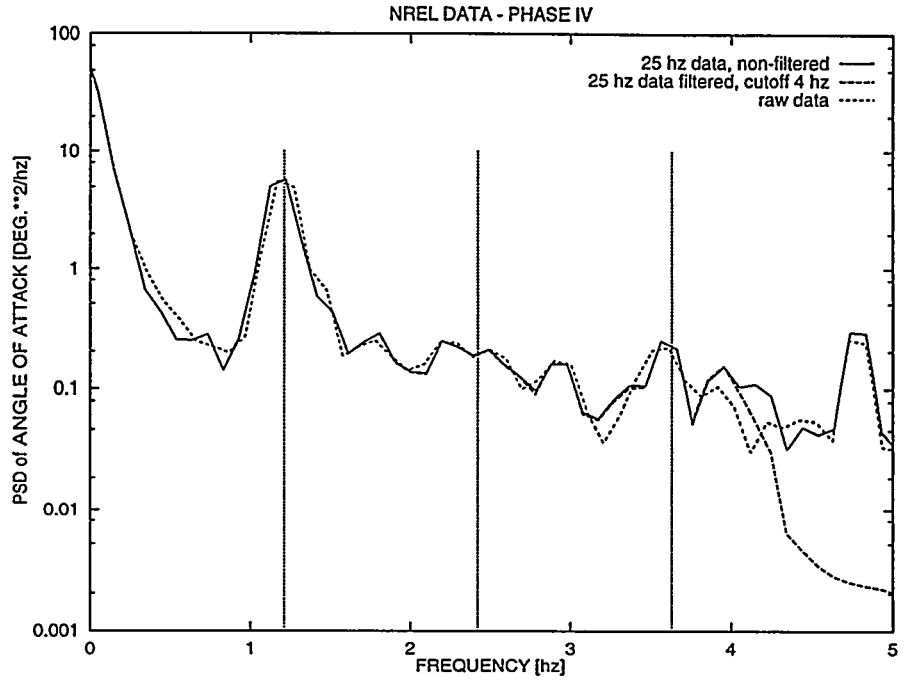
*Figure 7-7   Details at the low frequencies of Figure 7-6 with the position of
1p, 2p and 3p illustrated with vertical lines.*
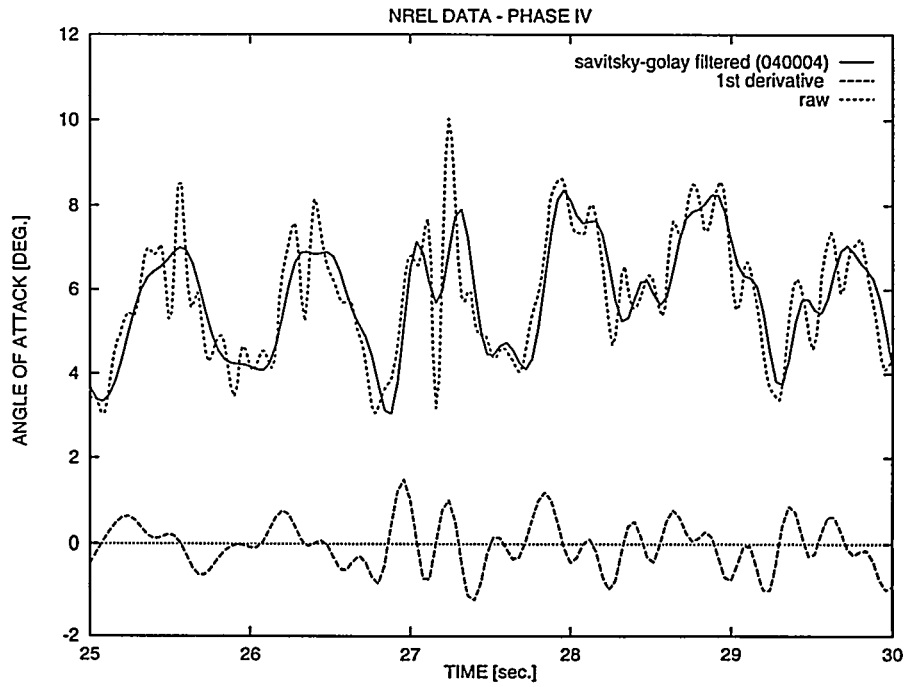
*Figure 7-8   The time derivatives of the angle of attack, used stall hysteresis
modelling, are derived by a savitsky-golay filter.*
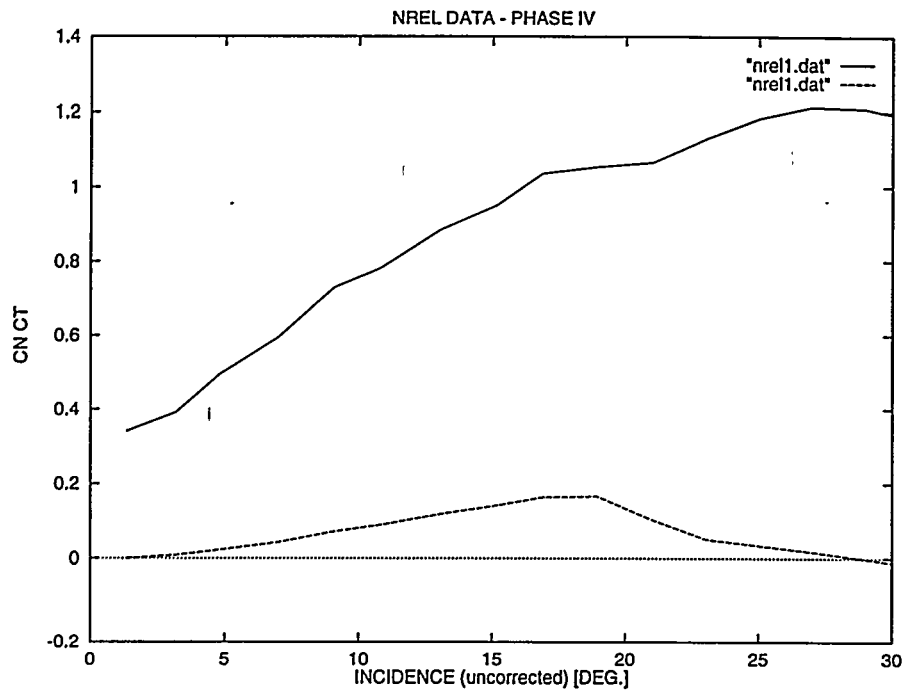
Figure 7-9 The normal and tangential force coefficients binned on angle of attack.
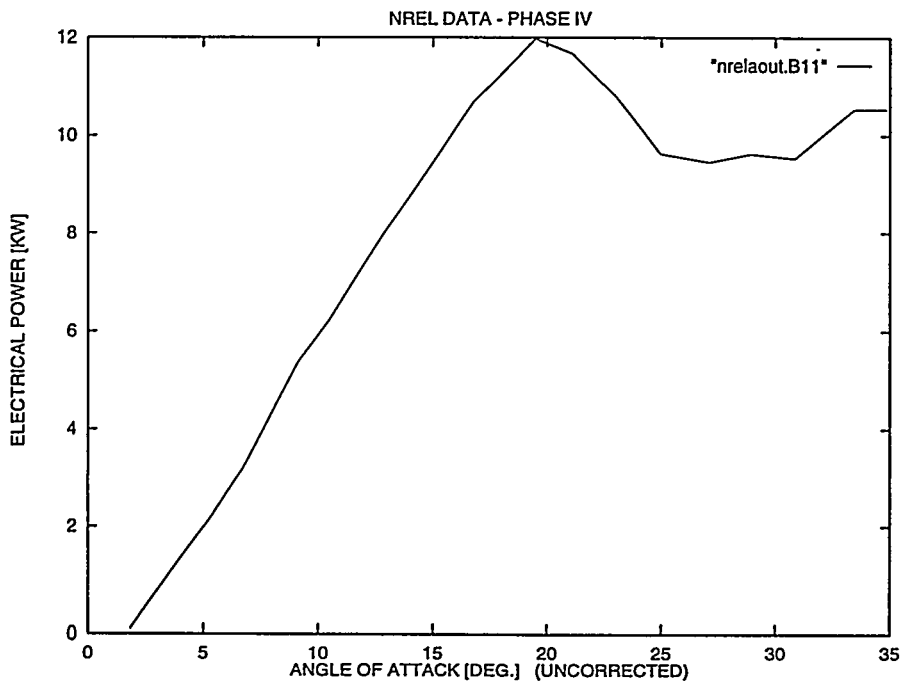
Figure 7-10 The electrical power binned as function of angle of attack.

NREL DATA - PHASE IV
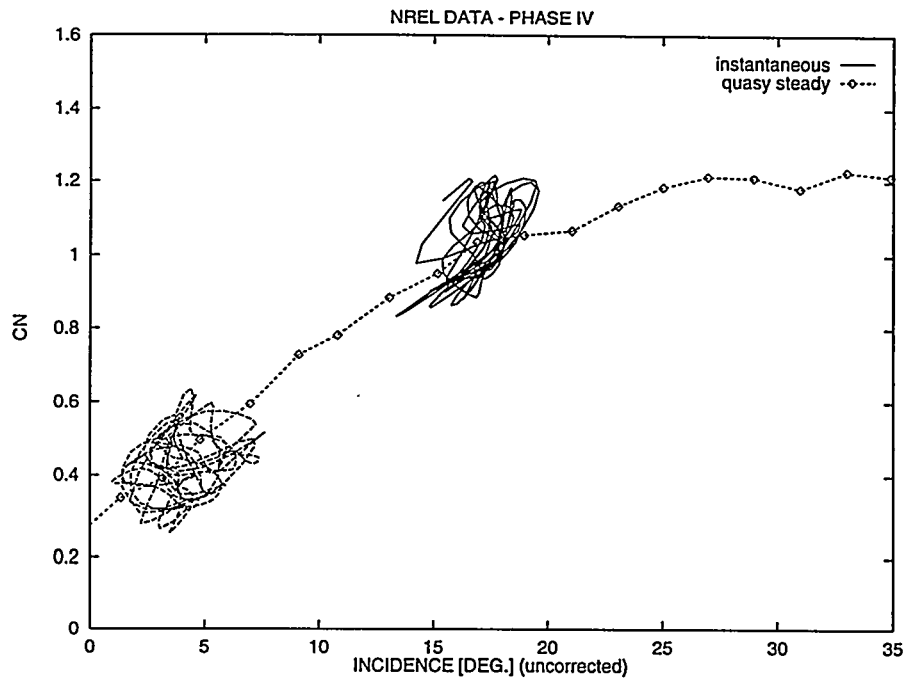
Figure 7-11   Hysteresis loops showed as instantaneous C_N vs. angle of attack. C_N normalized with airfoil stagnation pressure.

NREL DATA - PHASE IV
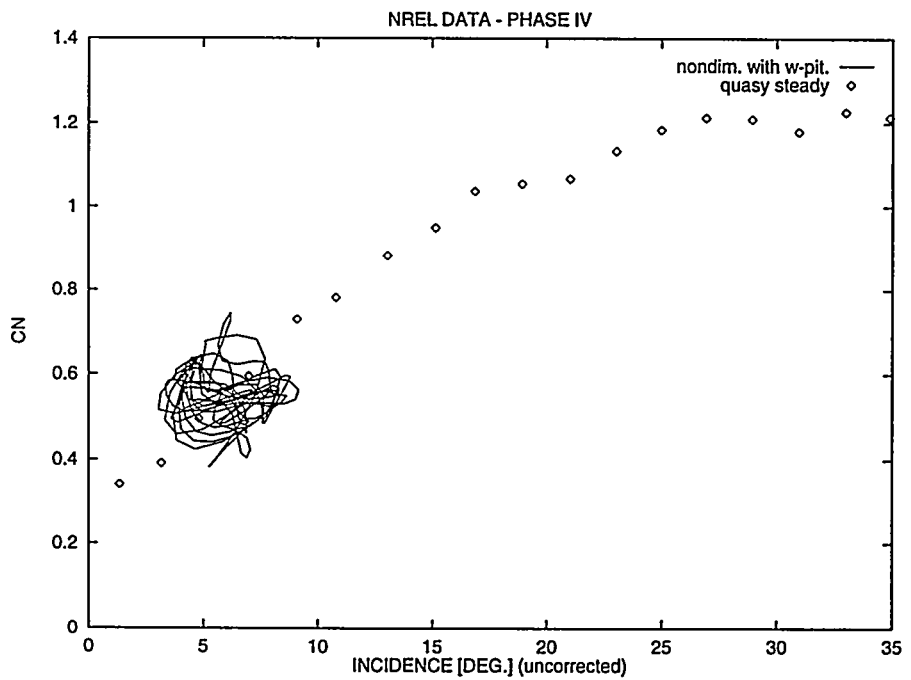
Figure 7-12 Hysteresis loops showed as instantaneous C_N vs. angle of attack. C_N normalized with the five hole pitot tube stagnation pressure

8 Concluding remarks and an example of use of the data

A detailed investigation of the influence of the postprocessing of the different data sets has been performed. Further, important statistical functions such as PSD spectra, coherence and transfer functions have been derived for the data sets which can be used as basis for evaluation of the quality of the data seen relative to actual application of the data. The importance of using an appropriate low pas filtering to remove high frequency noise has been demonstrated when the relation between instantaneous values of e.g. α and C_N is considered.

In general, the complicated measurement on a rotor of α and w and the interpretation of these parameters combined with the strongly three-dimensional, turbulent flow field around the rotating blade has the consequence that it seems difficulty to derive systematic information from the different data sets about stall hysteresis. In particular, the measurement of α, which has been performed by different methods, is complicated. Derivation of α on basis of determination of the stagnation point gives reasonable data below stall but fails in stall. Measurements of α with a five hole pitot tube seems to give reasonable results. Another main problem is the non-dimensionalisation of the coefficients C_N and C_T. If the dynamic pressure used for the non-dimensionalization is not fully correlated with the aerodynamic pressure over the considered airfoil section due to e.g. influence of the gravity on the pressure pipes, the hysteresis loops will be distorted.

However, using the data with caution and applying a suitable postprocessing as described by the different participants it will probably be possible to obtain some information of stall hysteresis from the field rotor data. An example of extracting information from one of the data sets is demonstrated below.

8.1 An example of use of data

As an example of use of the data the determination of the empirical functions in the fgh stall hysteresis model will be shown The fgh stall model [8-1], [8-2] was originally developed with the particular objective to study the general characteristics of the field rotor data. The basic assumption in the model is that the hysteresis loops can be derived on basis of the variations of the angle of attack α and the relative velocity w and the time derivatives of these two parameters:

$$C_N = C_{N,q}(\alpha) + f(\alpha)\frac{c}{w}\frac{d\alpha}{dt} + g(\alpha)\left(\frac{c}{w}\right)^2\frac{d^2\alpha}{dt^2} + h(\alpha)\frac{c}{w^2}\frac{dw}{dt}$$

$$(8-1)$$

Here $C_{N,q}$ means the quasy steady normal force coefficient, c is the chord length and the f,g and h are empirical functions of α which have to be determined on basis of experiments.

In the present case f,g,h were derived by numerical optimisation in order to minimise the deviation between simulated and measured C_N for some time series. Using the two data files tl200101 and tl210101 shown previously in paragraph 6 the f,g and h functions shown in Figure 8-1 were derived. The f function controls mainly the opening of the hysteresis loops whereas the g function

controls the effective slope of the hysteresis loops, seen relative to the slope of the quasy steady values. Finally, the h function gives the influence of the varying velocity and has considerable influence on the size of the loops as will be shown below.

Generated data with the model using the measured variations of α and w are compared with measurements in Figure 8-2 to Figure 8-4. Below stall a good correlation is found whereas considerable deviations are found in stall and deep stall.

As the variations of the measured α and w have a big stochastic contents a better insight in the nature of the hysteresis of the data gathered through the f,g, and h functions can be visualised by using harmonic variations of α and w. The chosen amplitude for α is 2.5 deg. and 2 m/s for w. These data are close to measured standard deviations of the same two parameters on the turbine (Table 6-2). Three cases have been simulated; 1) w constant Figure 8-5 and Figure 8-6, 2) α and w in phase Figure 8-7 and Figure 8-8, and 3) α and w in counter-phase Figure 8-9 and Figure 8-10. With the harmonic input, regular loops are now observed and the overall characteristics of stall hysteresis known from wind tunnel measurements are found with the model tuned only on basis of the field rotor measurements. In the linear region below stall, the loops are counter-clockwise due to the shed wake effects. However, above stall, the viscous effects and the lag in the trailing edge separation are dominant and the direction of the loops changes to clockwise and the opening of the loops increases. It is also seen that w has a considerable influence on the loops depending on the phase between α and w. On a real rotor there will possibly be big variations of the phase and based on the present data it seems to be important to take into account the influnce on the hysteresis from the variations of w.
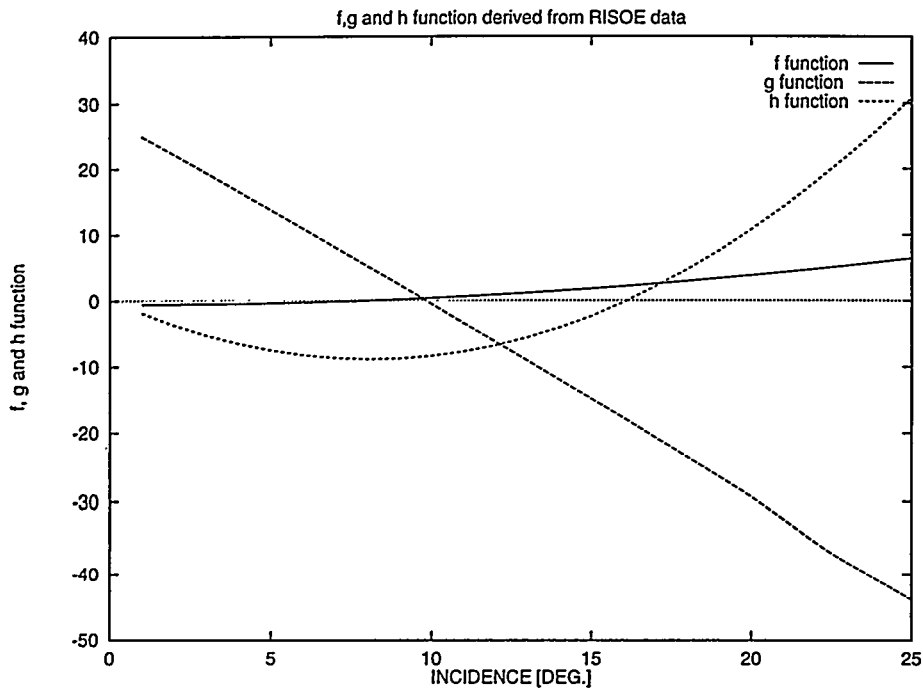
8.2 Figures

Figure 8-1   The f, g and h functions derived on basis of the Risoe data.
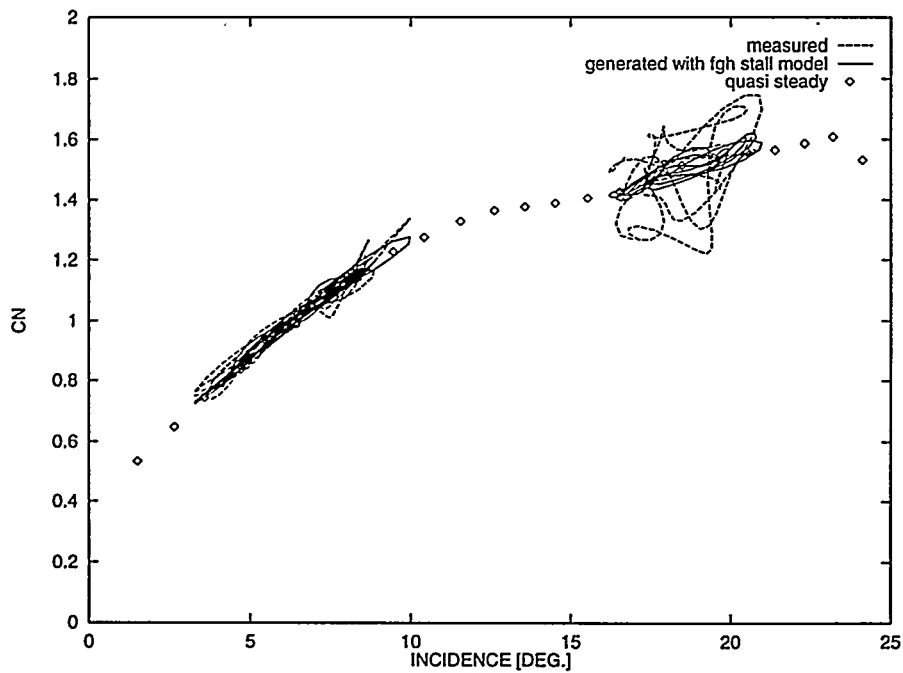

Figure 8-2   Generated hysteresis loops with the fgh model, compared with measurements
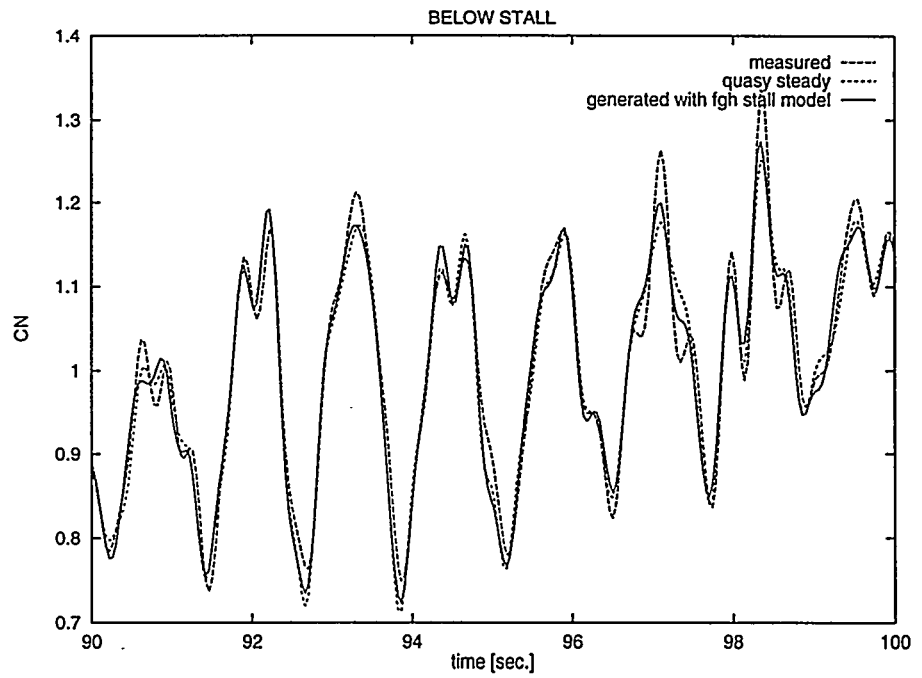
Figure 8-3 Time trace of generated hysteresis loops with the fgh model, compared with measurements. Operation below stall.
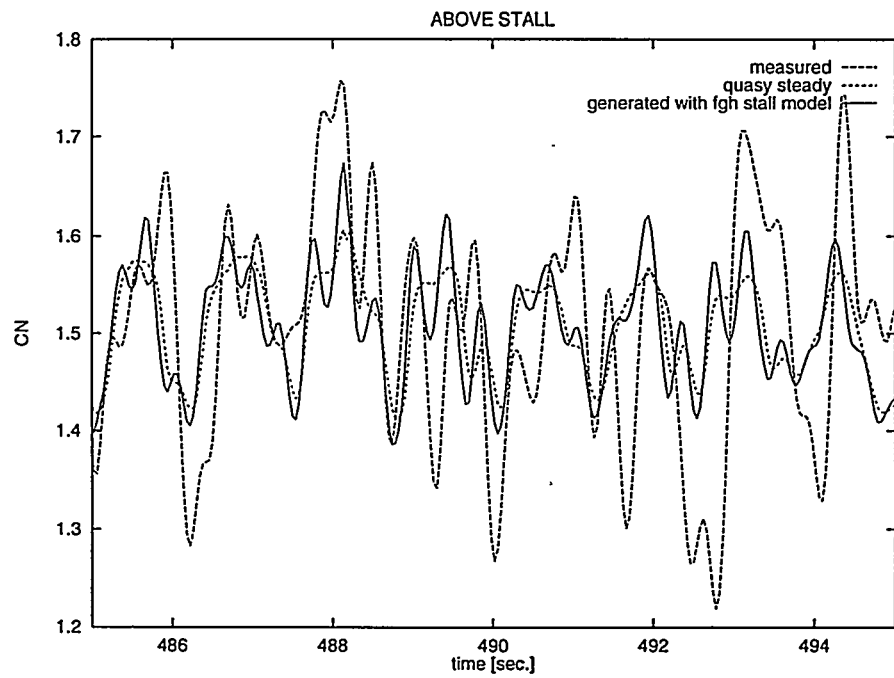

Figure 8-4 Time trace of generated hysteresis loops with the fgh model, compared with measurements. Operation above stall.
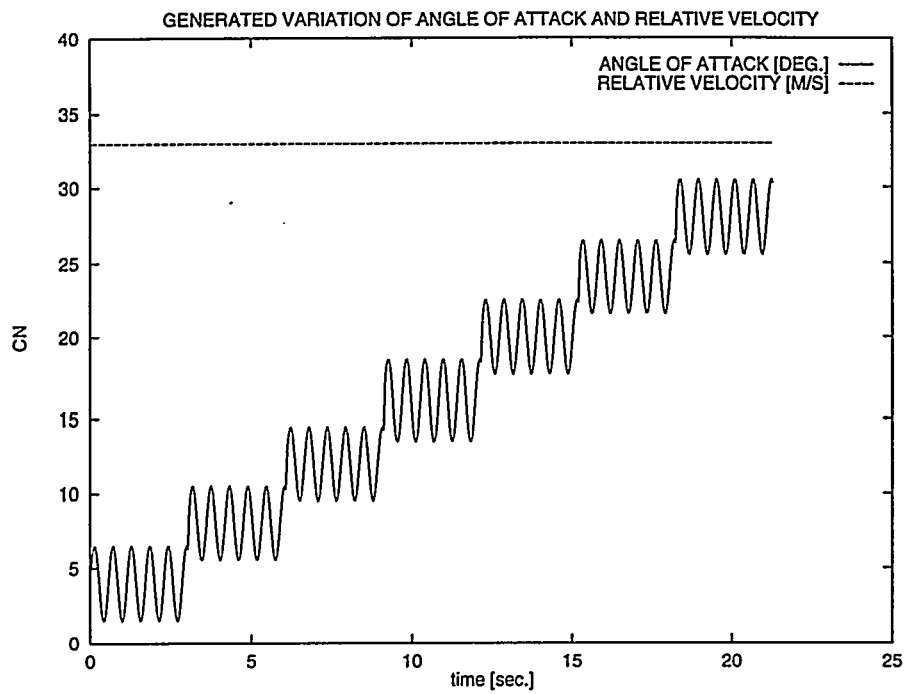
Figure 8-5   Harmonic variation of α and constant relative velocity w corresponding to a reduced frequency of 0.1.
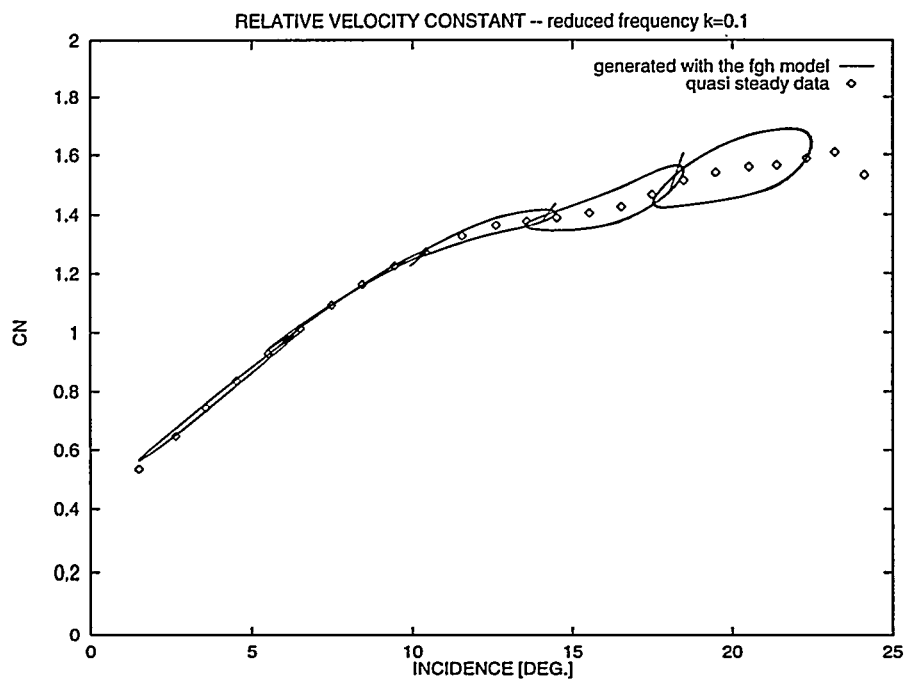
Figure 8-6   Generated hysteresis loops with variation of α and w as shown in Figure 8-5.

GENERATED VARIATION OF ANGLE OF ATTACK AND RELATIVE VELOCITY
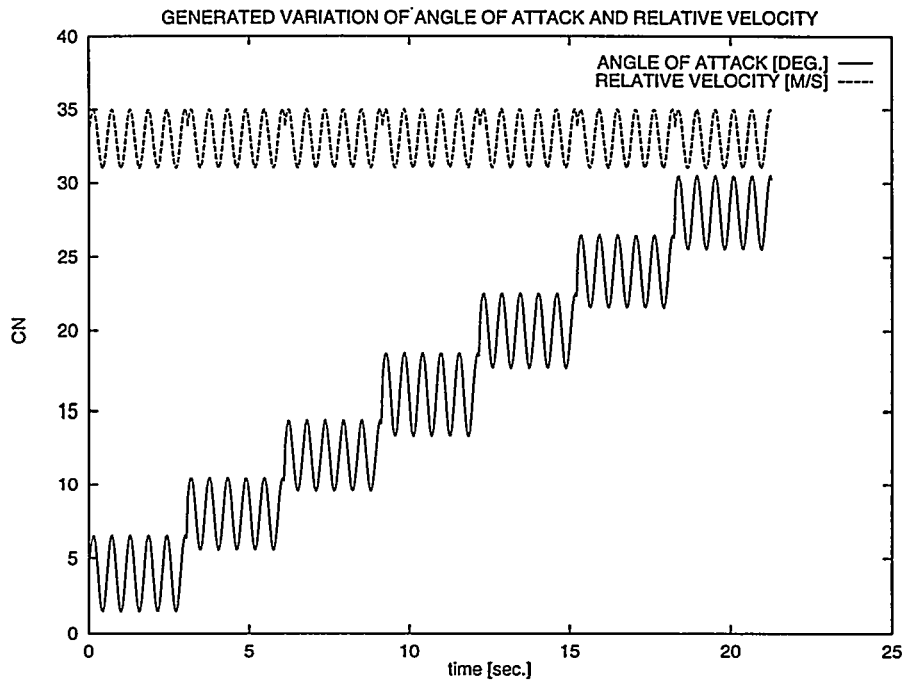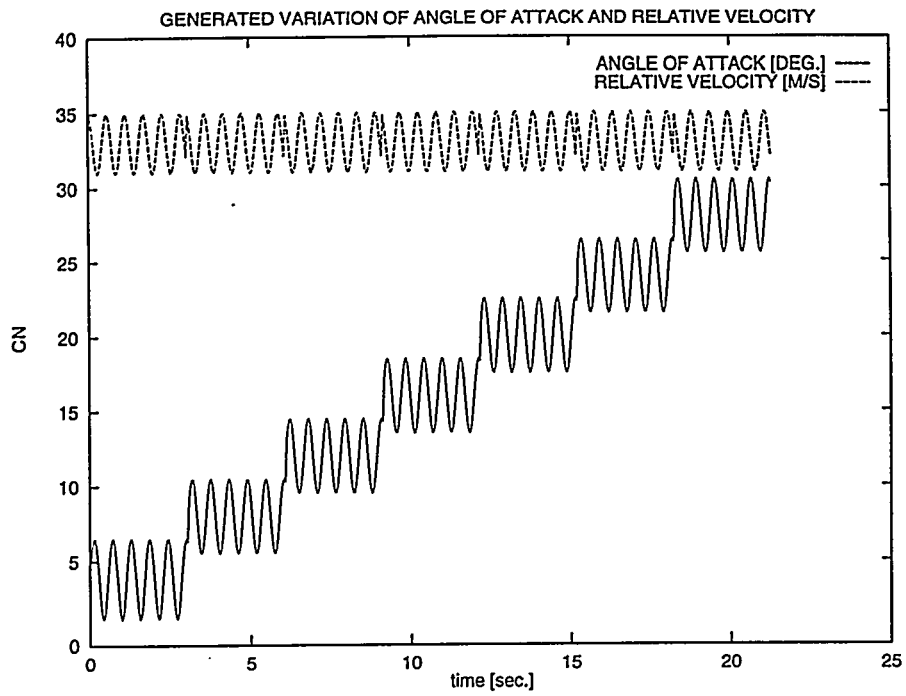

Figure 8-7 Harmonic variation of α and the relative velocity w corresponding to a reduced frequency of 0.1. Amplitude of α is 2.5 deg. and 2.0 m/s for w. α and w in phase.

ALPHA AND W IN PHASE -- reduced frequency k=0.1
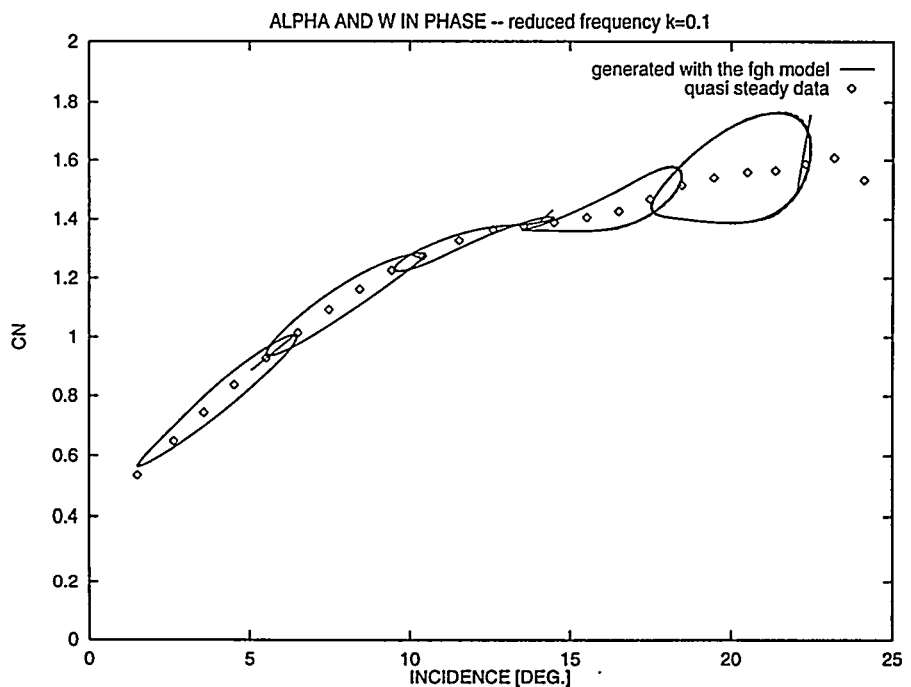
Figure 8-8 Generated hysteresis loops with variation of α and w as shown in Figure 8-7.

Figure 8-9   Harmonic variation of α and the relative velocity w corresponding to a reduced frequency of 0.1. Amplitude of α is 2.5 deg. and 2.0 m/s for w. α and w in counter-phase.
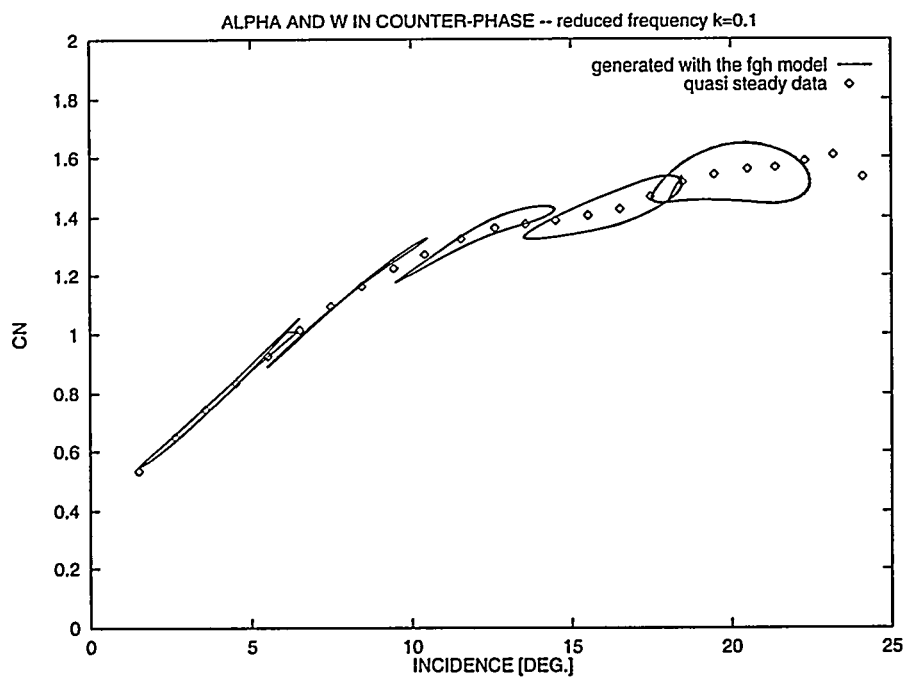

Figure 8-10   Generated hysteresis loops with variation of α and w as shown in Figure 8-9.

8.3 References

[8-1]
Rasmussen, F. "Dynamic Stall of a Wind Turbine Blade Section". Proceedings
(edited by B. Maribo Petersen) of the 8th IEA Joint Action Symposium on
Aerodynamics of Wind Turbines, held at Lyngby, November 21-22, 1994.

[8-2]
Rasmussen, F., Petersen, J.T. and Madsen, H.A. "Response Predictions by Ap-
plication of a New Dynamic Stall Model". Proceedings of the 1996 European
Union Wind Energy Conference, held at Göteborg, Sweeden, 20-24 May 1996.
Pp. 838-842.

Abstract (Max. 2000 characters)

As part of the JOULE-3 project "STALLVIB" an analysis and synthesis of the data from the field rotor experiments at ECN, Delft University, Imperial College, NREL and Risø has been carried out. This has been done in order to see to what extent the data could be used for further development and validation of engineering dynamic stall models. A detailed investigation of the influence of the post-processing of the different data sets has been performed. Further, important statistical functions such as PSD spectra, coherence and transfer functions have been derived for the data sets which can be used as basis for evaluation of the quality of the data seen relative to actual application of the data. The importance of using an appropriate low- pass filtering to remove high frequency noise has been demonstrated when the relation between instantaneous values of e.g. α and C_N is considered.

In general, the complicated measurement on a rotor of α and w and the interpretation of these parameters combined with the strongly three-dimensional, turbulent flow field around the rotating blade has the consequence that it seems difficult to derive systematic information from the different data sets about stall hysteresis. In particular, the measurement of α, which has been performed by different methods, is complicated. Derivation of α on basis of determination of the stagnation point gives reasonable data below stall but fails in stall. On the other hand, measurements of α with a five hole pitot tube can be used also in the stall region. Another main problem is the non-dimensionalization of the coefficients C_N and C_T. If the dynamic pressure used for the non-dimensionalization is not fully correlated with the aerodynamic pressure over the considered airfoil section due to e.g. influence of the gravity on the pressure pipes, the hysteresis loops will be distorted.

However, using the data with caution and applying a suitable post-processing as described by the different participants, it will probably be possible to obtain some information on stall hysteresis from the field rotor data. An example of use of the data for derivation of the empirical constants in the fgh dynamic stall model is shown at the end of the report.